F 1503/3

BULETINUL INSTITUTULUI POLITEHNIC DIN IAŞI

Tomul XL (XLIV)
Fasc. 1–4

Secţia III

ELECTROTEHNICĂ. ENERGETICĂ. ELECTRONICĂ

1994

ORSZÁGOS MŰSZAKI INFORMÁCIÓS KÖZPONT ÉS KÖNYVTÁR
1883

BULETINUL INSTITUTULUI POLITEHNIC DIN IAŞI

Tomul XL (XLIV)
Fasc. 1–4

Secţia III

ELECTROTEHNICĂ. ENERGETICĂ. ELECTRONICĂ

1994

EDITORIAL STAFF

Prof. dr. eng. **VITALIE BELOUSOV** (President)
Prof. dr. eng. **PAULICĂ RĂILEANU** (Secretary)
Prof. dr. eng. **EFTIMIE NIŢESCU**
Prof. dr. doc. **ALFRED BRAIER** (Editor)
Prof. dr. eng. **HUGO ROSMAN** (Editor)
Prof. dr. eng. **MIHAIL VOICU** (Head of the Exchange Service)
Prof. dr. **AUREL BEJANCU**
Prof. dr. eng. **VICTOR BULACOVSCHI**
Prof. dr. eng. **DIMITRIE ALEXA**
Prof. dr. eng. **SPIRIDON CREŢU**
Prof. dr. eng. **ADRIAN RADU**
Prof. dr. eng. **ION GIURMA**
Prof. dr. eng. **MIRCEA MATEESCU**

L 329248

TEXredaction:
Computing Centre of the Technical University of Iaşi

BULETINUL INSTITULUI POLITEHNIC DIN IAŞI
BULLETIN OF THE POLYTECHNIC INSTITUTE OF JASSY
Tomul XL (XLIV), Fasc. 1–4 1994

Secţia III

ELECTROTEHNICĂ. ENERGETICĂ. ELECTRONICĂ

SUMAR

Pag.

CAMELIA PETRESCU, Distribuţia puterii absorbite într-un dielectric cu simetrie cilindrică, încălzit în două tipuri de instalaţii de încălzire, funcţionând în domeniul radio-frecvenţelor (engl., rez. rom.) 7

D.P. HOWSON şi M. NASER-MOGHADASI, Rezonatoare acordabile cu ferită pentru circuite cu microunde (engl., rez. rom.) 15

HUGO ROSMAN, Asupra condiţiilor de reciprocitate şi simetrie ale unui diport liniar neautonom, generalizat, în regim permanent armonic (franc., rez. rom.) 23

PAUL COTAE, Metodă de calcul a densităţii spectrale de putere în modulaţia digitală de frecvenţă cu semnale modulatoare corelate (engl., rez. rom.) 31

ILIE POPESCU, IUSTINA ZAHARIA şi CAMELIA PETRESCU, Asupra determinării puterii şi energiei armonice active în reţelele electrice funcţionând în regim deformant (franc., rez. rom.) 39

VALERIU MUNTEANU, M. LUCANU şi DANIELA TARNICERIU, Creşterea siguranţei în funcţionarea dispozitivelor electronice prin folosirea unui cod bloc liniar corector de o eroare (I) (engl., rez. rom.) 49

MARIANA BUZDUGA, Asupra condiţiilor de apariţie a oscilaţiilor mecanice într-un sistem electromecanic. I. Stabilirea ecuaţiilor de mişcare (franc., rez. rom.) 55

CRISTIAN FOŞALĂU, Măsurări de capacităţi şi conductanţe folosind detectoare sensibile la fază (engl., rez. rom.) 65

I. SUCHAR şi RADU URSULEAN, Asupra unui limitator parametric de cursă fără contacte (engl., rez. rom.) 71

C. POŞA şi DORU-FLORIN CHIPER, Asupra utilizării multiplexoarelor în sinteza funcţiilor logice (engl., rez. rom.) 79

N.D. ALEXANDRU şi I.F. MASHEH, Asupra decodorului *M*2 modificat (engl., rez. rom.) 83

N.D. ALEXANDRU şi PAUL COTAE, Un decodor simplificat pentru semnale codate Miller (engl., rez. rom.) 87

	Pag.
ADRIAN BARABOI, EUGEN HNATIUC şi MARICEL ADAM, Intensificarea răcirii căilor de curent cu ajutorul tuburilor termice (franc., rez. rom.)	91
EUGEN HNATIUC, ALBIN CZERNICHOWSKI, JEAN-MARIE CORMIER şi FRÉDÉRIC RICHARD, Cu privire la bilanţul de puteri în instalaţiile de alimentare a generatoarelor de plasmă rece de tip „GLIDARC" (franc., rez. rom.)	97
MIRCEA-SORIN OPRIŞOR şi ANA-SIMONA CABA, Şuntarea indusului motorului de curent continuu cu excitaţie separată (engl., rez. rom.)	103
C. ASAFTEI, N. GAVRILAŞ, MIRCEA GUŞĂ şi MARCEL ISTRATE, Aspecte teoretice cu privire la propagarea semnalelor emise de indicatoarele de defect pe liniile de medie tensiune aeriene (franc., rez. rom.)	111
GH. GEORGESCU şi M. GAVRILAŞ, Contribuţii privind analiza spectrală a graficelor de sarcină ale reţelelor electrice de distribuţie (engl., rez. rom.)	115
N. GAVRILAŞ, C. ASAFTEI, MIRCEA GUŞĂ şi MARCEL ISTRATE, Consideraţii privind detectarea şi localizarea scurtcircuitelor în reţelele electrice aeriene de distribuţie (engl., rez. rom.)	123
M. GAVRILAŞ şi GH. GEORGESCU, Identificarea categoriilor de consum ale sarcinilor reţelelor electrice de distribuţie cu ajutorul reţelelor neuronale (engl., rez. rom.)	127
RECENZII	135

BULETINUL INSTITULUI POLITEHNIC DIN IAŞI
BULLETIN OF THE POLYTECHNIC INSTITUTE OF JASSY
Tome XL (XLIV), Fasc. 1–4 1994

Section III

ELECTROTECHNICS. ENERGETICS. ELECTRONICS

CONTENTS

Pp.

CAMELIA PETRESCU, Power Distribution in Cylindrical Dielectric Heated in Two Different Types of Radio-Frequency Stray-Field Applicators (English, Romanian summary) 7

D.P. HOWSON and M. NASER-MOGHADASI, Ferrite Tuned Resonators for Microwave Circuits (English, Romanian summary) 15

HUGO ROSMAN, Sur les conditions de réciprocité et de symétrie d'un biporte généralisé non-autonome en régime permanent harmonique (French, Romanian summary) 23

PAUL COTAE, Method to Calculate Power Spectral Density of Digital Frequency Modulation with Correlated Data Symbols (English, Romanian summary) 31

ILIE POPESCU, IUSTINA ZAHARIA et CAMELIA PETRESCU, Sur la détermination de la puissance et de l'énergie harmonique active dans les réseaux électriques fonctionnant en régime déformant (French, Romanian summary) 39

VALERIU MUNTEANU, M. LUCANU and DANIELA TARNICERIU, Increasing of the Safety in the Working of the Electronic Devices Using a Single-Error Correcting Linear Block Code (I) (English, Romanian summary) 49

MARIANA BUZDUGA, Sur les conditions d'apparition des oscillations mécaniques dans un système électromecanique. I. Etablissement des équations du mouvement (French, Romanian summary) 55

CRISTIAN FOŞALĂU, Conductance and Capacitance Measurements Using Phase-Sensitive Detection (English, Romanian summary) 65

I. SUCHAR and RADU URSULEAN, On Parametric Limiting Rabbets without Contacts (English, Romanian summary) 71

C. POŞA and DORU-FLORIN CHIPER, About the Use of Multiplexers in the Synthesis of Logical Functions (English, Romanian summary) 79

N.D. ALEXANDRU and I.F. MASHEH, A Modified *M*2 Decoder (English, Romanian summary) 83

N.D. ALEXANDRU and PAUL COTAE, A Simplified Decoder for Miller Coded Data (English, Romanian summary) 87

Pp.

ADRIAN BARABOI, EUGEN HNATIUC et MARICEL ADAM, Intensification du refroidissement des conducteurs à l'aide des caloducs (French, Romanian summary) .. 91

EUGEN HNATIUC, ALBIN CZERNICHOWSKI, JEAN-MARIE CORMIER et FRÉDÉRIC RICHARD, Sur le bilan des puissances pour les installations d'alimentation des générateurs de plasma froid de type „GLIDARC" (French, Romanian summary) ... 97

MIRCEA-SORIN OPRIŞOR and ANA-SIMONA CABA, Shunting of the Armature of the Separately Excited D.C. Motor (English, Romanian summary) 103

C. ASAFTEI, N. GAVRILAŞ, MIRCEA GUŞĂ et MARCEL ISTRATE, Quelques aspects théoriques concernant la propagation des signaux émis par les indicateurs de défaut sur les lignes de moyenne tension (French, Romanian summary) 111

GH. GEORGESCU and M. GAVRILAŞ, Some Aspects about the Spectral Analysis of Load Curves of Electric Distribution Networks (English, Romanian summary) 115

N. GAVRILAŞ, C. ASAFTEI, MIRCEA GUŞĂ et MARCEL ISTRATE, General Considerations on the Detecting and the Location of the Short-circuits on Overhead Distribution Lines (English, Romanian summary) 123

M. GAVRILAŞ and GH. GEORGESCU, Consumer Category Identification of the Loads from Electric Distribution Systems Using Artificial Neural Networks (English, Romanian summary) 127

BOOK REVIEWS 135

BULETINUL INSTITUTULUI POLITEHNIC DIN IAŞI
Tomul XL (XLIV), Fasc. 1–4, 1994
Secţia III
ELECTROTEHNICĂ. ENERGETICĂ. ELECTRONICĂ

D.C. 621.3.017.21

POWER DISTRIBUTION IN CYLINDRICAL DIELECTRIC HEATED IN TWO DIFFERENT TYPES OF RADIO-FREQUENCY STRAY-FIELD APPLICATORS

BY
CAMELIA PETRESCU

1. Introduction

The most important requirement in the dielectric heating problem is the uniformity of heating, and thus the uniformity of the electric field inside the charge. There are industrial processes that rely on the constant temperature of the dielectric for further processing, for example blowing compressed air in a hollow heated dielectric tube in order to increase its diameter.

This paper presents the mathematical model and computes the dissipated power inside the dielectrical tube for two configurations of the applicator. A comparative study is then carried out to point the better solution with respect to the uniformity of heating.

2. Axial Stray-Field Applicator

2.1. Physical Model

The first analyzed applicator is a classical stray-field one with electrodes in the form of rings coaxial with the dielectric tube (Fig. 1).

The electric potential varies periodically in axial direction the period being equal to the distance between two neighbouring electrodes having the same potential.

Thus the electric field may be studied in the basic cell presented in Fig. 2. The installation is usually shielded and this is done by a grounded cylinder coaxial with the whole device.

The electric potential satisfies the P o i s s o n equation:

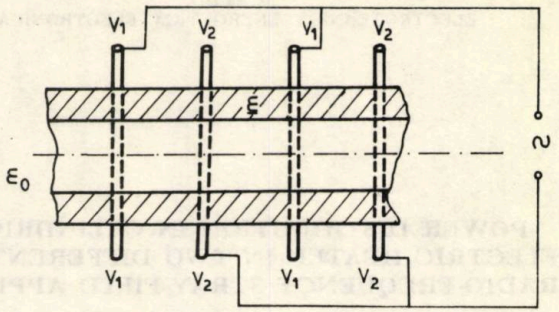

Fig. 1

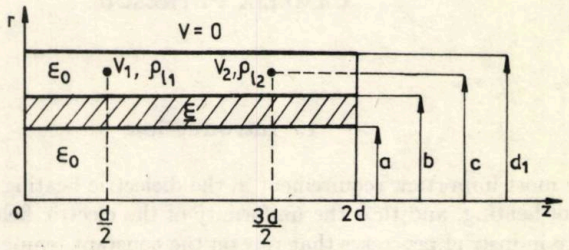

Fig. 2

$$(1) \qquad \Delta V(r,z) = -\frac{\rho_{l_1}}{\varepsilon_0}\delta\left(z-\frac{d}{2}\right)\delta(r-c) - \frac{\rho_{l_2}}{\varepsilon_0}\delta\left(z-\frac{3d}{2}\right)\delta(r-c),$$

where $\delta(x) = \begin{cases} \infty, & x = 0 \\ 0, & x \neq 0 \end{cases}$ is the D i r a c generalised function, ρ_{l_1} and ρ_{l_2} are the line charges on the ring electrodes connected at the potential V_1 and V_2, respectively. The boundary conditions for eq. (1) are:

$$(2) \qquad V(0,r) = V(2d,r), \quad V(z,d_1) = 0,$$

$$(2') \qquad V(d/2,c) = V_1, \quad V(3d/2,c) = V_2.$$

The solution for eq.(1) with the boundary conditions (2), (2′) may be expressed by means of the G r e e n function:

$$(3) \qquad V(r,z) = \rho_{l_1} G(r,z|\, c,d/2) + \rho_{l_2} G(r,z|\, c,3d/2),$$

where $G(r,z|\ r_0,z_0)$ is the potential at point (r,z) established by an unity line charge placed at the point (r_0,z_0).

The G r e e n function for the domain in Fig. 2 satisfies the P o i s s o n equation:

$$\Delta G = -\frac{1}{\varepsilon_0}\delta(r-r_0)\delta(z-z_0) \tag{4}$$

and is given by:

$$G(r,z)|\ r_0,z_0) = \sum_{k=1}^{\infty}[B_k\mathrm{I}_0(\lambda r) + C_k\mathrm{K}_0(\lambda r)]\cos\lambda(z-z_0) + a_1\ln r + a_2, \tag{5}$$

where $\mathrm{I}_0(\lambda r)$ and $\mathrm{K}_0(\lambda r)$ are the modified B e s s e l functions of zero order and of the first and second kind respectively, and $\lambda = k\pi/d$, $(k = 1,2,...)$, are the eigenvalues for eq.(4). The coefficients B_k, C_k, a_1, a_2 are piece-wise constant in radial direction corresponding to the domains where ε =const. The values of these coefficients are derived from the continuity conditions for $G(r,z|\ r_0,z_0)$ and for the electric flux density (the radial component), on the surfaces $r = a$, $r = b$, from the boundary condition $V(z,d_1) = 0$ and from G a u s s theorem applied on the surface $r = c$.

The line charges ρ_{l_1} and ρ_{l_2} are derived from the conditions $(2')$.

The electric field and the power density may be computed using the relations:

$$E = -\frac{\partial V}{\partial z}\mathbf{e}_z - \frac{\partial V}{\partial r}\mathbf{e}_r, \tag{6}$$

$$p_v = \omega\varepsilon_0\varepsilon_r''\left(E_r^2 + E_z^2\right). \tag{7}$$

2.2. Numerical Results and Discussion

A numerical experiment was conducted in order to study the influence of the geometrical parameters on the absorbed power and its uniformity, both in radial and axial direction. The results of some simulations are presented in Figs. 3, 4 and in Table 1.

Table 1

V_1, [V]	V_2, [V]	d_1, [cm]	d, [cm]	c, [cm]	$\tilde{p}_v$, [W/m^3]		
					a	$(a+b)/2$	b
2 000	−2 000	8	10	4	27 933	29 460	32 103
4 000	0	8	10	4	47 526	51 966	59 801
4 000	0	8	15	4	37 369	40 269	45 291
4 000	0	12	10	4	49 477	53 935	61 771
4 000	0	8.55	10	3.55	69 623	78 516	95 857

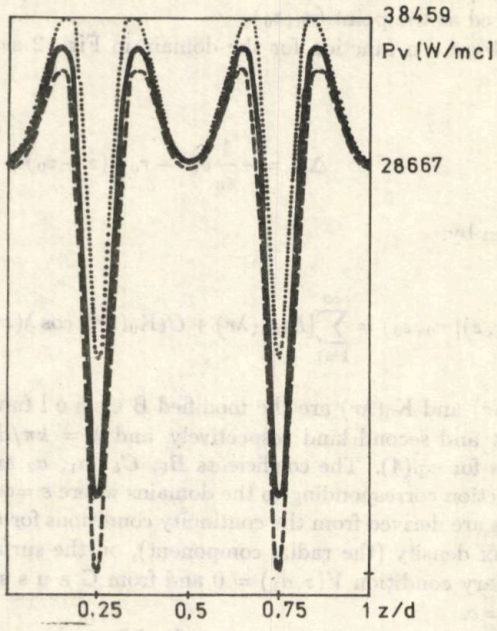

Fig. 3

Fig. 3 and Fig. 4 present the power density in axial direction for the model presented in Fig. 2. The three curves refer to $r = a$, $r = (a + b)/2$ and $r = b$, respectively. The lower values of p_v correspond to $r = a$ and the higher ones to $r = b$, respectively.

The absorbed power density has peak values in the neighbourhood of the electrodes and minimum values in the plane of the electrodes. This is due to the fact that the axial component of the electric field is larger that the radial one at all points excepting $z = d/2$, $z = 3d/2$, where $E_z = 0$. The nonuniformity of the power density in radial direction, computed with the relation:

$$K_r = \left.\frac{p_{v_{\min}}(r,z)}{p_{v_{\max}}(r,z)}\right|_{z=\text{const.}}, \tag{8}$$

may be over 10 in the neighbourhood of the active electrodes (electrodes that have a nonzero potential) and is negligible elsewhere. The nonuniformity of the power density in axial direction, computed with the relation:

$$K_z = \left.\frac{p_{v_{\min}}(r,z)}{p_{v_{\max}}(r,z)}\right|_{r=\text{const.}}, \tag{9}$$

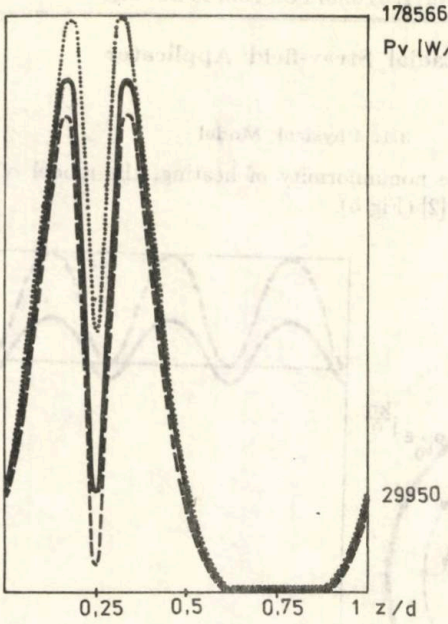

Fig. 4

is rather large (31 in the considered example) when two active electrodes are used ($V_1 = V_0,\ V_2 = -V_0$) and is extremely large when only one electrode is active ($V_1 = 2V_0,\ V_2 = 0$).

Table 1 presents the mean value of the absorbed power defined as:

$$\tilde{p}_v(r) = \frac{1}{2d}\int_0^{2d} p_v(r,z)\mathrm{d}z, \tag{10}$$

for $r = a,\ r = (a+b)/2,\ r = b$ and for several values of $V_1,\ V_2,\ d_1,\ d,\ c$.

These results show that the closer the electrodes, and the further the shield, the higher the mean absorbed power is.

This analysis makes possible the design of the device that gives a certain power with a certain degree of uniformity to the treated dielectric. It also shows that the two important goals of dielectric heating: greater absorbed power and greater temperature uniformity may not be achieved simultaneously. Generally speaking, a modification of a geometric parameter of the installation leads to an increase in the absorbed power and a decrease in power density uniformity.

3. Radial Stray-field Applicator

3.1. Physical Model

In order to reduce the nonuniformity of heating, the model of an original installation was conceived, [2] (Fig 5).

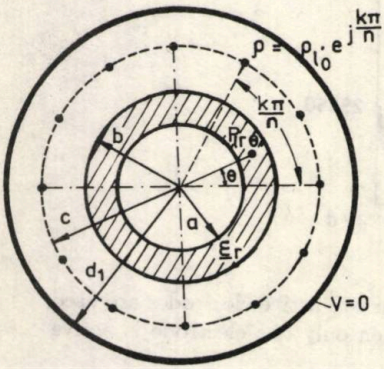

Fig. 5

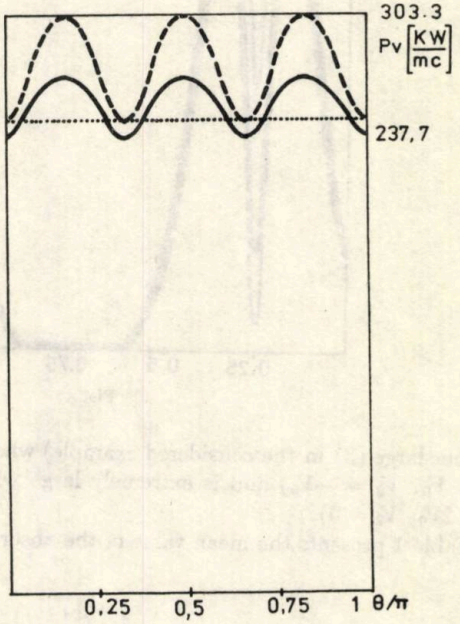

Fig. 6

A number of $2n$ electrodes in the form of long rods are placed in axial direction on the cylinder $r = c$, coaxial with the dielectric tube. In Fig. 5 the electrodes are placed at the points $(c,\ k\pi/n)$, $(k = 0, 1, ..., 2n-1)$. The kth electrode has a complex line charge:

$$\underline{\rho}_l = \rho_{l_0} e^{j\frac{k\pi}{n}} . \tag{11}$$

The complex potential satisfies the P o i s s o n equation:

$$\Delta \underline{V} = -\frac{\rho_{l_0}}{\varepsilon_0} \sum_{k=0}^{2n-1} e^{j\frac{k\pi}{n}} \delta(r-c)\delta\left(\theta - \frac{k\pi}{n}\right) \tag{12}$$

with the boundary condition

$$\underline{V}(d_1,\ \theta) = 0. \tag{13}$$

The solution of eq. (8) is

$$\underline{V}(r,\ \theta) = \frac{\rho l_0}{\pi\varepsilon_0} \sum_{k=0}^{n-1} e^{j\frac{k\pi}{n}} \sum_{p=0}^{\infty} \left(B_{2p+1} r^{2p+1} + \frac{D_{2p+1}}{r^{2p+1}} \right) \cos(2p+1)\left(\theta - \frac{k\pi}{n}\right), \tag{14}$$

where the coefficients B_{2p+1} and D_{2p+1} depend on r and are constant in the regions with constant ε. The expressions for B_{2p+1} and D_{2p+1} are derived from the potential and normal flux density continuity on the surfaces $r = a$ and $r = b$ and from the boundary condition (11).

The complex electric field intensity is given by:

$$\underline{E} = -\frac{\partial \underline{V}}{\partial r}\mathbf{e}_r - \frac{1}{r} \cdot \frac{\partial \underline{V}}{\partial \theta}\mathbf{e}_\theta \tag{15}$$

and the power density is:

$$p_v(r,\theta) = \omega\varepsilon_0\varepsilon_r''(|\underline{E}_r|^2 + |\underline{E}_\theta|^2). \tag{16}$$

3.2. Numerical Results and Discussions

A numerical study was conducted in order to compute the absorbed power density, and especially to examine its nonuniformity in radial and in tangential direction. Table 2 presents the results obtained when 6 or 12 electrodes are used, for several values of the radius c. The values listed in this table represent the ratio between minimum power density in radial and in tangential direction respectively, computed with relations:

$$K_\theta = \left.\frac{p_{v_{\min}}(r,\theta)}{p_{v_{\max}}(r,\theta)}\right|_{r=\text{const.}}, \quad K_r = \left.\frac{p_{v_{\min}}(r,\theta)}{p_{v_{\max}}(r,\theta)}\right|_{\theta=\text{const.}} \tag{17}$$

Table 2

No. of Electrodes	c cm	K_θ			$\min\{K_r\}_{\theta\in[0,\pi]}$
		$r = a$	$r = (a+b)/2$	$r = b$	
6	3.5	0.752	0.911	0.787	0.768 ($\theta = \pi/6$)
	4	0.810	0.880	0.996	0.812 ($\theta = \pi/6$)
12	3.5	0.981	0.997	0.951	0.835 ($\theta = \pi/12$)
	4	0.990	0.996	0.996	0.854 ($\theta = \pi/12$)

The nonuniformity in direction θ is very low compared to that of the device analyzed in the previous paragraph; K_θ tends to unity for increasing number of electrodes and increasing radius c. The nonuniformity in radial direction is also considerably lower for this installation than for the previous one.

Fig. 6 represents power density in the tangential direction when 6 electrodes are used. The other numerical values used in computations are:

$$a = 2.25 \text{ cm}, \quad b = 2.75 \text{ cm}, \quad c = 4 \text{ cm}, \quad d_1 = 10 \text{ cm}, \quad \varepsilon_r = 4, \quad V_0 = 4000 \text{ V}.$$

It is thus obvious that the second installation, although more difficult to realize in practice, is the best choice if a high uniformity of the dissipated power is required in the dielectric tube.

Received, October 7, 1993

Technical University "Gh.Asachi", Jassy,
Department of Electrotechnics

REFERENCES

1. S m y t h e W.R., *Static and Dynamic Electricity.* Mc Graw Hill, New York, 1950.
2. Ţ u g u l e a A., P e t r e s c u C., *Heating Lossy Dielectric Tubes in a New Type of Radio – Frequency Applicator.* Rev. Roum. Sci. Techn., **37**, *3* (1992).
3. * * * High Frequency / Microwave Proccesing and Heating Internat. Conf., Sept. 26-29, 1989, Arnhem, Netherlands.
4. M a r c h a n d C., *Le logiciel stray, un outil de simulation des applicateurs à barreaux utilisés en chauffage haute fréquence.* Électricité de France, Direction des Études et recherches, 1988.

DISTRIBUŢIA PUTERII ABSORBITE ÎNTR-UN DIELECTRIC CU SIMETRIE CILINDRICĂ, ÎNCĂLZIT ÎN DOUĂ TIPURI DE INSTALAŢII DE ÎNCĂLZIRE, FUNCŢIONÂND ÎN DOMENIUL RADIO-FRECVENŢELOR

(Rezumat)

Se determină pe cale analitică potenţialul, intensitatea câmpului electric, densitatea de putere şi puterea medie absorbită în două tipuri de instalaţii de încălzire dielectrică destinate procesării unor sarcini cu simetrie cilindrică şi se efectuează o analiză comparativă a lor privind densitatea de putere absorbită şi uniformitatea acesteia.

BULETINUL INSTITUTULUI POLITEHNIC DIN IAŞI
Tomul XL (XLIV), Fasc. 1–4, 1994
Secţia III
ELECTROTEHNICĂ. ENERGETICĂ. ELECTRONICĂ

D.C. 621.396.6; 621.3.029.6

FERRITE TUNED RESONATORS FOR MICROWAVE CIRCUITS

BY

D.P. HOWSON and M. NASER-MOGHADASI

1. Introduction

Various techniques are available for the rapid tuning of microwave resonators, including the use of ferrites, varactors, or PIN switches. This paper is concerned with high Q resonators at low microwave frequencies (0.9...2 GHz), at which the use of dielectric resonators keeps the total resonator dimensions relatively small. Such a high Q resonator may be used in the base station of a mobile radio system, as part of the transmitter combiner.

A performance comparison of various tuning mechanisms for high Q resonators is given in Table 1, for which it can be seen that the use of ferrite to tune the dielectric resonator is attractive.

Table 1

A Performance Comparison of Various Tuning Mechanisms

Configuration	Ferrite	Varactor	PIN Diode
Tuning range, [%]	1.25	0.3	0.045
Tuning Degradation (Q_0/Q_u), [%]	50	40	40
Power handling	good	poor	good
Non-linearity	good	poor	moderate

Q_0 – unloaded quality factor of resonator (MAX.perturbation); Q_u – unloaded quality factor of resonator (unperturbed).

Although ferrite tining requires a bulky electromagnet and a standing current, it was decided that the advantages laid out in Table 1 make it worthwhile to design a series of ferrite-tuned resonators, as described in the next two sections.

2. Single-tuned Ferrite Resonators

Wide tuning ranges were found to be possible in preliminary experiments on low Q resonators operating at 8.5 GHz. Use of a YIG sphere showed 20% was practicable. In the high Q single tuned resonator that was subsequently [1], [2], a

cylindrical DR was supported on low-loss low permittivity foam within a copper cavity. The DR was excited in its dominant TE_{01} mode being coupled via a coaxial connector to the transmitter. Tuning was effected by variation of the magnetic field applied to the magnetic discs, which were attached above and below the cylindrical DR. Several configurations of field, disc and DR were investigated – an unit is shown in Fig. 1 and a typical result in Fig. 2. Both longitudinal and transverse magnetisation was investigated – the latter was found preferable. Units with a single ferrite disc above the DR and none below showed similar characteristics, but a lower tuning range say 75% of the double unit.

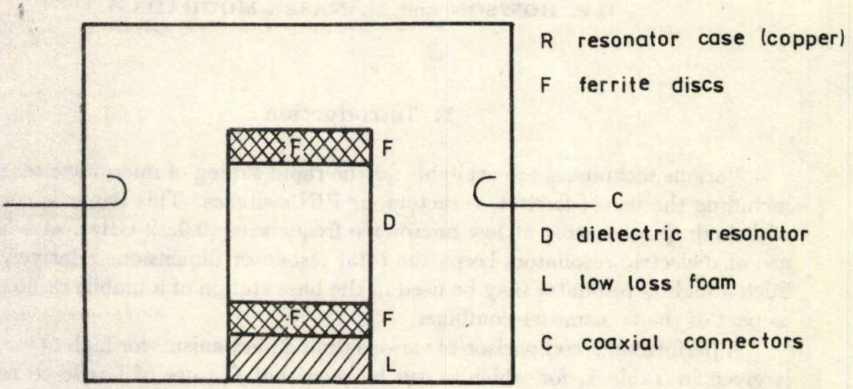

Fig. 1.– Ferrite tuned dielectric resonator.

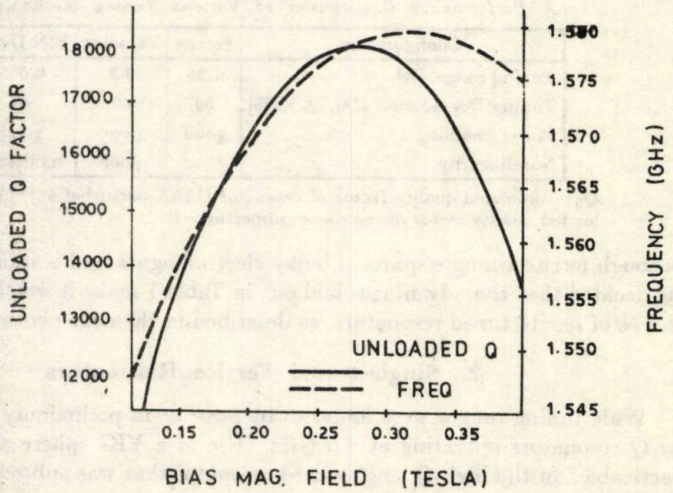

Fig. 2.– Performance of typical signale-tuned resonator.

A similar unit at 900 MHz exhibited an unloaded Q of 13 000, that was degraded to 9 000 by 1% tuning, and further to 8 000 by 2% tuning.

Operation above the natural resonant frequency of the unit in all cases gave highest Q – the ferrite was most lossy when unsaturated.

3. Double-tuned Dielectric Resonator

Dual mode filters, in which two resonances are coupled in a single structure, have significant advantages of weight and size. Dual mode dielectric resonator filters have been reported by several authors. For this work a ferrite tuned dual mode filter is designed which offers excellent temperature and electrical characteristics [3].

The mode of operation is the degenerate hybrid mode HE_{111}. The input/output coupling is achieved by using two SMA type coaxial connectors in which the centre pin is extended into the cavity, positioned at 90°to each other in the maximum radial electric field. Coupling between the two modes is achieved by means of a coupling screw oriented at 45°with respect to the electrical fields of the two orthogonal modes (s. Fig. 3).

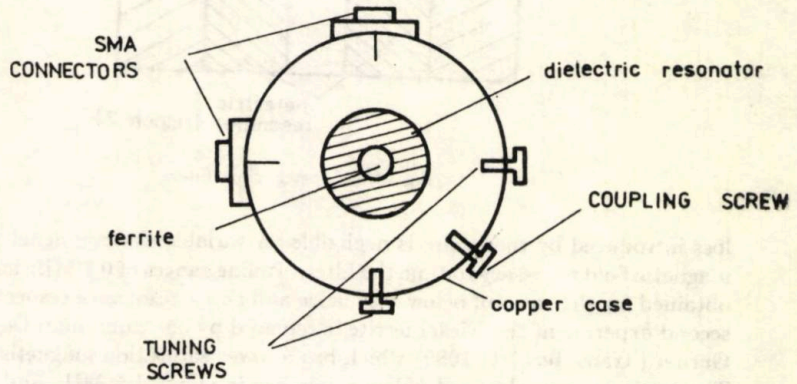

Fig. 3.– Dual mode ferrite tuned DR.

For independent tuning, two tuning screws are mounted at the direction of maximum electric field of each mode, being perpendicular to each other and each facing to one of the coaxial probes.

Experiments have been performed which show that dual mode as well as the previously reported single mode filters can be magnetically tuned using ferrite. This is accomplished by inserting a thin ferrite rod through an axial hole in the dielectric resonator [4]. The magnetic field controls the permeability of ferrite and hence the resonant frequency of the system. The tuning range is a function of the ferrite properties and also the magnetic field applied.

In this experiment two different types of ferrite have been investigated. In both cases the tuning of the dual mode filter is achieved either at below resonance or above resonance state of the ferrite. The tuning in the resonance area of the ferrite is strongly affected by the spin wave properties of the ferrite. In the first part a Nickel ferrite rod (Trans-Tech.TT2.113) of dimension 4 mm dia. × 16 mm height was a close fit inside a ring Dielectric Resonator of 35.5 mm dia. (Trans-Tech. C88(10)1400(Y)630(B)162) housed inside a circular metal cavity as shown in Fig. 4. The presence of ferrite does not alter the dual mode coupling and the

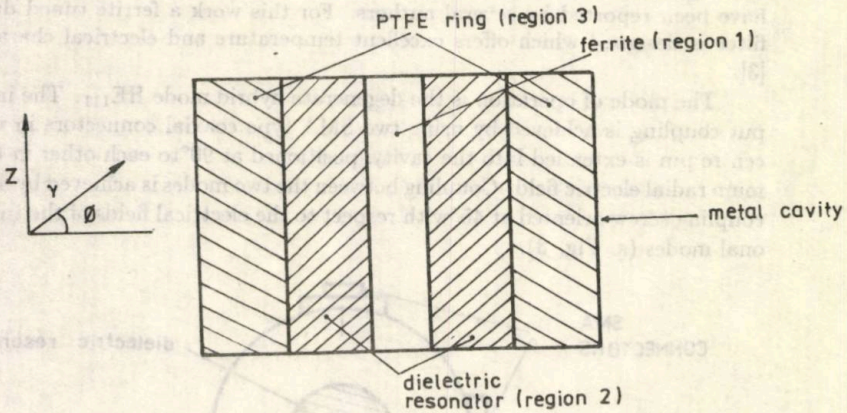

Fig. 4.– Shorter ring filter.

loss introduced by the ferrite is negligible. A variable electromagnet provided the magnetic field necessary to tune the filter. Tuning ranges of 0.7 MHz and 5 MHz are obtained for the cases of below resonance and above resonance respectively. In the second experiment the Nickel ferrite is replaced by an Aluminium Doped Yttrium Garnet (Trans-Tech. G-1009) which has a lower saturation magnetisation of 175. The tuning range obtained below resonance is about 1.5 MHz and furthermore above resonance, the tuning range is similar to the Nickel ferrite. This is shown in Fig. 5. The main difference of the two types of ferrites is in their saturation magnetisation. This has a direct effect on the amount of necessary DC magnetic field required to tune the dual mode filter. It is observed that the Yttrium garnet, in a comparison to the Nickel ferrite, offers more tuning range in the below resonance state, but more importantly due to its lower saturation magnetisation ($4\pi M_s$) requires less magnetic field to reach the above resonance state. It is noteworthy that the dual mode response is preserved over a reasonable frequency range as the magnetic field is altered.

The unloaded Q of the unit reported above is modest (2000) but other units have been made in which the ferrite/DR combination of Fig. 3 is located within a larger cavity in the manner of Fig. 1, without the ferrite discs. In this case,

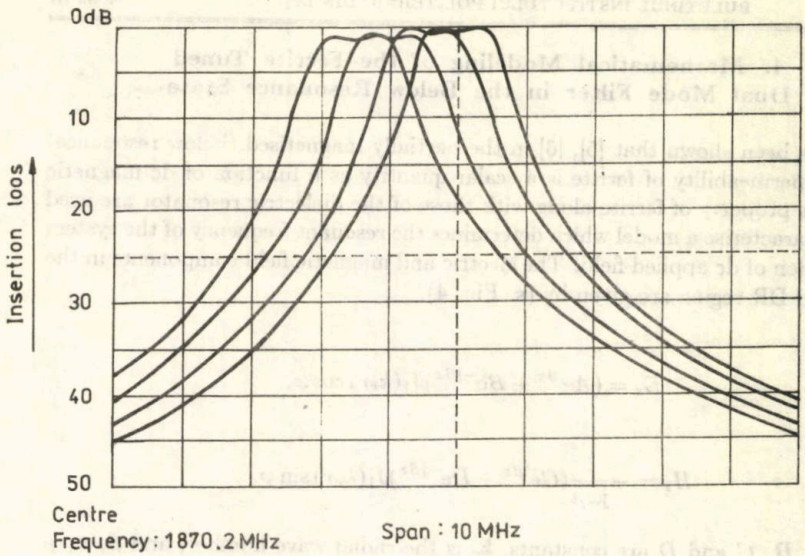

Fig. 5 *a*.– Dual-mode frequency response below resonance (Yttrium garnet).

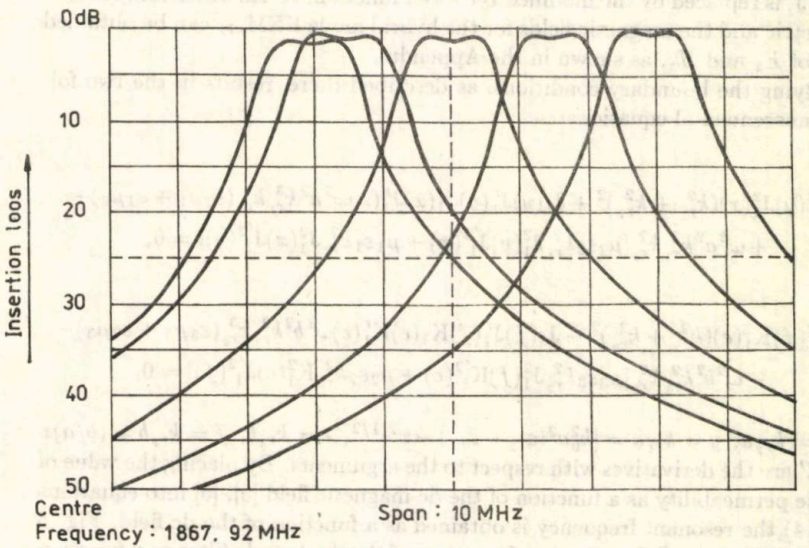

Fig. 5 *b*.– Dual-mode frequency response above resonance (Yttrium garnet).

an unloaded Q of 11 000 at 1.47 GHz was obtained, with a tuning bandwidth of 1 MHz.

4. Mathematical Modeling of the Ferrite Tuned Dual Mode Filter in the Below Resonance State

It has been shown that [5], [6] in the partially magnetised (below resonance) state the permeability of ferrite is a scalar quantity as a function of dc magnetic field. This property of ferrite along with those of the dielectric resonator are used here to characterise a model which determines the resonant frequency of the system as a function of dc applied field. The electric and magnetic field components in the ferrite and DR region are given by (s. Fig. 4):

$$E_z = (Ae^{j\beta z} + Be^{-j\beta z})J_1(k_r r)\cos\varphi, \tag{1}$$

$$H_z = -\frac{1}{j\omega\mu}(Ce^{j\beta z} + De^{-j\beta z})J_1(k_r r)\sin\varphi, \tag{2}$$

where A, B, C and D are constants, k_r is the radial wave number, and β, ε, μ and ω have usual meanings. In the air region for the above equations the Bessel function, J, is replaced by the modified B e s s e l function, K. All other components of the electric and the magnetic fields for the hybrid mode HEM_{111} can be obtained in terms of E_z and H_z, as shown in the Appendix.

Applying the boundary conditions, as described there, results in the two following transcendental equations:

$$\begin{aligned}(3)\quad &-\beta^2 J_1^2(y)J_1^2(x)(k_{r_1}^2 + k_{r_2}^2)^2 + J_1(y)J_1'(y)J_1(x)J_1'(x)\omega^2 a^2 k_{r_1}^3 k_{r_2}^3(\varepsilon_2\mu_1 + \varepsilon_1\mu_2) + \\ &+ \omega^2 a^2 k_{r_1}^2 k_{r_2}^2[\mu_2\varepsilon_2 k_{r_1}^2 J_1^2(y)J_1'^2(x) + \mu_1\varepsilon_1 k_{r_2}^2 J_1^2(x)J_1'^2(y)] = 0,\end{aligned}$$

$$\begin{aligned}(4)\quad &\beta^2 J_1^2(f)K_1^2(e)(k_{r_2}^2 + k_{r_3}^2)^2 - J_1(f)J_1'(f)K_1(e)K_1'(e)\omega^2 b^2 k_{r_2}^3 k_{r_3}^3(\varepsilon_3\mu_2 + \varepsilon_2\mu_3) - \\ &- \omega^2 b^2 k_{r_2}^2 k_{r_3}^2[\mu_3\varepsilon_3 k_{r_2}^2 J_1^2(f)K_1'^2(e) + \mu_2\varepsilon_2 k_{r_3}^2 K_1^2(e)J_1'^2(f)] = 0,\end{aligned}$$

where $x = k_{r_2}a$, $y = k_{r_1}a = [k_0^2 a^2(\varepsilon_{r_2} - \varepsilon_{r_1}) - x^2]^{1/2}$, $e = k_{r_3}b$, $f = k_{r_2}b = (b/a)x$ and J′, K′ are the derivatives with respect to the arguments. By placing the value of the ferrite permeability as a function of the dc magnetic field [5], [6] into equations (3) and (4) the resonant frequency is obtained as a function of the dc field. Fig. 6 illustrates variations of the resonant frequency of the dual mode filter as a function of dc magnetic field in the below resonance state for the second of the two samples used in these experiments.

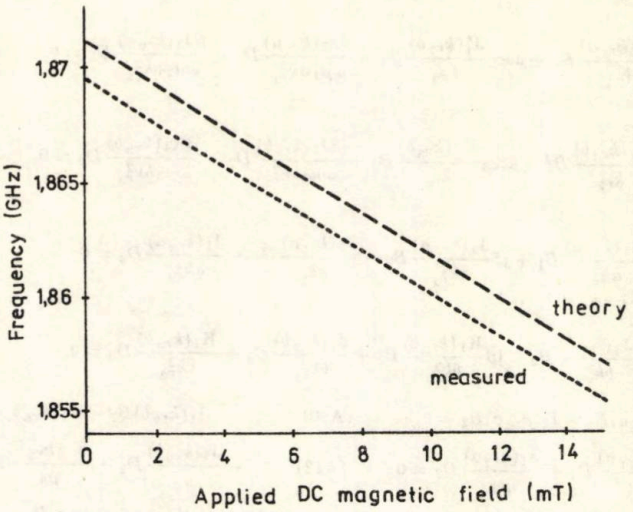

Fig. 6.– Resonant frequency vs. magnetic field (Yttrium garnet).

Appendix [3]

Dimensions of cavity in expt: height = 16 mm, radius of ferrite rod $a = 2$ mm, radius of DR $b = 17.75$ mm.

For the HEM_{111} mode the required electric and magnetic field components are:

(A1)
$$E_\varphi = -\left[j\beta\frac{A}{r}J_1(k_r r) + Ck_r J_1'(k_r r)\right]\frac{e^{j\beta z}\sin\varphi}{(j\beta)^2 + k^2} + \left[j\frac{B\beta}{r}J_1(k_r r) - Dk_r J_1'(k_r r)\right]\frac{e^{-j\beta z}\sin\varphi}{(j\beta)^2 + k^2},$$

(A2)
$$H_r = -\left[j\omega\frac{\varepsilon A}{r}J_1(k_r r) + \frac{\beta k_r C}{\omega\mu}J_1'(k_r r)\right]\frac{e^{j\beta z}\sin\varphi}{(j\beta)^2 + k^2} - \left[j\omega\frac{\varepsilon B}{r}J_1(k_r r) + \frac{\beta k_r D}{\omega\mu}J_1'(k_r r)\right]\frac{e^{-j\beta z}\sin\varphi}{(j\beta)^2 + k^2},$$

(A3)
$$H_\varphi = -\left[j\omega\varepsilon k_r A J_1'(k_r r) + \frac{\beta C}{\omega\mu r}J_1(k_r r)\right]\frac{e^{j\beta z}\cos\varphi}{(j\beta)^2 + k^2} - \left[j\omega\varepsilon k_r B J_1'(k_r r) - \frac{\beta D}{\omega\mu r}J_1(k_r r)\right]\frac{e^{-j\beta z}\cos\varphi}{(j\beta)^2 + k^2},$$

(A4)
$$E_r = \left[j\beta k_r A J_1'(k_r r) + \frac{C}{r}J_1(k_r r)\right]\frac{e^{j\beta z}\cos\varphi}{(j\beta)^2 + k^2} + \left[-j\beta k_r B J_1'(k_r r) + \frac{D}{r}J_1(k_r r)\right]\frac{e^{-j\beta z}\cos\varphi}{(j\beta)^2 + k^2}.$$

Applying the boundary conditions leads to:

$$(A5)\qquad j\omega\varepsilon_1\frac{J_1'(k_{r_1}a)}{k_{r_1}}B_1+j\omega\varepsilon_2\frac{J_1'(k_{r_2}a)}{k_{r_2}}B_2-\frac{\beta J_1(k_{r_1}a)}{\omega\mu_1 ak_{r_1}^2}D_1-\frac{\beta J_1(k_{r_2}a)}{\omega\mu_2 ak_{r_2}^2}D_2=0,$$

$$(A6)\qquad -j\omega\varepsilon_2\frac{J_1'(k_{r_2}b)}{k_{r_2}}B_2-j\omega\varepsilon_3\frac{K_1'(k_{r_3}b)}{k_{r_3}}B_3+\frac{\beta J_1(k_{r_2}b)}{\omega\mu_2 bk_{r_2}^2}D_2+\frac{\beta K_1(k_{r_3}b)}{\omega\mu_3 bk_{r_3}^2}D_3=0,$$

$$(A7)\qquad j\beta\frac{J_1(k_{r_1}a)}{ak_{r_1}^2}B_1+j\beta\frac{J_1(k_{r_2}a)}{ak_{r_2}^2}B_2-\frac{J_1(k_{r_1}a)}{ak_{r_1}^2}D_1-\frac{J_1(k_{r_2}a)}{ak_{r_2}^2}D_2=0,$$

$$(A8)\qquad -j\beta\frac{J_1(k_{r_2}b)}{bk_{r_2}^2}B_2-j\beta\frac{K_1(k_{r_3}b)}{bk_{r_3}^2}B_3+\frac{J_1(k_{r_2}b)}{bk_{r_2}^2}D_2+\frac{K_1(k_{r_3}b)}{bk_{r_3}^2}D_3=0,$$

$$(A9)\qquad J_1(k_{r_1}a)B_1-J_1(k_{r_2}a)B_2=0,\qquad (A10)\qquad J_1(k_{r_2}b)B_2-K_1(k_{r_3}b)B_3=0,$$

$$(A11)\qquad -\frac{J_1(k_{r_1}a)}{\mu_1}D_1+\frac{J_1(k_{r_2}a)}{\mu_2}D_2=0,\qquad (A12)\qquad -\frac{J_1(k_{r_2}b)}{\mu_2}D_2+\frac{K_1(k_{r_3}b)}{\mu_3}D_3=0.$$

Equations (A5)...(A12) form two 4×4 matrices. In order that the parameters B_1, B_2, B_3, D_1, D_2 and D_3 are not zero, the determinant of their coefficient must vanish. This leads to equations (3) and (4) in the main text.

Received, November 4, 1993

University of Bradford,
England, UK

REFERENCES

1. Kazeminejad S., Zargar-Ershadi T., Mahdi A., Khanifar A., Howson D.P., *Electronically Reconfigurable Cellular Radio Multicouplers.* IEE Fifth International Conference on Mobile Radio and Personal Communications, Warwick, December 1989, 57-59.
2. Zargar-Ershadi T., *Electronic Tuning of a Composite Ferrite/Dielectric Loaded Cavity Resonator.* PhD Thesis, University of Bradford, 1991.
3. Naser-Moghadasi M., *Ferrite Tuned Dual-Mode Dielectric Resonator Filters.* PhD Thesis, University of Bradford, 1992.
4. Farr A.N., Blackie G.N., Williams D., *Novel Techniques for Electronic Tuning of Dielectric Resonators.* Proc. 13th Eur. Microwave Conf., Germany, 1983, 791-796.
5. Lecraw R.C., Spencer E.G., *Tensor Permeabilities of Ferrites below Magnetic Saturation.* IRE Convention Record, Part 5, 1956, 66-74.
6. Green J.J., Sandy F., *Microwave Characterisation of Partially Magnetised Ferrites.* IEEE Trans. Microwave Theory Tech., **MTT-22**, *6*, 641-645 (1974).

REZONATOARE ACORDABILE CU FERITĂ PENTRU CIRCUITE CU MICROUNDE

(Rezumat)

Se studiază unele tipuri de rezonatoare cu ferită cu factor de calitate ridicat pentru domeniul de frecvenţe 0,9...2 GHz.

Sunt prezentate o serie de detalii constructive precum şi rezultate teoretice şi experimentale privind comportarea rezonatoarelor sub acţiunea tensiunii de control.

BULETINUL INSTITUTULUI POLITEHNIC DIN IAŞI
Tomul XL (XLIV), Fasc. 1–4, 1994
Secţia III
ELECTROTEHNICĂ. ENERGETICĂ. ELECTRONICĂ

C.D. 621.329.5

SUR LES CONDITIONS DE RÉCIPROCITÉ ET DE SYMÉTRIE D'UN BIPORTE GÉNÉRALISÉ NON-AUTONOME EN RÉGIME PERMANENT HARMONIQUE

PAR
HUGO ROSMAN

1. Introduction

C'est V.P. S i g o r s k y qui a le mérite d'avoir élaboré une théorie cohérente et unitaire des biportes linéaires généralisés dans une monographie publiée en 1955 [1] où il a synthétisé les principaux résultats obtenus soit par lui même soit par autres chercheurs (surtout par R.A. V o r o n o v [2] et G.E. P u k h o v [3]). La théorie des biportes linéaires généralisés a prouvé sa utilité dans l'étude de certains circuits électroniques [4] ou des circuits qui contiennent des générateurs Hall [5]...[7].

L'idée fondamentale se trouvant à la base de la définition d'un biporte généralisé est soutenue par l'observation qu'un tel biporte (Fig. 1 *a*) constitue une extension du celui représentant un biporte en sens *restreint* (Fig. 1 *b*), qui est caractérisé par $Z_3 \to \infty$.

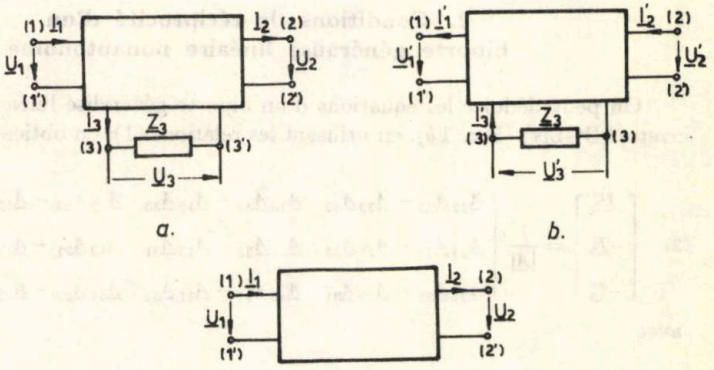

Fig. 1

Quoique dans le système d'équations:

$$(1) \qquad \begin{bmatrix} \underline{U}_1 \\ \underline{I}_1 \\ \underline{U}_3 \end{bmatrix} = \begin{bmatrix} \underline{A}_{11} & \underline{A}_{12} & \underline{A}_{13} \\ \underline{A}_{21} & \underline{A}_{22} & \underline{A}_{23} \\ \underline{A}_{31} & \underline{A}_{32} & \underline{A}_{33} \end{bmatrix} \begin{bmatrix} \underline{U}_2 \\ \underline{I}_2 \\ \underline{I}_3 \end{bmatrix},$$

qui caractérise un biporte généralisé nonautonome en régime permanent harmonique interviennent tant les signaux aux portes d'accès proprement dites, $(1) - (1')$ et $(2) - (2')$, que ceux à la porte de couplage $(3) - (3')$, il ne faut pas omettre le fait que, sous aspect logique, afin d'etablir les conditions qui assurent le caractère réciproque ou symétrique d'un tel biporte, il s'avère nécessaire à utiliser seulement les signaux aux portes d'accès (principales) sans inclure dans celles-ci et la porte de transfert (secondaire). Or, le raisonnement développé par S i g o r s k y afin d'établir soit les conditions de réciprocité, soit celles de symétrie d'un biporte généralisé, ne fait pas resortir cette distinction obligatoire entre les deux catégories de portes, de sorte que les résultats obtenus caractérisent plutot un *triporte (hexapole)* (ayant $(1) - (1')$ - porte d'entrée et $(2) - (2')$, $(3) - (3')$ - portes de sortie), qu'un biporte généralisé.

Dans ce qui suit on poursuit à établir, d'une façon correcte, les conditions de réciprocité ou de symétrie d'un biporte généralisé linéaire, en tenant compte, d'une façon systématique, que les seules portes d'accès d'un tel biporte sont $(1) - (1')$ et $(2) - (2')$. En réalité, dans la structure du biporte il y a plusieures portes de couplage (actives ou passives), la porte $(3) - (3')$ se caractérisant par la propriété de réaliser, en particulier, le couplage entre la porte d'entrée et celle de sortie.

2. Conditions de réciprocité d'un biporte généralisé linéaire nonautonome

On peut déduire les équations d'un biporte généralisé linéaire nonautonome inversé (BGLN) (Fig. 1 *b*), en utilisant les relations (1); on obtient:

$$(2) \qquad \begin{bmatrix} \underline{U}_2' \\ -\underline{I}_2' \\ -\underline{I}_3' \end{bmatrix} = \frac{1}{|\underline{A}|} \begin{bmatrix} \underline{A}_{22}\underline{A}_{33} - \underline{A}_{23}\underline{A}_{32} & \underline{A}_{13}\underline{A}_{32} - \underline{A}_{12}\underline{A}_{33} & \underline{A}_{12}\underline{A}_{23} - \underline{A}_{13}\underline{A}_{22} \\ \underline{A}_{23}\underline{A}_{31} - \underline{A}_{21}\underline{A}_{33} & \underline{A}_{11}\underline{A}_{23} - \underline{A}_{13}\underline{A}_{31} & \underline{A}_{13}\underline{A}_{21} - \underline{A}_{11}\underline{A}_{23} \\ \underline{A}_{21}\underline{A}_{32} - \underline{A}_{22}\underline{A}_{31} & \underline{A}_{12}\underline{A}_{31} - \underline{A}_{11}\underline{A}_{32} & \underline{A}_{11}\underline{A}_{22} - \underline{A}_{12}\underline{A}_{21} \end{bmatrix} \begin{bmatrix} \underline{U}_1' \\ -\underline{I}_1' \\ -\underline{U}_3' \end{bmatrix},$$

avec

$$(3) \qquad |\underline{A}| = \det[\underline{A}_{ij}], \quad (i,j = 1,2,3).$$

Afin d'établir les conditions de réciprocité d'un BGLN il este suffisant à considérer les régimes de celui-ci représentés dans la Fig. 2 et d'appliquer, dans ces cas, le théoréme de la réciprocité à savoir:

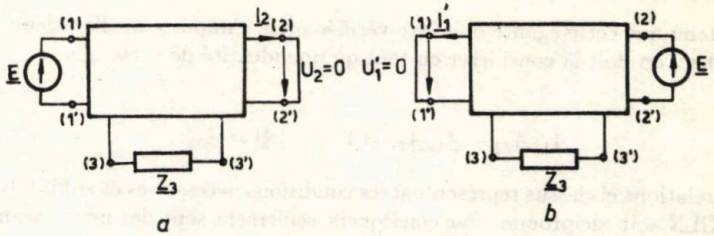

Fig. 2

$$\underline{I}_2\Big|_{\substack{\underline{U}_1=\underline{E}\\ \underline{U}_2=0}} = \underline{I}'_1\Big|_{\substack{\underline{U}'_2=\underline{E}\\ \underline{U}_1=0}}. \tag{4}$$

Si on utilise les équations (1) ainsi que la relation évidente:

$$\underline{U}_3 = \underline{Z}_3\underline{I}_3, \tag{5}$$

en admettant à l'instar de S i g o r s k y (*op.cit.*) que la branche $(3) - (3')$ est passive, il résulte:

$$\underline{I}_2\Big|_{\substack{\underline{U}_1=\underline{E}\\ \underline{U}_2=0}} = \frac{(\underline{Z}_3 - \underline{A}_{33})\underline{E}}{\underline{A}_{12}\underline{Z}_3 + \underline{A}_{13}\underline{A}_{32} - \underline{A}_{12}\underline{A}_{33}}. \tag{6}$$

Toutefois les équations (2) et la relation

$$\underline{U}'_3 = \underline{Z}_3\underline{I}'_3 \tag{7}$$

conduisent à

$$\underline{I}'_1\Big|_{\substack{\underline{U}'_2=\underline{E}\\ \underline{U}_1=0}} = \frac{(\underline{A}_{11}\underline{A}_{22} - \underline{A}_{12}\underline{A}_{21})\underline{Z} - |\underline{A}|}{\underline{A}_{12}\underline{Z}_3 + \underline{A}_{13}\underline{A}_{32} - \underline{A}_{12}\underline{A}_{33}}\underline{E}, \qquad (|\underline{A}| \neq 0). \tag{8}$$

Par susbstitution des relations (6) et (8) dans (4) il résulte:

$$\underline{Z}_3 - \underline{A}_{33} = (\underline{A}_{11}\underline{A}_{22} - \underline{A}_{12}\underline{A}_{21})\underline{Z}_3 - |\underline{A}|. \tag{9}$$

Compte tenu que cette égalité doit être vérifiée pour n'importe quelle valeur de $\underline{Z}_3$ il s'énsuit qu'on doit la considérer en tant qu'une identité de sorte que

$$\underline{A}_{11}\underline{A}_{22} - \underline{A}_{12}\underline{A}_{21} = 1, \qquad |\underline{A}| = \underline{A}_{33}. \tag{10}$$

Les relations ci-dessus représentent les conditions nécessaires et suffisantes afin qu'un BGLN soit réciproque. Par conséquent seulement sept des neuf paramètres d'un BGLN sont indépendants (et pas six, selon la voie utilisée par S i g o r s k y).

O b s e r v a t i o n. Les conditions de réciprocité (10) ont comme conséquences les relations:

$$\begin{cases} \underline{A}_{13}(\underline{A}_{21}\underline{A}_{32} - \underline{A}_{22}\underline{A}_{31}) = \underline{A}_{23}(\underline{A}_{11}\underline{A}_{32} - \underline{A}_{12}\underline{A}_{31}), \\ \underline{A}_{31}(\underline{A}_{12}\underline{A}_{23} - \underline{A}_{13}\underline{A}_{22}) = \underline{A}_{32}(\underline{A}_{11}\underline{A}_{23} - \underline{A}_{13}\underline{A}_{21}). \end{cases} \tag{11}$$

D'ailleurs on peut retrouver les conditions de réciprocité (10) par une autre voie. Si on élimine, entre les équations (1) et (5), $\underline{U}_3$, $\underline{I}_3$, il résulte le système:

$$\begin{bmatrix} \underline{U}_1 \\ \\ \underline{I}_1 \end{bmatrix} = \begin{bmatrix} \underline{A}'_{11} & \underline{A}'_{12} \\ \\ \underline{A}'_{21} & \underline{A}'_{22} \end{bmatrix} \begin{bmatrix} \underline{U}_2 \\ \\ \underline{I}_2 \end{bmatrix}, \tag{12}$$

avec

$$\begin{cases} \underline{A}'_{11} = \underline{A}_{11} + \frac{\underline{A}_{13}\underline{A}_{31}}{\underline{Z}_3 - \underline{A}_{23}}, \quad \underline{A}'_{12} = \underline{A}_{12} + \frac{\underline{A}_{13}\underline{A}_{32}}{\underline{Z}_3 - \underline{A}_{33}}, \\ \underline{A}'_{21} = \underline{A}_{21} + \frac{\underline{A}_{23}\underline{A}_{31}}{\underline{Z}_3 - \underline{A}_{33}}, \quad \underline{A}'_{22} = \underline{A}_{22} + \frac{\underline{A}_{23}\underline{A}_{32}}{\underline{Z}_3 - \underline{A}_{33}}. \end{cases} \tag{13}$$

Evidemment les équations (12) caractérisent un biporte linéaire nonautonome, au sens restreint, que l'on va denommer *biporte primitif* (BP). Celui-ci a un caractère réciproque si ses paramètres $\underline{A}'_{ij}$, $(i,j = 1,2)$, satisfont la relation bien-connue:

$$|\underline{A}'| = \underline{A}'_{11}\underline{A}'_{22} - \underline{A}'_{12}\underline{A}'_{21} = 1. \tag{14}$$

Compte tenu des expressions (13), tous calculs effectués on obtient:

$$|\underline{A}'| = \frac{(\underline{A}_{11}\underline{A}_{22} - \underline{A}_{12}\underline{A}_{21})\underline{Z}_3 - |\underline{A}|}{\underline{Z}_3 - \underline{A}_{33}}. \tag{15}$$

On constate aisément que la condition de réciprocite (14) du BP est satisfaite seulement si les paramètres $\underline{A}_{ij}$, $(i,j = 1,2,3)$, du BGLN vérifient les relations

(10) qui assurent, en même temps, le caractère réciproque de celui-ci (qui génère le BP considéré). Le résultat obtenu est naturel puisque, compte tenu de quelques considérations d'ordre physique élémentaires, si un BGLN est réciproque, alors le BP généré par celui-ci est à son tour réciproque.

Il est intéréssant à observer que dans le cas des BP nonréciproques (v. la rel. (15)) la grandeur complexe (adimensionelle) $|\underline{A}'|$ a des valeurs situées à l'intérieur ou sur la frontière d'un certain cercle si l'impédance $\underline{Z}_3$ est variable (avec $\Re e \underline{Z}_3 \geq \geq 0$).

3. Conditions de symétrie d'un biporte généralisé, linéaire, nonautonome

Dans la théorie des BGLN, élaborée par S i g o r s k y, les conditions de symétrie sont établies par rapport à certains axes analytiques (denommés axes de symétrie) [1]. Une autre possibilité d'envisager la symétrie d'un BGLN tient compte de la symétrie globale d'un BGLN ainsi qu'on a procédé dans un travail précedent [8].

Si on accepte, même dans le cas du problème étudié dans ce paragraphe, l'hypothèse concernant le rôle des trois portes (v. § **2**) à savoir, deux d'accès et la troisième de couplage, il est tout-à-fait naturel à considérer la symétrie d'un BGLN seulement par rapport aux portes d'accès proprement dites. Ainsi, il est logique à considérer qu'un tel biporte est symétrique seulement si les relations:

$$\underline{U}'_2 = \underline{U}_1, \quad \underline{I}'_2 = \underline{I}_1, \quad \underline{U}'_1 = \underline{U}_2, \quad \underline{I}'_1 = \underline{I}_2 \tag{16}$$

sont satisfaites. Dans ces conditions on réalise la symétrie d'un BGLN lorsque le BP généré par celui-ci est à son tour symétrique. Cette situation est réalisée si

$$\underline{A}'_{11} = \underline{A}'_{22}, \tag{17}$$

ou, compte tenu de (13):

$$\underline{A}_{11}\underline{Z}_3 + \underline{A}_{13}\underline{A}_{31} - \underline{A}_{11}\underline{A}_{33} = \underline{A}_{22}\underline{Z}_3 + \underline{A}_{23}\underline{A}_{32} - \underline{A}_{22}\underline{A}_{33}. \tag{18}$$

Or, vu que cette égalité doit être satisfaite pour n'importe quelle valeur de $\underline{Z}_3$ elle est, proprement dit, une identité et par conséquent:

$$\underline{A}_{11} = \underline{A}_{22}, \quad \underline{A}_{13}\underline{A}_{31} = \underline{A}_{23}\underline{A}_{32}, \tag{19}$$

conditions qui sont nécessaires et suffisantes pour assurer le caractère symétrique d'un BGLN. Par conséquent seulement sept des neuf paramètres d'un BGLN symétrique sont indépendants et si le biporte est en même temps et réciproque, le nombre des paramètres indépendants est de cinq.

Au fond, si les symétries d'un BGLN par rapport à ses axes on peut les denommer *axiales* et celle étudié en [8] – *totale*, la symétrie définie dans ce paragraphe peut être considérée comme *ordinaire*, usuelle pour un tel biporte. Il est possible à definir même une symétrie *partielle* qui est réalisée si la condition

$$\underline{I}_3\Big|_{\underline{U}_1=\underline{E}} = \underline{I}'_3\Big|_{\underline{U}'_2=\underline{E}} \tag{20}$$

est satisfaite pour n'importe quelles valeurs de l'impédance du récepteur. L'étude détaillée des conditions qui assurent la réalisation d'un tel régime fera l'objet d'un travail subséquent.

4. Exemple

On considère le BGLN passif représenté dans la Fig. 3. Ses paramètres fondamentaux sont donnés par les expressions (par ex. [1]):

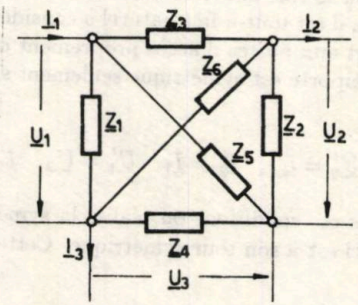

Fig. 3

$$\underline{A}_{11} = -\frac{\underline{Z}_2(\underline{Z}_3+\underline{Z}_6)(\underline{Z}_4+\underline{Z}_5)+\underline{Z}_3\underline{Z}_6(\underline{Z}_4+\underline{Z}_5)+\underline{Z}_4\underline{Z}_5(\underline{Z}_3+\underline{Z}_6)}{\underline{Z}_2(\underline{Z}_3\underline{Z}_4-\underline{Z}_5\underline{Z}_6)},$$

$$\underline{A}_{12} = -\frac{\underline{Z}_3\underline{Z}_6(\underline{Z}_4+\underline{Z}_5)+\underline{Z}_4\underline{Z}_5(\underline{Z}_3+\underline{Z}_6)}{\underline{Z}_3\underline{Z}_4-\underline{Z}_5\underline{Z}_6}, \quad \underline{A}_{13} = \frac{\underline{Z}_4\underline{Z}_5(\underline{Z}_3+\underline{Z}_6)}{\underline{Z}_3\underline{Z}_4-\underline{Z}_5\underline{Z}_6},$$

$$\underline{A}_{21} = -\frac{(\underline{Z}_4+\underline{Z}_5)[\underline{Z}_2(\underline{Z}_1+\underline{Z}_6)+\underline{Z}_3(\underline{Z}_2+\underline{Z}_6)]+\underline{Z}_1(\underline{Z}_4+\underline{Z}_6)(\underline{Z}_3+\underline{Z}_5)}{\underline{Z}_1\underline{Z}_2(\underline{Z}_3\underline{Z}_4-\underline{Z}_5\underline{Z}_6)}+$$

$$+\frac{(\underline{Z}_3+\underline{Z}_6)(\underline{Z}_4\underline{Z}_5+\underline{Z}_1\underline{Z}_2)}{\underline{Z}_1\underline{Z}_2(\underline{Z}_3\underline{Z}_4-\underline{Z}_5\underline{Z}_6)}, \tag{21}$$

$$\underline{A}_{22} = -\frac{\underline{Z}_1(\underline{Z}_3+\underline{Z}_5)(\underline{Z}_4+\underline{Z}_6)+\underline{Z}_4\underline{Z}_6(\underline{Z}_3+\underline{Z}_5)+\underline{Z}_3\underline{Z}_5(\underline{Z}_4+\underline{Z}_6)}{\underline{Z}_1(\underline{Z}_3\underline{Z}_4-\underline{Z}_5\underline{Z}_6)},$$

$$\underline{A}_{23} = \frac{\underline{Z}_4[\underline{Z}_1(\underline{Z}_3+\underline{Z}_5)+\underline{Z}_5(\underline{Z}_3+\underline{Z}_6)]}{\underline{Z}_1(\underline{Z}_3\underline{Z}_4-\underline{Z}_5\underline{Z}_6)}, \quad \underline{A}_{31} = -\frac{\underline{Z}_4[\underline{Z}_6(\underline{Z}_3+\underline{Z}_5)+\underline{Z}_2(\underline{Z}_3+\underline{Z}_6)]}{\underline{Z}_2(\underline{Z}_3\underline{Z}_4-\underline{Z}_5\underline{Z}_6)},$$

$$\underline{A}_{32} = -\frac{\underline{Z}_4\underline{Z}_6(\underline{Z}_3+\underline{Z}_5)}{\underline{Z}_3\underline{Z}_4-\underline{Z}_5\underline{Z}_6}, \quad \underline{A}_{33} = \frac{\underline{Z}_4\underline{Z}_5\underline{Z}_6}{\underline{Z}_3\underline{Z}_4-\underline{Z}_5\underline{Z}_6}.$$

Tous calculs effectués on constate aisément que les coefficients $\underline{A}_{ij}$, $(i,j = 1,2,3)$, ci-dessus, vérifient les relations de réciprocité (10).

Si le BGLN représenté dans la Fig. 3 est symétrique, ses paramètres satisfont les relations:

$$\underline{Z}_1 = \underline{Z}_2 = \underline{Z}', \quad \underline{Z}_3 = \underline{Z}_4 = \underline{Z}'', \quad \underline{Z}_5 = \underline{Z}_6 = \underline{Z}''' . \tag{22}$$

Dans ce cas:

$$\begin{aligned}
&\underline{A}_{11} = -\frac{\underline{Z}'(\underline{Z}'' + \underline{Z}''') + 2\underline{Z}''\underline{Z}'''}{\underline{Z}'(\underline{Z}'' - \underline{Z}''')}, \quad \underline{A}_{12} = -\frac{2\underline{Z}''\underline{Z}'''}{\underline{Z}'' - \underline{Z}'''}, \quad \underline{A}_{13} = \frac{\underline{Z}''\underline{Z}'''}{\underline{Z}'' - \underline{Z}'''}, \\
&\underline{A}_{21} = -\frac{(\underline{Z}' + \underline{Z}'')(\underline{Z}' + \underline{Z}''') + \underline{Z}'(\underline{Z}' + \underline{Z}'' + \underline{Z}''') + \underline{Z}''\underline{Z}'''}{\underline{Z}'^2(\underline{Z}'' - \underline{Z}''')}, \\
&\underline{A}_{22} = -\frac{\underline{Z}'(\underline{Z}'' + \underline{Z}''') + 2\underline{Z}''\underline{Z}'''}{\underline{Z}'(\underline{Z}'' - \underline{Z}''')}, \quad \underline{A}_{23} = \frac{\underline{Z}''(\underline{Z}' + \underline{Z}''')}{\underline{Z}(\underline{Z}'' - \underline{Z}''')}, \\
&\underline{A}_{31} = -\frac{\underline{Z}''(\underline{Z}' + \underline{Z}''')}{\underline{Z}'(\underline{Z}'' - \underline{Z}''')}, \quad \underline{A}_{32} = -\frac{\underline{Z}''\underline{Z}'''}{\underline{Z}'' - \underline{Z}'''}, \quad \underline{A}_{33} = \frac{\underline{Z}''\underline{Z}'''^2}{\underline{Z}''^2 - \underline{Z}'''^2}.
\end{aligned} \tag{23}$$

Même cette fois on peut vérifier rapidement que les paramètres (23) satisfont, en dehors des conditions de réciprocité (10) et celles de symétrie (19).

5. Conclusions

1. Afin de délimiter les biportes (quadripôles) généralisés linéaires nonautonomes par rapport aux triportes (hexapôles) on apporte nombre de clarifications concernant la réciprocité et la symétrie d'un tel biporte. Les conditions établies diffèrent de celles trouvées par S i g o r s k y [1].

2. On introduit la notion de biporte primitif qui s'avère utile dans l'étude des biportes généralisés.

3. On met en évidence les distinctions nécessaire à faire entre la symétrie axiale, totale et ordinaire d'un biporte généralisé linéaire nonautonome et on esquisse la possibilité de définir même une symétrie partielle d'un tel biporte.

Reçue le 8 octobre 1993

Université Technique „Gh. Asachi", Jassy,
Chaire d'Electrotechnique

BIBLIOGRAPHIE

1. S i g o r s k y V.P., *Théorie générale des quadripôles* (en russe). Ed. Acad. Sci. d'Ukr., Kiev, 1955.
2. V o r o n o v R.A., *Théorie générale des quadripôles et des multipôles* (en russe). Ed. Energ. d'Etat, Moscou, 1951.
3. P o u k h o v C.E., *Sur les bases d'un nouvelle théorie des quadripôles* (en russe). Trav. sci., Inst. Polyt. de Lvov, *5* (1949).
4. S i g o r s k y V.P., *Analyse des circuits électroniques* (en russe). Ed. d'Etat de la Litter. Techn., Kiev, 1960.
5. D o b r e S., *Ecuaţiile generatorului Hall şi schemele echivalente în cadrul teoriei cuadripolului general.* Bul. Inst. polit., Timişoara, **14 (28)**, *2*, s. Electrot., 13-18 (1979).

6. Şora C., Dobre S., *Application of the General Quadripole Theory for the Investigation of Circuits Including a Hall Generator.* Rev. Roum. Sci. Techn., Electrot. et Energ., **24**, *1*, 15-22 (1979).
7. Dobre S., *Analysis of Unidirectional Hall Generator Circuits Based on the General Quadripole Theory.* Bul. Inst. polit., Iaşi, **XXVI (XXX)**, *1-2*, s. III, 17-24 (1980).
8. Rosman H., *Über die Symmetriebedingugen eines allgemeinen nichtautonomen Vierpole in harmonischen Danerbetrieb.* Beiträge zur theoretischen Elektrotechnik, **1**, 78-89 (1988).

ASUPRA CONDIŢIILOR DE RECIPROCITATE ŞI SIMETRIE ALE UNUI DIPORT LINIAR NEAUTONOM, GENERALIZAT, ÎN REGIM PERMANENT ARMONIC

(Rezumat)

Se aduc unele precizări referitoare la condiţiile de reciprocitate şi simetrie ale diporţilor (cuadripolilor) liniari neautonomi generalizaţi cu scopul de a-i delimita pe aceştia de triporţi (hexapoli), cu care au în comun anumite elemente structurale (topologice). Stabilirea condiţiilor de reciprocitate şi simetrie ale unor astfel de diporţi este favorizată de introducerea noţiunii de diport primitiv, care se dovedeşte a fi deosebit de avantajoasă. Se fac distincţiile necesare între simetria axială, totală şi ordinară şi se schiţează posibilitatea de a defini şi o simetrie parţială a diporţilor liniari generalizaţi.

BULETINUL INSTITUTULUI POLITEHNIC DIN IAŞI
Tomul XL (XLIV), Fasc. 1–4, 1994
Secţia III
ELECTROTEHNICĂ. ENERGETICĂ. ELECTRONICĂ

D.C. 621.394

METHOD TO CALCULATE POWER SPECTRAL DENSITY OF DIGITAL FREQUENCY MODULATION WITH CORRELATED DATA SYMBOLS

BY

PAUL COTAE

1. Introduction

For FSK modulation with continuous phase (CPFSK), the instantaneous frequency is proportional with the data signals in the baseband (BB), so that in time domain, the expression of the modulated signal FSK is:

$$y(t) = A\cos[2\pi f_p t + 2\pi f_d \int_{-\infty}^{t} \sum_{i=-\infty}^{\infty} a_i h(\tau - iT)\mathrm{d}\tau], \tag{1}$$

where A is the amplitude of the carrier, $f_p = f_d \sum_i a_i h(t - iT)$ – the frequency deviation according to the carrier. The complex envelope of the modulated signal FSK is given by the relation:

$$x(t) = A\exp\left[\mathrm{j}k_F \int_{-\infty}^{t} \sum_{i=-\infty}^{\infty} a_i h(\tau - iT)\mathrm{d}\tau\right] = a\exp\varphi(t). \tag{2}$$

The phase variation of the CPFSK signal between two moments of succesive sampling on the interval $KT \leq t < (K+1)T$, is:

$$\varphi(t) = k_F \int_{-\infty}^{KT} \sum_{i=-\infty}^{\infty} a_i h(\tau - iT)\mathrm{d}\tau + k_F \int_{t}^{(K+1)T} \sum_{i=-\infty}^{\infty} a_i h(\tau - iT)\mathrm{d}\tau = \tag{3}$$

$$= \left[q(T) \sum_{i=-\infty}^{\infty} a_i + a_k q(t - KT) \right] u_T(t - KT),$$

where $k_F = 2\pi f_d$ and $q(t)$ is the integral of shaping function and is given by the relation:

$$q(t) = \begin{cases} 0, & t < 0, \\ k_F \int_0^t h(\tau)\mathrm{d}\tau, & 0 \le t \le T, \\ q(T), & t > T. \end{cases} \tag{4}$$

According to relations (3) and (4) we deduce that the complex envelope of FSK signal is:

$$x(t) = \exp\{\mathrm{j}[\varphi_k + a_k q(t - KT)]\}, \tag{5}$$

where:

$$\varphi_k = q(T) \sum_{i=-\infty}^{k-1} a_i. \tag{6}$$

2. Calculation of Power Spectral Density for *M*-ary FSK with Correlated Data Symbols

The shaping filter has the transfer function defined in the interval $[0, KT]$, and its response depends on the last K symbols emitted by the source.

We calculate the shaping function defined in a single interval and which depends on the last K symbols. For example, for $K = 2$, we have:

$$h(t, a_i) = h_0(t, a_i) u_T(t) + h_1(t - T, a_1) u_T(t - T), \tag{7}$$

$$h_K(t, a_i) = h_K(t + KT, a_i)u_T(t). \tag{8}$$

According to relations (3),...,(5) and changing the sum index in (6), it results:

$$\begin{aligned}\phi_i &= \sum_{-\infty}^{i-1} q(T, a_K) = \sum_{-\infty}^{i-1} [q_0(T, a_K) + q_1(T, a_{K-1})] = \\ &= \sum_{-\infty}^{i-1} q(2T, a_{K-1}) + q_0(T, a_{i-1}).\end{aligned} \tag{9}$$

To facilitate the calculus, the notation:

$$\exp[\mathrm{j}q(t, a_i)]u_T(t) \triangleq c(t, a_i) \tag{10}$$

is introduced and the statistical average of the above terms will be noted with:

$$m_{c,0}(t) = \overline{c_0(t, a_0)}, \tag{11}$$

taking into consideration the stationarity of the source symbols.

We consider the autocorrelation function

$$R_{c,0}(t, t') = \overline{c(t, a_0)c^*(t', a_0)}. \tag{12}$$

According to W i e n e r - K h i n č i n theorem, (12) becomes:

$$X_{c,i}(f) = \int_0^T \int_0^T R_{c,0}(t, t') \exp[-\mathrm{j}2\pi f(t - t')]\mathrm{d}t\mathrm{d}t' \tag{13}$$

and thus we can deduce the spectrum of $x(t)$ given by relation (2):

$$X(f) = \sum_{i=-\infty}^{\infty} X_{c,i}(f) \exp(-\mathrm{j}2\pi f i T). \tag{14}$$

Replacing (12) in (13) and using (14), it results:

$$\begin{aligned}X(f) &= \sum_{i=-\infty}^{\infty} \left(\int_0^T \int_0^T R_{c,0}(t, t') \exp[-\mathrm{j}2\pi f(t - t')]\mathrm{d}t\mathrm{d}t' \right) \exp(-\mathrm{j}2\pi i T) = \\ &= \sum_{i=-\infty}^{\infty} \left(\int_0^T \int_0^T \overline{c_i(t, a_i)c_i^*(t', a_i)}\mathrm{d}t\mathrm{d}t' \right) \exp(-\mathrm{j}2\pi f T).\end{aligned} \tag{15}$$

Although relation (15) is more general then the one known in the references, it can be easier turn into particular cases for signals having a partial response signal, to obtain their analytical expressions.

3. The PSD of *M*-ary FSK with Duobinary Shaping Function

According to relations (7)...(11) the transfer function of the filter to single symbol will be:

$$h(t, a_i) = a_i[h_0(t)u_T(t) + h_1(t-T)u_T(t-T)] = a_i h(t) \tag{16}$$

and in the same way:

$$q(t, a_i) = a_i q_0(t) + a_{i-1} q_1(t), \tag{17}$$

$$q(t) = K_F \int_0^T h(t) u_{2T}(t) \mathrm{d}t, \tag{18}$$

$$q_K(t) = K_F \int_0^t h_K(t') u_T(t') \mathrm{d}t'. \tag{19}$$

In the duobinary case, $h_0(t) = h_1(t) = u_T(t)$ and at the same time $q_1(t) = q_0(t) = q(t) = 2\pi f_d t$. We calculate, according to the autocorrelation function, making the mediation, first of all. From (11) it results:

$$m_c(t) = \overline{c(t, a_0)} = \frac{\sin M(\sin 2\pi f_d t)}{M \sin 2\pi f_d t}. \tag{20}$$

According to relation (12), the autocorrelation function will be:

$$\begin{aligned} R_{c,0}(t, t') &= \overline{c(t, \alpha_0) c^*(t', \alpha_0)} = \overline{\exp\{\mathrm{j}[q(t, a_0) - q(t', a_0)]\}} = \\ &= \frac{\sin^2(M \sin 2\pi f_d t)}{M^2 \sin^2(2\pi f_d t)}. \end{aligned} \tag{21}$$

In (15) the term for $i = 1$ is calculated. For this purpose it is necessary, first, to perform:

$$\begin{aligned} c_1(t, a_0) c_0(T, a_0) c_0^*(t', a_0) &= \frac{\sin M[q_1(t) + q_0(T) - q_0(t')]}{M \sin[q_1(t) + q_0(T) - q_0(t')]} = \\ &= \frac{\sin M[2\pi f_d(t + T - t')]}{M \sin[2\pi f_d(t + T - t')]}, \end{aligned} \tag{22}$$

then:

$$c_1(T, a_{-1})c_1^*(t, a_{-1}) = \frac{\sin M[q_1(T) - q_1(t')]}{M[q_1(T) - q_1(t')]}$$

and thus:

$$(24) \qquad R_{c,1}(t, t') = \frac{\sin M2\pi f_d t}{M \sin 2\pi f_d t} \cdot \frac{\sin M2\pi f_d(t + T - t')}{M \sin 2\pi f_d(t + T - t')} \cdot \frac{\sin M2\pi f_d(T - t')}{M \sin 2\pi f_d(T - t')}.$$

For $M = 2$, in Fig. 1, is represented the PSD of binary FSK with duobinary shaping function for various values of $f_d T$.

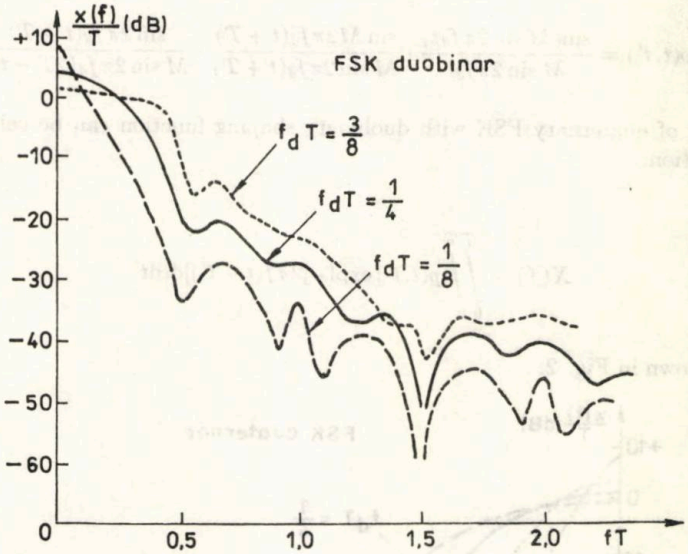

Fig. 1

For $M = 4$ and also considering the duobinary shaping function, we can also calculate the PSD of quaternary FSK. This time, the relation (10) can also be written as:

$$(25) \qquad p(t, t') = m_{c,0}(t, t')[x(t)][y(t)][z(t)],$$

where:

$$(26) \qquad x(t) = \overline{c_1(t, a_0)c_0(t', a_0)}, \qquad (27) \qquad y(t) = \overline{c_1(T, a_0)c_1^*(t', a_0)},$$

$$z(t) = \overline{c(2T, a_0)c_0^*(t', a_0)}, \tag{28}$$

but

$$c(2T, a_0)c_0^*(t', a_0) = \frac{\sin M[q(2T) - q_0(t')]}{M \sin[q(2T) - q_0(t')]} = \frac{\sin M[2\pi f_d(2T - t')]}{M \sin[2\pi f_d(2T - t')]} \tag{29}$$

and therefore:

$$p(t, t') = \frac{\sin(M \sin 2\pi f_d t)}{M \sin 2\pi f_d t} \cdot \frac{\sin M 2\pi f_d(t + T)}{M \sin 2\pi f_d(t + T)} \cdot \frac{\sin 2\pi f_d(t + T)}{M \sin 2\pi f_d(2T - t')}. \tag{30}$$

PSD of quaternary FSK with duobinary shaping function can be calculated with relation:

$$X(f) = \int_0^T \int_0^T p(t, t') \exp[-j2\pi f(t - t')] dt dt' \tag{31}$$

and is shown in Fig. 2.

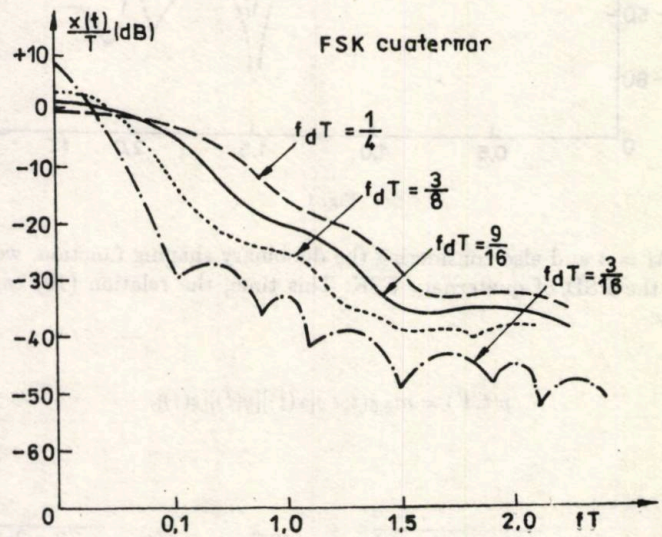

Fig. 2

4. Conclusions

The band with necessary for a data transmission system is an important factor in determination of their performances. In connection with this, is the PSD calculus of digital modulated signal. In contrast with methods proposed in the references, which makes use of quantifications for the shaping functions, we calculate a shaping function equivalent for the signals with partial response. First of all, the statistic average is made, after wich the PSD is deduced applying the W i e n e r - K h i n č i n theorem. The results are graphically plotted for the –60 dB domain.

Received, April 30, 1992

Technical University "Gh. Asachi", Jassy, Department of Communications

REFERENCES

1. A u l i n T., L i n d e l l G., S u n d b e r g C.E., *Selecting Smooting Pulses for Partial Response Digital FM.* IEEE Proc., **128**, part F, *4* (1981).
2. A u l i n T., S u n d b e r g C.E., *An Easy Way to Calculate Power Spectra for Digital FM.* IEEE Proc., **130**, part F, *6* (1983).
3. C o t a e P., *Contribuţii la îmbunătăţirea tehnicilor de modulaţie din sistemele de transmisiuni de date cu mare viteză.* Ph. D. Diss., Polyt. Inst., Bucharest, 1991.
4. C o t a e P., *Comunicaţii digitale. I. Modulaţia digitală.* Polyt. Inst., Jassy, 1992.
5. G a r r i s o n G.J., *A Power Spectral Density Analysis for Digital FM.* IEEE Trans. Commun., **COM-23**, *11*, 1228-1243 (1975).

METODĂ DE CALCUL A DENSITĂŢII SPECTRALE DE PUTERE ÎN MODULAŢIA DIGITALĂ DE FRECVENŢĂ CU SEMNALE MODULATOARE CORELATE

(Rezumat)

Se prezintă o metodă pentru calculul DSP a FSK *M*-ar care este mai generală decât cea cunoscută în literatura de specialitate, dar care prezintă avantajul unei simplităţi în cazul semnalelor cu răspuns parţial.

Se deduce expresia analitică DSP a FSK duobinar şi cuaternar şi se prezintă rezultatul obţinut sub formă grafică până în domeniul –60 dB.

BULETINUL INSTITUTULUI POLITEHNIC DIN IAŞI
Tomul XL (XLIV), Fasc. 1–4, 1994
Secţia III
ELECTROTEHNICĂ. ENERGETICĂ. ELECTRONICĂ

C.D. 621.3.025.0183

SUR LA DÉTERMINATION DE LA PUISSANCE ET DE L'ÉNERGIE HARMONIQUE ACTIVE DANS LES RÉSEAUX ÉLECTRIQUES FONCTIONNANT EN RÉGIME DÉFORMANT

PAR

ILIE POPESCU, IUSTINA ZAHARIA et CAMELIA PETRESCU

1. Introduction

Il est bien connu le fait que dans les réseaux fonctionnant en régime déformant les puissances électriques se conservent. En outre, dans la littérature on trouve des bilans concernant les puissances actives et on a établi des relations pour la détermination de la puissance active harmonique dans un réseau qui fournit l'énergie à des récepteurs nonlinéaires [2], [3].

Dans ce qui suit on poursuit la détermination des puissances et des énergies actives harmoniques dans les réseaux électriques qui alimentent des récepteurs tant linéaires que nonlinéaires, en fonctionnant à charge soit constate, soit variable.

2. Schéma électrique du réseau fonctionnant en régime déformant

On considère, dans la Fig. 1, le schéma électrique d'un réseau qui alimente par l'intermédiaire d'une station de raccord profond des récepteurs tant linéaires que nonlinéaires (la batterie de condensateurs étant connectée aux barres collectrices de moyenne tension). Toutefois on admet que la tension fournie par le système énergétique est pratiquement sinusoïdale. Par suite de la présence de l'élément nonlinéaire le réseau électrique fonctionne en régime permanent nonsinusoïdal (déformant) et, par conséquent, les courants dans le réseau, aussi que les tensions en divers points de celui-ci, ont une forme de variation nonsinusoïdale par rapport au temps.

On peut déterminer les puissances actives harmoniques pour le réseau de la Fig. 1 *a*, en se basant sur les schémas électriques équivalents des Figs. 1 *b*, 1 *c* [5] qui correspondent au bilan des puissances actives et où on a noté par: R_1 – la résistance équivalente du réseau et des transformateurs d'alimentation; R_L – la résistance équivalente du récepteur linéaire; G_1 – le générateur équivalent au système énergétique (qui fournit la puissance active à la fréquence fondamentale); Ga – le générateur d'harmoniques équivalent à l'élément nonlineaire.

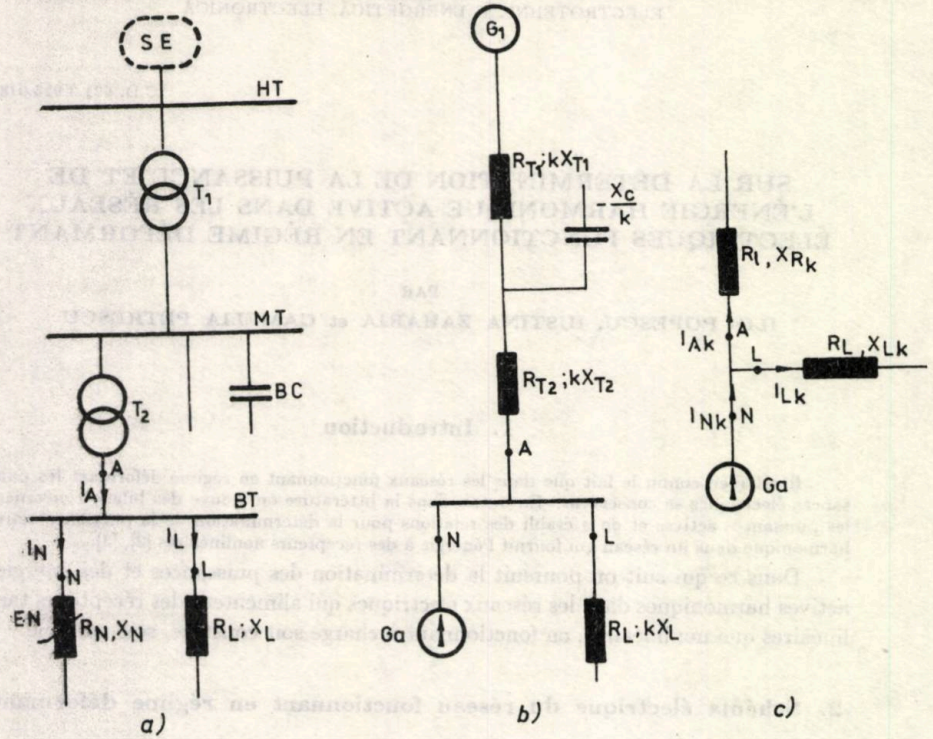

Fig. 1.– Schémas équivalentes: *a* – d'un réseau fonctionnant en régime déformant; *b* – pour les harmoniques; *c* – pour le bilan des puissances actives harmoniques.

Compte tenu que *Ga* est connecté au réseau par l'intermédiaire des transformateurs, celui-ci fournit dans le réseau la puissance active seulement par l'entremise des harmoniques et pas par celui du composant continu. Par puissance active harmonique, P_a, on définit la puissance active des harmoniques qui circulent dans une section d'un réseau électrique, dont l'expression est:

$$P_a = \sum_{k=2}^{\infty} U_k I_k \cos \varphi_k, \tag{1}$$

où: P_a – la puissance active harmonique dans chaque phase; U_k, I_k – les valeurs efficaces des harmoniques de tension et de courant; φ_k – leurs déphasages.

La puissance active totale, P, dans une section quelconque du réseau représenté dans la Fig. 1, est donnée par la somme algébrique de la puissance active harmonique, P_a, et la puissance active P_1 qui correspond à la fréquence fondamentale, c'est-à-dire:

$$P = P_1 + P_a, \tag{2}$$

où la puissance active P_a est considérée positive lorsqu'elle est absorbée et respectivement négative lorsqu'elle est fournie par la section du réseau considéré ($P > 0$, $P_1 > 0$, $P_a \gtrless 0$).

3. Détermination de la puissance et de l'énergie active harmonique

Dans ce qui suit on poursuit la détermination de la puissance et de l'énergie harmonique (P_{Aa}, W_{Aa}) échangées avec le réseau d'alimentation dans le point A où l'on mesure, d'habitude, la puissance et l'énergie active totale (P_A, W_A – Fig. 1).

Pour apprécier le régime de fonctionnement du récepteur il suffit de suivre l'évolution, en fonction de temps, dans le point A, seulement de la valeur efficace du courant I_A et du facteur de distorsion K_{IA} de celui-ci.

Les relations qui permettent à déterminer la puissance et l'énergie active harmonique dépendent du mode de fonctionnement du récepteur linéaire, respectivement nonlinéaire, en pouvant prendre en considération différentes situations possibles, les plus fréquentes étant celles présentées ci-dessous.

3.1. Récepteurs linéaires et nonlinéaires fonctionnant à charge variable

C'est le cas général lorsque les charges des récepteurs (linéaires et nonlinéaires) sont variables d'une telle façon que dans le point de mesure, A, les grandeurs K_{IA} et I_A soient variables.

La puissance active harmonique P_{Na}, fournie par le générateur d'harmoniques $Ga(EN)$ par le point N, est dissipée sur les résistances R_1, R_L (Fig. 1 *c*), à savoir:

$$P_{Na} = R_{ec} \sum_{k=2}^{\infty} I_{Nk}^2 = R_{ec} I_{Na}^2 = R_{ec} K_{NI}^2 I_N^2, \tag{3}$$

où: I_{Na} – la valeur efficace du courant harmonique généré par $GA(EN)$; K_{NI} – le facteur de distorsion du courant I_N; R_{ec} – la résistance équivalente déterminée avec la relation:

$$R_{ec} = \frac{R_1 R_L (R_1 + R_L) + K^2 (R_1 X_L^2 + R_L X_1^2)}{(R_1 + R_L)^2 + K^2 (X_1 + X_L)^2} \approx R_1 + R_L \left(\frac{X_1}{X_L} \right)^2 \tag{4}$$

dans les conditions:

$$R_1 < R_L; \quad R_1 < X_1; \quad X_1 < X_L; \quad R_L < X_L,$$

compte tenu que, pour des harmoniques rencontrés habiteullement dans les réseaux électriques, on peut admettre $kx_T \ll x_C$ [5] (s. Fig. 1 *b*).

La puissance harmonique P_{Na} qui circule par le point N est transférée tant au réseau électrique par le point $A(P_{Aa})$ qu'au récepteur linéaire par le point $L(P_{La})$. On peut déterminer les valeurs P_{Aa}, P_{La} à l'aide des expressions ci-dessous:

(5) $$P_{Aa} = \frac{R_1}{R_{ec}} P_{Na},$$ (6) $$P_{La} = \frac{R_L}{R_{ec}} \cdot \frac{X_1^2}{(X_1 + X_L)^2} P_{Na},$$

en tenant compte que dans les réseaux électriques $X_1 \ll X_L$ et par conséquent $X_L/(X_1 + X_L) \approx 1$.

On observe que la puissance active harmonique P_{Aa} dépend surtout du régime de chargement du récepteur nonlinéaire (I_N) et moins du celui linéaire (R_L), donc:

(7) $$P_{Aa} = R_1 K_{NI}^2 I_N^2 \approx P_{Na}.$$

Pour le réseau représenté dans la Fig. 1, les valeurs efficaces des courants et leurs facteurs de distorsion sont:

(8) $$I_N^2 = I_{N1}^2 + I_{NA}^2, \quad I_L \approx I_{NA}, \quad I_A^2 = I_{A1}^2 + I_{Aa}^2, \quad I_{Aa} \approx I_{Na};$$

(9) $$K_{NI} = \frac{I_{Na}}{I_N}, \qquad K_{IA} = \frac{I_{Aa}}{I_A}, \qquad K_{IL} \approx 0.$$

Compte tenu des relations (8) et (9) on obtient:

(10) $$K_{NI} I_N = K_{IA} I_A$$

et ensuite on peut exprimer la puissance active harmonique P_{Aa} par la relation:

(11) $$P_{Aa} = R_1 K_{IA}^2 I_A^2.$$

Par conséquent on peut déterminer par voie expérimentale la puissance active harmonique P_{Aa}, fournie au réseau dans le point de mesure, en utilisant un ampermètre (I_A) et un distorsiomètre (K_{IA}), connectés dans le point A si on connaît la résistance R_1.

On peut déterminer la puissance harmonique P_{Aa} même à l'aide de la relation (1) qui implique la nécessité de connaître les valeurs efficaces des harmoniques et leurs déphasages. Pour un régime de fonctionnement donné et en utilisant les relations (1) et (11), on peut déterminer la résistance équivalente R_1 du réseau d'alimentation, évidemment valable pour n'importe quel autre régime de fonctionnement.

Il en résulte que l'énergie active harmonique, W_{Aa}, fournie au réseau dans le point A, peut être déterminée à l'aide de la relation:

(12) $$W_{Aa} = \int_0^t P_{Aa} \mathrm{d}t = R_1 \int_0^t K_{IA}^2 I_A^2 \mathrm{d}t.$$

Dans ce cas, tout à fait général, on peut apprécier l'énergie harmonique W_{Aa} à l'aide de la relation (12) si l'on enregistre les courbes de variation en fonction du temps, du facteur de distorsion et du courant I_A. D'une façon pratique on peut

déterminer l'énergie harmonique fournie au réseau dans un certain intervalle de temps (par exemple 24 heures) à l'aide de la relation approximative:

$$W_{Aa} = R_1 \sum_{j=1}^{24} (K_{IAj} I_{Aj})^2, \qquad [\mathrm{W \cdot h}], \tag{13}$$

où: I_{Aj} – valeurs moyennes horaires qui correspondent aux énergies actives totales horaires; K_{IAj} – facteurs de distorsion qui correspondent aux courants I_{Aj}.

3.2. Récepteur nonlinéaire fonctionnant à une charge variable et celui linéaire à une charge constante

Ce cas correspond à la situation caractérisée par les conditions:

$$I_A,\ K_{IA},\ I_N \ - \text{ variables}; \quad I_L = \text{const.}, \quad K_{NI} = \text{const.} \tag{14}$$

La puissance active harmonique P_{Aa}, fournie au réseau dans le point A, est donnée, même dans ce cas, par la relation (7). Si l'on considère que tous les deux récepteurs fonctionnent à des facteurs de puissance dont les valeurs sont très approchées, les valeurs efficaces des courants fondamentaux satisfont la relation:

$$I_{A1} = I_{N1} + I_{I1}, \tag{15}$$

où

$$I_{A1} = I_A \sqrt{1 - K_{IA}^2}, \quad I_{L1} = I_L. \tag{16}$$

Compte tenu de (8), (15) et (16) on obtient, pour le courant I_N, l'expression:

$$I_N^2 = I_A^2 + I_L^2 - 2 I_A I_L \sqrt{1 - K_{IA}^2}. \tag{17}$$

Dans les cas assez fréquents lorsque $K_{IA} \leq 0,3$ et $I_N \approx I_A - I_L$ on peut calculer la puissance harmonique P_{Aa} à l'aide de la relation:

$$P_{Aa} = R_1 K_{NI}^2 I_N^2 \approx R_1 K_{NI}^2 (I_A - I_L)^2. \tag{18}$$

Le courant I_A, qui intervient dans cette relation, peut être mesuré par voie directe, tandis que K_{NI} et I_L, conformément à (10), peuvent être déterminés en utilisant les relations:

$$K_{NI} = K_{IA} \frac{I_A}{I_A - I_L}, \quad I_L = \left(1 - \frac{K_{iA}}{K_{Ni}}\right) I_A. \tag{19}$$

Pour satisfaire la conditions (14) K_{NI} et I_L doivent conserver des valeurs constantes pour des régimes différents de fonctionnement (K_{IA1}, I_{A1}; K_{IA2}, I_{A2}; ...) mais, d'habitude, on ne peut pas mesurer directement ces valeurs. (On effectue des

mesures seulement dans le point A). Afin de déterminer les valeures de K_{IA} et I_L et de vérifier que les conditions (14) soient satisfaites, on mesure, successivement, dans le point A, au moins trois paires de valeurs distinctes (K_{IA1}, I_{A1}; K_{IA2}, I_{A2}; K_{IA3}, I_{A3}) et à l'aide de la relation (19) on obtient trois expressions pour k_{Ni} et trois pour I_L. Si les trois valeurs obtenues sont tres approchées, alors le réseau correspond à la situation considérée dans le § **3.2** (K_{NI} = const. et I_L = const.).

Conformément à (18) on peut déterminer la puissance harmonique P_{Aa}, fournie au réseau dans le point A, si l'on effectue des mesures seulement dans ce point.

La puissance active totale, P_N, absorbée par le récepteur nonlinéaire, est donnée par:

$$P_N = P_{N1} + P_{Na}, \quad P_{Na} < 0, \tag{20}$$

où l'on a tenu compte du sens de circulation de la puissance harmonique P_{Na} par rapport à P_1.

Compte tenu que dans la plupart des réseaux électriques sont satisfaites les conditions:

$$P_{Na} \ll P_{N1};\ U_A = U_N \approx U_{N1};\ \cos\varphi_{N1} \approx \cos\varphi_N \approx \text{const.}, \tag{21}$$

on peut exprimer la puissance active P_N à l'aide de la relation:

$$P_N = U_A I_{N1} \cos\varphi_N. \tag{22}$$

Ayant en vue que:

$$I_{N1} = I_N\sqrt{1 - K_{NI}^2} \tag{23}$$

et en se basant sur (22) et (23) on obtient:

$$I_N^2 = \frac{P_N}{U_A^2(1 - K_{NI}^2)\cos^2\varphi_N}. \tag{24}$$

Si l'on introduit l'expression (24) dans (7) on peut obtenir l'expression suivante de la puissance harmonique:

$$P_{Aa} = \lambda_N P_N^2, \tag{25}$$

où le facteur λ_N est donné par la relation:

$$\lambda_N = \frac{K_{NI}^2}{1 - K_{NI}^2} \cdot \frac{R_1}{U_A^2 \cos^2\varphi_N} = \text{const.} \tag{26}$$

On peut observer que la puissance harmonique, P_{Aa}, fournie au réseau par le point A, est fonction du carré de la puissance active totale P_N. Ayant en vue qu'on ne

peut pas mesurer par voie directe la puissance P_N, on la détermine à l'aide de la relation:

$$P_N = P_A - P_L, \tag{27}$$

où

$$P_L = U_A I_L \cos \varphi_L. \tag{28}$$

On obtient ainsi l'expression de la puissance active harmonique P_{Aa} sous la forme:

$$P_{Aa} = \lambda_N (P_A - P_L)^2. \tag{29}$$

On peut exprimer l'énergie active harmonique W_{Aa}, fournie au réseau dans le point A et dans un intervalle de temps t, à l'aide de la relation:

$$W_{Aa} = \int_0^t P_{Aa} \mathrm{d}t = \lambda_N \int_0^t (P_A - P_L)^2 \mathrm{d}t, \tag{30}$$

où l'on a tenu compte de (20).

Toutefois on peut exprimer l'énergie active harmonique en fonction de l'énergie active totale W_A et de celle absorbée par le récepteur linéaire W_L. Dans ce but il est nécessaire à tenir compte de la forme de la courbe de charge $P_A(t)$ dans un certain intervalle de temps t, respectivement du coefficient de forme K_f de la courbe de charge [5] défini par:

$$K_f = \frac{P_{\text{med}\cdot p}}{P_{\text{med}}}, \tag{31}$$

où $P_{\text{med}\cdot p}$ représente la racine carrée de la moyenne quadratique de la puissance active dans l'intervalle de temps t:

$$P_{\text{med}\cdot p} = \sqrt{\frac{1}{t} \int_0^t P^2(t) \mathrm{d}t} \tag{32}$$

et

$$P_{\text{med}} = \frac{1}{t} \int_0^t P(t) \mathrm{d}t = \frac{W}{t} \tag{33}$$

– la moyenne aritmétique de la puissance active dans le même intervalle de temps.

Si l'on introduit (31), (32) et (33) dans la relation (30) on obtient:

$$W_{Aa} = \lambda_N K_f^2 \frac{W_A}{t} \left[1 - \frac{W_L}{K_f^2 W_A} \left(2 - \frac{W_L}{W_A} \right) \right], \tag{34}$$

qui permet à déterminer l'énergie active harmonique W_{Aa}, dans le cas considéré, où W_A représente l'énergie active enregistrée par le compteur placé dans le point A et W_L – l'énergie active absorbée par les récepteurs linéaires.

Dans les cas où l'on ne dispose d'aucune possibilité de mesurer par voie directe l'énergie W_L on la détermine à l'aide de la relation:

$$W_L = P_L t = U_A I_L \cos\varphi \cdot t, \quad P_L = \text{const.}, \tag{35}$$

où $I_L = \text{const.}$ est déterminé avec (19) et $\cos\varphi_L$ représente le facteur de puissance correspondant.

Si l'on introduit dans la relation (34) les notations:

$$K_W = \frac{W_L}{W_A}, \quad K_L = \frac{K_W}{K_f^2}(2 - K_W) \tag{36}$$

on obtient l'expresion de l'énergie active harmonique sous la forme:

$$W_{Aa} = W_{Aa\max}(1 - K_L), \tag{37}$$

où $W_{Aa\max}$ représente la valeur maximum de l'énergie active harmonique fournie au réseau dans le point A et donnée par:

$$W_{Aa\max} = \lambda_N K_f^2 \frac{W_A^2}{t}. \tag{38}$$

Pour les courbes de charge fréquemment rencontrées dans l'industrie on a $K_f \approx 1...1,1$ [5].

Conformément à (42) et (45), l'énergie active harmonique W_{Aa} est nulle si $K_L = 1$, ($W_A = W_L$, $K_f = 1$) et devient maximum (v.(38)) pour $K_L = 0$ ($W_L = 0$, $W_A = W_N$).

4. Exemple de calcul

En tant qu'exemple numérique on considére le cas

$$U = \sqrt{3}U_A = 6 \text{ KV}, \quad W_{At} = 3W_A = 72 \text{ MWh/24h},$$
$$\cos\varphi_N \approx \cos\varphi_L = 0,92, \quad K_f = 1,15, \quad R_1 = 0,5\ \Omega.$$

Par des mesures successives dans le point A on obtient les valeurs:

$$I_1 = 200 \text{ A}, \quad I_2 = 400 \text{ A}, \quad I_3 = 800 \text{ A}, ...$$

$$K_1 = 0,1, \quad K_2 = 0,2, \quad K_3 = 0,25, ...$$

A l'aide de (19) on détermine

$$K_{NI} = 0,3 = \text{const.}, \quad I_L = \frac{400}{3} \text{ A} = \text{const.},$$

en confirmant que le cas étudié peut être considéré du type présenté ci-dessus. En se basant sur les mesures effectuées seulement dans le point A on détermine, à l'aide de la relation (35),

l'énergie W_L absorbée par chaque phase des récepteurs linéaires triphasés pendant 24 heures, en résultant l'énergie totale:

$$W_{Lt} = 3W_L = 3U_A I_L \cos\varphi_L \cdot t = 28,34 \text{ MWh/24h}.$$

À l'aide de (26) on détermine

$$\lambda_N = 6,13 \cdot 10^{-9} \text{ W}^{-1}$$

et à l'aide de (34), l'énergie active harmonique sur phase, W_{Aa}, et puis l'énergie active harmonique totale:

$$W_{Aat} = 3W_{Aa} = 3 \cdot 102,771 = 308,3 \text{ MWh/24h},$$

ce qui représente, en pourcents:

$$W_{Aat} = 0,43W_{At} \%.$$

5. Conclusions

Conformément au bilan des puissances actives dans des circuits électriques nonlinéaires on établit des relations qui permettent à déterminer la puissance active harmonique fournie au réseau dans le cas où celui-ci alimente des récepteurs tant linéaires que nonlinéaires.

Compte tenu du régime de fonctionnement des récepteurs et des expressions des puissances actives harmoniques établies on réussit à déterminer les relations qui permettent à calculer l'énergie active harmonique fournie dans le réseau électrique.

On a poursuivi que toutes les relations proposées pour la détermination de la puissance et de l'énergie active harmonique soient exprimées seulement en fonction des grandeurs facilement mesurables à l'aide des appareils usuels (amperemètre, compteur, distorsiomètre).

La littérature de specialité n'offre pas des relations et des procédés pour la détermination concrète de l'énergie active harmonique dans des réseaux électriques qui fonctionnent en régime déformant et à des charges variables, tenant compte que l'énergie harmonique dépend essentiellement du régime variable de fonctionnement dans le point de mesure considéré.

Reçue le 29 juin 1993

Université Technique „Gh. Asachi", Jassy,
Chaire d'Electrotechnique

BIBLIOGRAPHIE

1. Ţugulea A., *Considérations concernant les effets énergétiques du régime déformant* (en roumain). Energetica, **34**, *1*, 27-31 (1986).
2. Tschappu F., *Champ et limite d'application des installations de régulation de puissance à thiristors dans l'optique de l'influence qu'elles exercent sur la mesure de l'énergie.* Rev. Landis and Gyr, **26**, *2*, 16-33 (1979).
3. Tschappu F., *Problèmes de la mesure exacte de l'énergie électrique dans les réseaux lors de la présence d'harmoniques dans le courant.* Rev. Landis and Gyr, **28**, *2*, 2-23 (1981).
4. Antoniu I.S., *Influence du régime déformant sur les conditions de mesure de la puissance et de l'énergie active.* Rapport CIGRE *301*, Paris, 4-14 juin 1958.
5. Iordănescu I. et al., *Alimentation avec de l'énergie électrique des entreprises* (en roumain). EDP, Bucureşti, 1979.

6. B ă r b u l e s c u D. et al., *Compteur pour enregistrer les pertes d'énergie active dans les réseaux électriques* (en roumain). Sess. sci. Inst. Polytechnique, Jassy, 16-17 mai 1986, s.IV, Mesures électriques, 113.

7. G e o r g e s c u Gh. et al., *Dispositif pour la mesure des pertes d'énergie active dans les réseaux électriques* (en roumain). Bul. Inst. polit., Iaşi, **XXIII (XXVII)**, *1-2*, s.III, 81 (1977).

ASUPRA DETERMINĂRII PUTERII ŞI ENERGIEI ARMONICE ACTIVE ÎN REŢELELE ELECTRICE FUNCŢIONÂND ÎN REGIM DEFORMANT

(Rezumat)

Se stabilesc relaţiile care permit determinarea puterii şi energiei active transmise pe armonici într-o reţea electrică ce alimentează simultan receptoare liniare şi neliniare care funcţionează la sarcină fie constantă, fie variabilă. Se determină energia armonică activă cu ajutorul câtorva măsurători simple efectuate doar în punctul de racord al staţiei electrice la reţeaua de alimentare.

BULETINUL INSTITUTULUI POLITEHNIC DIN IAŞI
Tomul XL (XLIV), Fasc. 1–4, 1994
Secţia III
ELECTROTEHNICĂ. ENERGETICĂ. ELECTRONICĂ

D.C. 621.3.088.6

INCREASING OF THE SAFETY IN THE WORKING OF THE ELECTRONIC DEVICES USING A SINGLE-ERROR CORRECTING LINEAR BLOCK CODE (I)

BY

VALERIU MUNTEANU, M. LUCANU and DANIELA TARNICERIU

1. Introduction

In many practical purposes, various electronic devices (thyristors, transistors, etc.) within an electrical circuit must be driven in time according to a certain program. For instance, in the scheme of any inverter there are some main thyristors that must be controlled for direct conduction in certain time intervals during a working period and some auxiliary thyristors that must be controlled in other time intervals, to get the reversed commutation of the main thyristors [5], [7].

In the most modern control systems there is a central computer that provides the proper commands for the electronic devices contained within various electronic circuits, placed in various places.

One marks a logical "1" the command for the conduction of an electronic device, and a logical "0" for its absence. If there are k electronic devices in an electrical circuit, at a certain moment of time, the computer must provide a sequence of k binary symbols, which are transmitted by the computer at a certain distance to the place where that circuit is. The sequence of the k binary symbols will be called information word. In a working cycle at discrete time moments t_1, $t_2, ..., t_p$, the computer will send p information words, according to the working program of that electrical circuit, afterwards the commands are repeated.

The information word provided by the computer may arrive erroneously to the electrical circuit, i.e.: a "1" might turn into a "0", or inversely a "0" into a "1", which could lead either to a disordered working, or, worse, to damages.

In principle, to eliminate this disadvantage, error-correcting codes should be used. So, the computer will provide a code-word which is supposed to contain besides the k information symbols dedicated to the electronic device drive, some other m binary symbols, called parity-check symbols, so that k or fewer errors, that might appear on the way from the computer to the electronic circuit, could be corrected. Since the electrical circuits mostly used in applications contain at least three electronic devices that must be driven to correct all possible errors, it would take on at least three-errors-correcting code. The implementing of a many-error-correcting decoder, that can correct a great number of errors, is very complex, unjustified economically comparing to other classical protection methods [7].

In this paper we propose a method of driving the electronic devices in any electrical circuit, so that it results in one of the p correct information words, dis-

regarding the error number that have occurred in the transmission process, from computer to electrical circuit and in addition using a minimum of components. To achieve this goal we will use a single-error-correcting linear block code [1],...,[4], [6], for which the decoder implementing is very simple, therefore economical.

2. Theoretical Fundament of the Method

We suppose an electrical circuit containing k electronic devices that must be controlled in a working cycle at the discrete time moments $t_1, t_2, ..., t_p$. The number of information words that can be formed of k binary symbols is 2^k. From the 2^k possible information words we choose p information words ($p \leq 2^k$), according to the program of correct working of the circuit.

To achieve a single-error-correcting linear block code it takes a number of parity-check symbols, m, determined by the relation [1], [6]:

$$2^m \geq m + k + 1. \tag{1}$$

In relation (1) one chooses the least positive integer, m. We construct then the parity-check matrix [1]:

$$[H] = [h_1 \; h_2 \; ... \; h_n], \tag{2}$$

where:

$$n = m + k. \tag{3}$$

The columns h_i, $(i = 1, ..., n)$, are m-binary component vectors, representing the transcription of the decimal number $i = 1, ..., n$ [1].

The codeword will have the following form:

$$[v] = [c_1 \; c_2 \; i_3 \; c_4 \; i_5 \; i_6 \; i_7 \; c_8 \; i_9 ... i_n], \tag{4}$$

where c_i are parity-check symbols and i_j – information symbols.

The parity-check symbols c_i are determinated by the classical relation [1],...,[4]:

$$[H][v]^{\mathrm{T}} = [0], \tag{5}$$

where $[v]^{\mathrm{T}}$ is the transposed of the matrix $[v]$.

If in the transmission process, from computer to electrical circuit, e errors have occurred, they may be characterized by the error word (error pattern):

$$[\epsilon] = [...\alpha_{i_1}...\alpha_{i_2}...\alpha_{i_e}...], \tag{6}$$

where:

$$\alpha_{i_1} = \cdots = \alpha_{i_2} = \cdots = \alpha_{i_e} = 1, \tag{7}$$

specifying that on the positions $i_1, ..., i_2, ..., i_e = 1$ errors have been introduced.

The erroneous word arriving to the electrical circuit has the following form:

$$[v_e] = [v] \oplus [\epsilon] \tag{8}$$

where $\oplus$ represents mod 2 sum.

The associated syndrome of the received-word is calculated by the relation:

$$[Z] = [H][v_e]^{\mathrm{T}}. \tag{9}$$

In case of a single-error-correcting linear block code, the decoder will contain a binary-decimal decoder and a shift register of n storage devices, where the symbols of the word that arrived the electrical circuit would be stored. The binary-decimal decoder is a combinational circuit that will have m inputs corresponding to the components of the syndrome $[Z]$ and n outputs.

The binary-decimal decoder will be so synthesized that a logical "1" should result only on the i output, representing the decimal transcription of syndrome's components. The remaining outputs stay on logical "0". By mod 2 summing of the logical "1" of the i binary-decimal decoder output and the symbol on the i position in the erroneous word $[v_e]$, a new word will result, denoted by $[v_e]$. Two new properties of the decoder of a single-error-correcting linear block code will be proved.

T h e o r e m. *The decoder of a linear-block-code, implemented for a single-error-correcting code will provide at its output a code-word irrespective of the number of errors in the received word if this one's syndrome coincides with one of the columns of the parity-check matrix.*

P r o o f. Substituting the relation (8) in (9) and considering relations (5),...,(7), it results:

$$[Z] = h_{i_1} \oplus \cdots \oplus h_{i_2} \oplus \cdots \oplus h_{i_e}, \tag{10}$$

where h_{i_1}, $h_{i_2}, ..., h_{i_e}$ are e distinct columns in the parity-check matrix.

If $[Z] = [0]$, it means that in the transmission process either no errors have been introduced, or the $e \leq n$ errors have transformed the transmitted code-word into other one.

In this case, the binary-decimal decoder will have all outputs on logical "0", and leave unmodified the received word, which is a code-word.

If $[Z] \neq [0]$, let us suppose that:

$$h_{i_1} \oplus \cdots \oplus h_{i_2} \oplus \cdots \oplus h_{i_e} = h_i \neq [0], \quad i \leq n. \tag{11}$$

In this case on the i output of the binary-decimal decoder, a logical "1" will result, which will invert the binary-symbol on the i position of the received word $[v_e]$. So, the decoder will provide at the output, the word:

$$[v_c] = [v_e] \oplus [...\alpha_i...], \quad i \leq n, \tag{12}$$

where $\alpha_i = 1$ specifies the modification of the i position symbol.

The syndrome of the decoder provided $[v_e]$ word, calculated by relation (12), is:

$$[Z] = h_{i_1} \oplus \cdots \oplus h_{i_2} \oplus \cdots \oplus h_{i_e} \oplus h_i = [0], \quad i \leq n. \tag{13}$$

It means that the decoder provides in this case also a code-word.

C o r o l l a r y. *The code-word provided out for the decoder of a single-error-correcting linear block code is at the minimum H a m m i n g distance from the received word.*

P r o o f. If $e \leq n$ errors have occurred in the received word, and the received-word syndrome is zero, all the outputs of the binary-decimal decoder are zero, so leaving unmodified the received-word.

Thus:

$$d(v_e, v_e) = 0, \tag{14}$$

where $d(.)$ denotes the H a m m i n g distance [1].

If the syndrome of the received-word is nonzero there could occur two situations:

a) $i \neq i_1, ..., i_2, ..., i_e$ and $i \leq n$. In this case, the binary decimal decoder will invert a correct symbol in the received-word $[v_e]$, thus resulting the code-word $[v_c]$, which has an incoincidence on the i position from the received word, therefore:

$$d(v_e, v_c) = 1; \tag{15}$$

b) i equals one of the $i_1, ..., i_2, ..., i_e$ numbers. In this case, the binary-decimal decoder will invert an erroneous symbol of the received word, resulting the code-word $[v_c]$ which has an incoincidence from the $[v_e]$ on the i position. The relation (15) is true in this case also.

From relations (14) and (15) it follows:

$$d(v_e, v_c) \leq 1. \tag{16}$$

On the other hand, according to the theorem, the decoder will provide always a code word $[v_c]$.

In order to correct a single error, the H a m m i n g distance between the code-words must satisfy the relation [1],...,[4]:

$$d(v_j, v_c) \geq 3, \tag{17}$$

where $[v_j]$ is any code-word, and $[v_j] \neq [v_c]$. But:

$$d(v_j, v_e) \geq d(v_j, v_c) - d(v_c, v_e), \quad [v_j] \neq [v_c]. \tag{18}$$

Taking (16) and (17) into account, relation (18) becomes:

$$d(v_j, v_e) \geq 2. \tag{19}$$

Comparing (16) to (19), the corollary results.

3. Conclusions

A method of protecting the electronic devices to any electrical circuit driven by a certain program and submitted to disturbances is presented. The disturbances may lead to an undesired command of the electronic devices, causing either a malfunction, or damages by destroying the electronic devices.

On the basis of a property of single-error-correcting linear block codes the possibility of a false command is significantly diminished, using to this purpose a supplementary equipment much more reduced than other classical protection schemes.

The protection is ensured against no matter how great number of errors that could occur in a command sequence even so the complexity of the protection scheme does not exceed the complexity of a single-error-correcting linear block codes.

Received, October 7, 1993

Technical University "Gh.Asachi", Jassy,
Department of Electronics

REFERENCES

1. Hamming R.W., *Error-Detecting and Error-Correcting Codes.* Bell System Tech. J., **29**, 147-160 (1950).
2. Berlekamp E.R., *Algebraic Coding Theory.* McGraw-Hill Book Company, New York, 1968.
3. Gallager R.G., *Information Theory and Reliable Communication.* John Wiley and Sons, New York, 1968.
4. Peterson W.W., Weldom E.J.Jr., *Error Correcting Codes.* The MIT Press, Massachusetts, 1972.
5. Lucanu T.M., *Industrial Electronic* (in Romanian). Polyt. Inst., Iaşi, 1980.
6. Munteanu B.V., *Theory of Information Transmission* (in Romanian). Polyt. Inst., Iaşi, 1979.
7. Bose B.K., *Microcomputer Control of Power Electronics and Drives.* IEEE Press, New York, 1987.

CREŞTEREA SIGURANŢEI ÎN FUNCŢIONAREA DISPOZITIVELOR ELECTRONICE PRIN FOLOSIREA UNUI COD BLOC LINIAR CORECTOR DE O EROARE

(Rezumat)

Se prezintă două noi proprietăţi ale codurilor bloc liniare corectoare de o eroare. Pe baza acestor proprietăţi este prezentată fundamentarea teoretică a metodei, prin intermediul căreia pot fi comandate dispozitive dintr-un circuit electric, supus perturbaţiilor, care pot cauza un număr nedefinit de erori în secvenţa de comandă.

BULETINUL INSTITUTULUI POLITEHNIC DIN IAŞI
Tomul XL (XLIV), Fasc. 1–4, 1994
Secţia III
ELECTROTEHNICĂ. ENERGETICĂ. ELECTRONICĂ

C.D. 621.3.018.6

SUR LES CONDITIONS D'APPARITION DES OSCILLATIONS MÉCANIQUES DANS UN SYSTÈME ÉLECTROMECANIQUE

I. ÉTABLISSEMENT DES ÉQUATIONS DU MOUVEMENT

PAR
MARIANA BUZDUGA

1. Introduction

Dans un système électromécanique composé par un circuit électrique de I-er ordre (Fig. 1) contenant une diode Tunnel, un générateur de tension constante, E, une résistance linéaire, l'enroulement d'un miliampèremètre magnétoélectrique et le système électromécanique de l'instrument de mesure (Fig. 2) ayant comme paramètres caractéristiques: J – le moment d'inertie, Φ_0 – le flux magnétique de l'aimant permanent, B – le coefficient d'amortissement et C – la constante élastique du ressort, dans certaines conditions, partiellement precisées en [1], on peut constater l'apparition des oscillations de basse fréquence du cadre de l'instrument.

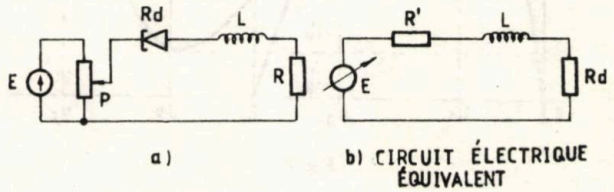

Fig. 1

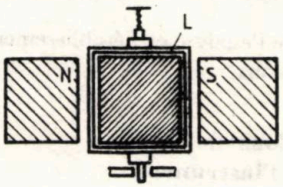

Fig. 2

On peut établir les équations d'évolution du système soit par l'évaluation du bilan énergétique du système hybride [2] soit, dans le cadre de la théorie unitaire des systèmes hybrides, par l'utilisation des équations de L a g r a n g e du deuxième ordre ou du principe variationnel [3].

L'équation du sous-système électrique résulte de la forme [1]:

$$E = Ri + u(i) + N\Phi_0 \frac{d\alpha}{dt} + L\frac{di}{dt}, \tag{1}$$

car $dL/d\alpha = 0$ (le mécanisme magnétoélectrique ayant une distribution constante du champ dans l'entrefer) et, pour le système mécanique, de la forme [1]:

$$J\frac{d^2\alpha}{dt^2} + B\frac{d\alpha}{dt} + C\alpha = N\Phi_0 i, \tag{2}$$

où α représente le déplacement angulaire de l'enroulement cadre de l'instrument magnétoélectrique.

Il est possible que des oscillations électriques apparaissent dans le circuit électrique quand la résistance R' du circuit est plus petite que la pente de la caractéristique de la diode Tunnel sur la portion de pente négative et l'intersection de la droite de charge avec la caractéristique en N est située dans cette zone (Fig. 3) [1].

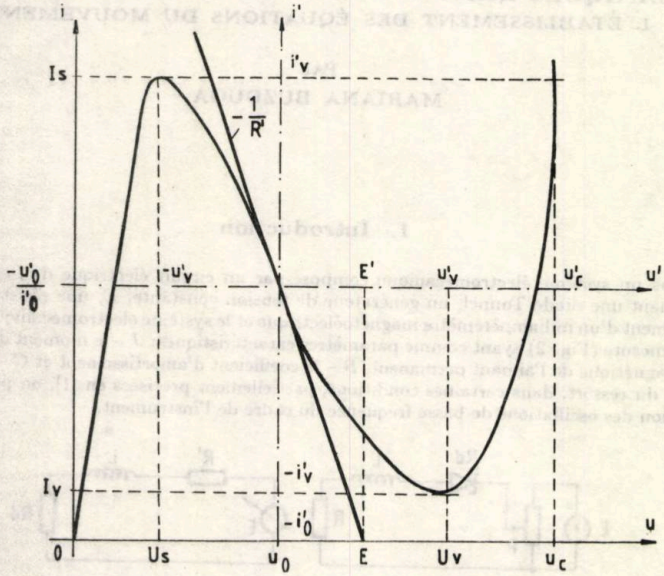

Fig. 3

En [1] on démontre aussi la possibilité d'apparition des oscillations mécaniques dans un système hybride, dues aux phénomènes de conversion de l'énergie par le système électromécanique de liaison.

Dans ce qui suit on essaye l'approfondissement de l'analyse et l'établissement des conditions qui assurent l'apparition de ces oscillations.

2. Établissement des équations de mouvement du cadre mobile de l'instrument

L'approximation analytique usuelle utilisée pour des caractéristiques nonlinéaires en N est exprimée par un polynôme incomplet de troisième degré, à condition que l'origine du système de coordonnées soit située aux centre de la zone à pente négative.

Pour une diode Tunnel caractérisée par (U_s, I_s), (U_v, I_v), l'origine des axes de coordonnées doit être translée dans le point $O'(u_0, i_0)$, avec:

$$u_0 = \frac{1}{2}(U_s + U_v), \quad i_0 = \frac{1}{2}(I_s + I_v). \tag{3}$$

Dorénavant les coordonnées rapportées au nouveau système d'axes seront notées avec l'indice ($'$).

Les coefficients a_1, a_3 du polynôme d'approximation de la caractéristique $i'(u')$ de la diode Tunnel:

$$i'(u') = -a_1 u' + a_3 u'^3, \tag{4}$$

sont en relation directe avec les paramètres concrets de la diode.

On peut aisément déduire que:

$$a_1 = \frac{3}{2|R_d|}, \tag{5}$$

où

$$|R_d| = \frac{U_v + U_s}{I_s - I_v} = \frac{u'_v}{i'_v} \tag{6}$$

'est le module de la pente moyenne de la portion descendante de la caractéristique et

$$a_3 = \frac{i'_v}{2u'^3_v}, \tag{7}$$

les extrêmes de la fonction étant situés à $u'_M = -u'_v$, respectivement $u'_m = u'_v$, ayant les valeurs $i'_M = i'_v$, $i'_m = -i'_v$.

Pour obtenir des oscillations électriques la droite de charge du circuit doit intersecter la caractéristique de la diode dans la zone de pente négative (R_d) et la résistance R' du circuit extérieur à la diode Tunnel (constituée par la résistance de l'enroulement cadre de l'instrument et la résistance interne de la source E) doit respecter la condition:

$$R_c + R = R' < |R_d|. \tag{8}$$

Dans le cas du système concret étudié, par le choix du point de fonctionnement en O', en tenant compte des équations du régime permanent, on peut négliger $L_c \mathrm{d}i'/\mathrm{d}t$ (qui représente la tension d'autoinduction) par rapport à $N\Phi_0 \mathrm{d}\alpha'/\mathrm{d}t$, qui représente la tension induite dans le cadre, due au mouvement dans le champ magnétique de l'aimant permanent, car

$$N\Phi_0 \frac{\mathrm{d}\alpha'}{\mathrm{d}t} = N\Phi_0 \frac{\mathrm{d}\alpha'}{\mathrm{d}i'} \cdot \frac{\mathrm{d}i'}{\mathrm{d}t}, \tag{9}$$

où $\mathrm{d}\alpha'/\mathrm{d}i' = \text{const.} = S$ représente la sensibilité de l'instrument magnétoélectrique et

$$N\Phi_0 S \gg L_c. \tag{10}$$

Pour les deux sous-systèmes, électrique et électromagnétique, on peut écrire les équations qui caractérisent le comportement du système de conversion électromécanique:

$$R'i' + u' + N\Phi_0 \frac{\mathrm{d}\alpha'}{\mathrm{d}t} = 0 \quad \text{et} \tag{11}$$

$$J\frac{\mathrm{d}^2\alpha'}{\mathrm{d}t^2} + B\frac{\mathrm{d}\alpha'}{\mathrm{d}t} + C\alpha' = N\Phi_0 i'. \tag{12}$$

Si on introduit en (11) la relation (4) il en résulte:

$$\frac{\mathrm{d}\alpha'}{\mathrm{d}t} = -\frac{1}{N\Phi_0}\left[(1 - R'a_1)u' + R'a_3 u'^3\right], \tag{13}$$

ou

$$\frac{\mathrm{d}\alpha'}{\mathrm{d}t} = -A'u' - B'u'^3. \tag{14}$$

On poursuit à trouver la fonction inverse $u' = f(\mathrm{d}\alpha'/\mathrm{d}t)$ pour obtenir une équation différentielle en α' capable à decrire le mouvement du cadre de l'instrument.

En respectant la condition (4) et en tenant compte de (5) on a:

$$|R'a_1| < \frac{3}{2}. \tag{15}$$

Pour $R' \in (0, R_d)$ le coefficient B' est positif et A' a des valeurs positives et négatives fonction exclusivement de la résistance du circuit extérieur à la diode.

On observe que pour $R' \in (0,\ 2|R_d|/3]$, $A' \geq 0$ et $A' \in [0,\ 1/N\Phi_0)$ tandis que pour $R' \in (2|R_d|/3,\ R_d)$, $A' < 0$ et $A' \in (-1/2N\Phi_0,\ 0)$.

2.1. Le cas $A' \geq 0$, équivalent à $R' \in (0,\ 2|R_d|/3]$

De l'analyse de la fonction $\mathrm{d}\alpha'/\mathrm{d}t = f(u')$, donnée par les relations (13) et (14), on constate que la fonction est strictement monotone et a un point d'inflexion en O'. En conséquence la fonction admet une inverse dans tout le domaine des valeurs de u', qui conformément aux formules de C a r d a n, a la forme:

$$u' = \sqrt[3]{-F + \sqrt{F^2 + G^3}} + \sqrt[3]{-F - \sqrt{F^2 + G^3}}, \tag{16}$$

où on a utilisé les notations:

$$\frac{1}{B'} \cdot \frac{\mathrm{d}\alpha'}{\mathrm{d}t} = F, \quad \frac{A'}{3B'} = G. \tag{17}$$

De la relation (11) il résulte:

$$i' = -\frac{1}{R'}\left(N\Phi_0 \frac{d\alpha'}{dt} + u'\right), \tag{18}$$

qui, substituée en (12) et compte tenu de (16), conduit à:

$$J\frac{d^2\alpha}{dt^2} + B\frac{d\alpha'}{dt} + C\alpha' = -\frac{N\Phi_0}{R'}\left(N\Phi_0\frac{d\alpha'}{dt} + \sqrt[3]{-F + \sqrt{F^2+G^3}} + \sqrt[3]{-F - \sqrt{F^2+G^3}}\right). \tag{19}$$

On obtient, donc, une équation différentielle du second ordre, de la forme:

$$J\frac{d^2\alpha'}{dt^2} + f\left(\frac{d\alpha'}{dt}\right) + C\alpha' = 0. \tag{20}$$

Cette équation doit être étudiée du point de vue de la stabilité, c'est-à-dire, de la possibilité d'existance des oscillations mécaniques.

On utilise souvent pour l'approximation de l'inverse de la fonction (17) une zone limitée de la fonction:

$$Y = -Px + Qx^3, \tag{21}$$

solution adoptée en [1].

2.2. Le cas $A' < 0$, équivalent à $R' \in (2|R_d|/3,\ |R_d|)$

De l'analyse de la fonction (13) il résulte l'existence des zéros à $u' = 0$ et $u' = \pm\sqrt{|A'|/B'}$, des extrêmes à $u' = \pm\sqrt{|A'|/3B'}$ et d'un point d'inflexion à $u' = 0$. Donc, la fonction, n'étant pas bijective n'admet pas d'inverse sur l'axe réele.

On est intéressé à connaître le comportement de la fonction dans les domaines concrets de variation de la variable u', pour déterminer les domaines de monotonie et les fonctions inverses qui correspondent à ces domaines. Il est donc nécessaire de tester si les extrêmes de la fonction (13) sont situés à l'intérieur de l'intervalle de variation de u'.

La tension u aux bornes de la diode Tunnel peut prendre des valeurs situées entre zero et E, dans le cas où il n'y a pas d'oscillations dans le circuit, respectif entre zero et u_c (Fig. 3) quand il y en a [4]. En conséquence la tension u' a des valeurs situées entre $-u'_0$ et $E' = E - u'_0$, respectivement $-u'_0$ et u'_0.

Pour le cas le plus restrictif, quand $u' \in (-u'_0,\ E')$, en considérant, conformément à l'hypothèse, que le point de travail est situé en O', on détermine la valeur de E' (qui à son tour dépend de R'):

$$E' = R'i_0. \tag{22}$$

Compte tenu de (3), il résulte:

$$(23)\qquad i'_v = i_0 - I_v = \frac{I_s - I_v}{2} \qquad \text{et} \qquad (24)\qquad u'_v = |R_d| i'_v = |R_d| \frac{I_s - I_v}{2}.$$

En rapportant (23) à (21) on obtient:

$$(25)\qquad \frac{u'_v}{E'} = \frac{|R_d| i_v}{R' i_0} = \frac{|R_d|}{R'} \cdot \frac{1 - I_v/I_s}{1 + I_v/I_s}.$$

Le cas le plus restrictif est obtenu pour la valeur minimum de E':

$$(26)\qquad E'(R'_{\min}) = E'\left(\frac{2}{3}|R_d|\right) = \frac{2}{3} u'_v \frac{1 + I_v/I_s}{1 - I_v/I_s} = \frac{2}{3} u'_v m,$$

avec

$$(27)\qquad m = \frac{1 + I_v/I_s}{1 - I_v/I_s} > 1,$$

coefficient surunitaire dont la valeur dépend de la diode utilisée. La position des extrêmes de la fonction $d\alpha'(u')/dt$ dépend aussi de la valeur de R', car les coefficients A', B' sont fonctions de R'. Il résulte:

$$(28)\qquad u' = \pm\sqrt{\frac{|A'|}{3B'}} = \pm u'_v \sqrt{1 - \frac{2}{3} \cdot \frac{|R_d|}{R'}}.$$

Si $R' \to 2|R_d|/3$ les extrêmes s'approchent vers O' et pour $R' \to |R_d|$ leurs positions s'éloignent jusqu'à:

$$(29)\qquad \lim_{R' \to |R_d|} \left(\pm\sqrt{\frac{|A'|}{3B'}}\right) = \frac{u'_v}{\sqrt{3}} < u'_v.$$

Afin que les extrêmes situés à $\pm u'_v/\sqrt{3}$ puissent être en dehors du domaine de variation de u' il faut que:

$$(30)\qquad E'_{\min} \leq \frac{u'_v}{\sqrt{3}},$$

c'est-à-dire

$$(31)\qquad m \leq \frac{\sqrt{3}}{2}.$$

Compte tenu que m est surunitaire, il résulte que la condition (29) n'est pas respectée, donc les extrêmes de la fonction (13) sont situés toujours à l'intérieur du domaine de variation de u'. En conséquence, dans l'intervalle respectif il y

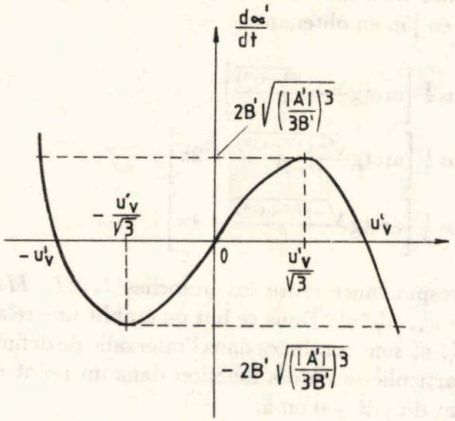

Fig. 4

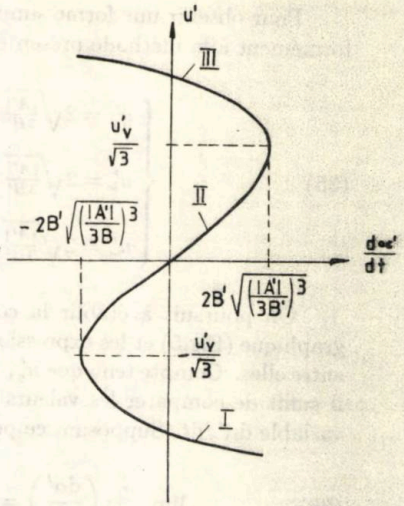

Fig. 5

a trois domaines de monotonie de la fonction (13), où elle admet des inverses. Conformément aux formules de C a r d a n, elles sont:

$$(32)\qquad \begin{cases} u'_1 = \sqrt[3]{-F+\sqrt{F^2+G^3}} + \sqrt[3]{-F-\sqrt{F^2+G^3}}, \\ u'_2 = \varepsilon\sqrt[3]{-F+\sqrt{F^2+G^3}} + \varepsilon^2\sqrt[3]{-F-\sqrt{F^2+G^3}}, \\ u'_3 = \varepsilon^2\sqrt[3]{-F+\sqrt{F^2+G^3}} + \varepsilon\sqrt[3]{-F-\sqrt{F^2+G^3}}, \end{cases}$$

où ε est la racine cubique primitive de l'unité:

$$(33)\qquad \varepsilon^2+\varepsilon+1=0$$

c'est-à-dire

$$\varepsilon_1 = \frac{-1+\mathrm{i}\sqrt{3}}{2} = \cos\frac{2\pi}{3}+\mathrm{i}\sin\frac{2\pi}{3}, \quad \varepsilon_2 = \frac{-1-\mathrm{i}\sqrt{3}}{2} = \cos\frac{4\pi}{3}+\mathrm{i}\sin\frac{4\pi}{3}.$$

Le discriminant $D = F^2+G^3$ étant négatif, car

$$(34)\qquad \left|\frac{\mathrm{d}\alpha'}{\mathrm{d}t}\right| \leq 2B'\sqrt{\left(\frac{|A'|}{3B'}\right)^3},$$

toutes les trois solutions u'_1, u'_2, u'_3 sont réeles.

Dans les Fig.4 et 5 on a représenté les graphiques de la fonction $\mathrm{d}\alpha'/\mathrm{d}t$ et des inverses respectives dans ces domaines.

Pour obtenir une forme simplifiée on transforme les solutions u'_1, u'_2, u'_3 conformément à la méthode présentée en [5], en obtenant:

$$(35)\qquad \begin{cases} u'_a = 2\sqrt{\frac{|A'|}{3B'}}\cos\frac{1}{3}\left[\operatorname{arctg}\frac{\sqrt{-(F^2+G^3)}}{-F}\right], \\ u'_b = 2\sqrt{\frac{|A'|}{3B'}}\cos\frac{1}{3}\left[\operatorname{arctg}\frac{\sqrt{-(F^2+G^3)}}{-F}+2\pi\right], \\ u'_c = 2\sqrt{\frac{|A'|}{3B'}}\cos\frac{1}{3}\left[\operatorname{arctg}\frac{\sqrt{-(F^2+G^3)}}{-F}+4\pi\right]. \end{cases}$$

On poursuit à établir la correspondance entre les branches I, II, III du graphique (Fig.5) et les expressions u'_a, u'_b, u'_c. Dans ce but on établit une rélation entre elles. Compte tenu que u'_a, u'_b, u'_c sont continues dans l'intervalle de définition il suffit de comparer les valeurs particulières de ces fonction dans un point de la variable $\mathrm{d}\alpha'/\mathrm{d}t$. Supposant ce point $\mathrm{d}\alpha'/\mathrm{d}t = 0$ on a:

$$(36)\qquad \lim_{\mathrm{d}\alpha'/\mathrm{d}t\nearrow 0}\varphi\left(\frac{\mathrm{d}\alpha'}{\mathrm{d}t}\right) = \lim_{\mathrm{d}\alpha'/\mathrm{d}t\searrow 0}\left[\operatorname{arctg}\frac{\sqrt{-(F^2+G^3)}}{-F}\right] = \frac{\pi}{2},$$

car le numérateur est toujours positif quelque soit $\mathrm{d}\alpha'/\mathrm{d}t$. Alors:

$$(37)\qquad \begin{cases} u'_a(0) = 2\sqrt{\frac{|A'|}{3B'}}\cos\frac{\pi}{6} = \sqrt{\frac{|A'|}{B'}}, \\ u'_b(0) = 2\sqrt{\frac{|A'|}{3B'}}\cos\left(\frac{\pi}{6}+\frac{2\pi}{3}\right) = -\sqrt{\frac{|A'|}{B'}}, \\ u'_c(0) = 2\sqrt{\frac{|A'|}{3B'}}\cos\left(\frac{\pi}{6}+\frac{4\pi}{3}\right) = 0. \end{cases}$$

En conclusion l'expression analytique de la branche I du graphique de la fonction inverse (Fig.5) est u'_b, celle de la branche II est u'_c et celle de la branche III est u'_a.

Les fonctions u'_a, u'_b, u'_c sont définies pour le même domaine de variation de $\mathrm{d}\alpha'/\mathrm{d}t$ à savoir:

$$(38)\qquad \frac{\mathrm{d}\alpha'}{\mathrm{d}t} \in \left[-2B'\sqrt{G^3},\ 2B'\sqrt{G^3}\right].$$

Dans les extrémités de l'intervalle on a:

$$(39)\qquad \lim_{\mathrm{d}\alpha'/\mathrm{d}t\to -2B'\sqrt{|G|^3}} u'_c = \lim_{\mathrm{d}\alpha'/\mathrm{d}t\to -2B'\sqrt{|G|^3}} u'_b = -\frac{u'_v}{\sqrt{3}},$$

$$(40)\qquad \lim_{\mathrm{d}\alpha'/\mathrm{d}t\to 2B'\sqrt{|G|^3}} u'_c = \lim_{\mathrm{d}\alpha'/\mathrm{d}t\to 2B'\sqrt{|G|^3}} u'_a = \frac{u'_v}{\sqrt{3}}.$$

Pour les domaines de variation de u' situés en dehors des limites $\pm 2u'_v/\sqrt{3}$, c'est-à-dire:

$$u' \in \left[-2u'_v,\ -2\frac{u'_v}{\sqrt{3}}\right] \bigcup \left[2\frac{u'_v}{\sqrt{3}},\ 2u'_v\right] \tag{41}$$

le discriminant D est positif. En conséquence pour ces intervalles la fonction $\mathrm{d}\alpha'(u')/\mathrm{d}t$ admet une seule inverse réele $u'_1(\mathrm{d}\alpha'/\mathrm{d}t)$. On a aussi les relations:

$$\lim_{\mathrm{d}\alpha'/\mathrm{d}t \to -2B'\sqrt{|G|^3}} u'_a = \lim_{\mathrm{d}\alpha'/\mathrm{d}t \to -2B'\sqrt{|G|^3}} u'_1 = \frac{2u'_v}{\sqrt{3}}, \tag{42}$$

$$\lim_{\mathrm{d}\alpha'/\mathrm{d}t \to 2B'\sqrt{|G|^3}} u'_b = \lim_{\mathrm{d}\alpha'/\mathrm{d}t \to 2B'\sqrt{|G|^3}} u'_1 = -\frac{2u'_v}{\sqrt{3}}, \tag{43}$$

qui montrent que la fonction inverse du polynôme (13), dans les domaines (41), est continuée par la branche *III*, respectivement *I*, du domaine $u' \in \left[-2u'_v/\sqrt{3},\ 2u'_v/\sqrt{3}\right]$.

En conséquence, dans les équations (17) et puis en (12) on doit introduire la fonction:

$$u' = \begin{cases} u'_1 & \text{pour} \quad u' \in \left[-2u'_v,\ -2u'_v/\sqrt{3}\right], \\ u'_b & \text{pour} \quad u' \in \left[-2u'_v/\sqrt{3},\ -u'_v/\sqrt{3}\right], \\ u'_c & \text{pour} \quad u' \in \left[-u'_v/\sqrt{3},\ u'_v/\sqrt{3}\right], \\ u'_a & \text{pour} \quad u' \in \left[u'_v/\sqrt{3},\ 2u'_v/\sqrt{3}\right], \\ u'_1 & \text{pour} \quad u' \in \left[2u'_v/\sqrt{3},\ 2u'_v\right]. \end{cases} \tag{44}$$

Il en résulte l'équation de mouvement du cadre mobile de l'instrument:

$$J\frac{\mathrm{d}^2\alpha'}{\mathrm{d}t^2} + B\frac{\mathrm{d}\alpha'}{\mathrm{d}t} + \frac{(N\Phi_0)^2}{R'} \cdot \frac{\mathrm{d}\alpha'}{\mathrm{d}t} + \frac{N\Phi_0}{R'}u'\left(\frac{\mathrm{d}\alpha'}{\mathrm{d}t}\right) + C\alpha' = 0, \tag{45}$$

où la fonction $u'(\mathrm{d}\alpha'/\mathrm{d}t)$ est définie par (44).

3. Conclusions

Dans le but d'établir les conditions d'apparition des oscillations électromécaniques dans un système hybride à diode Tunnel, on a déduit les équations différentielles qui décrivent le comportement du système et leurs domaines de valabilité.

L'analyse a été effectuée en acceptant l'hypothèse que le point de fonctionnement du système se trouve situé au centre de la zone de pente négative de la caractéristique de la diode Tunnel et qu'on respecte la condition (8), pour l'existence des oscillations dans le circuit électrique.

On constate que, en fonction de la valeur de la résistance R' du circuit électrique extérieur à la diode, l'équation différentielle correspondante a la forme (19) où (45).

L'analyse de ces équations du point de vue de la stabilité met en évidence l'éventuelle possibilité d'apparition des oscillations dans le mouvement de l'enroulement de l'instrument magnétoélectrique. On établit les conditions concrètes d'apparition de ces oscillations.

Reçue le 4 août 1993

Université Technique „Gh. Asachi", Jassy,
Chaire de Mesures électriques

BIBLIOGRAPHIE

1. Savin Gh., Grosu M., *Elektromechanische Schwingungen, die mit nichtlinearen aktiven Netzwerken selbsterregt werden.* Archiv für Elektrotechnik, **62**, 5-12 (1980).
2. Fitzgerald S., *Electric Machinery.* McGraw-Hill, NY, 1965.
3. Stanomir D., *Teoria fizică a sistemelor electromecanice.* Ed. Acad. RSR, Buc., 1982.
4. Sandu D.D., *Probleme moderne de tehnica impulsurilor.* Ed. Acad. RSR, Buc., 1980.
5. Buzduga M., Buzduga V., *Sur l'inversion des polynômes d'approximation des caractéristiques des éléments nonlinéaires.* Bul. Inst. polit., Iaşi, **XXXIX (XLIII)**, *1-4*, s.III (1993).

ASUPRA CONDIŢIILOR DE APARIŢIE A OSCILAŢIILOR MECANICE ÎNTR-UN SISTEM ELECTROMECANIC

I. Stabilirea ecuaţiilor de mişcare

(Rezumat)

Pentru un circuit particular ce conţine o diodă Tunnel şi bobina cadru a unui instrument de măsură magnetoelectric, în care s-a observat apariţia unor oscilaţii mecanice de joasă frecvenţă, se stabilesc ecuaţiile diferenţiale ce descriu mişcarea cadrului instrumentului şi domeniile lor de valabilitate.

Se constată că în funcţie de valoarea rezistenţei circuitului exterior diodei ecuaţiile diferenţiale au forme diferite.

BULETINUL INSTITUTULUI POLITEHNIC DIN IAŞI
Tomul XL (XLIV), Fasc. 1–4, 1994
Secţia III
ELECTROTEHNICĂ. ENERGETICĂ. ELECTRONICĂ

D.C. 621.317.335; 621.317.331

CONDUCTANCE AND CAPACITANCE MEASUREMENTS USING PHASE-SENSITIVE DETECTION

BY
CRISTIAN FOŞALĂU

1. Introduction

Frequently in the case of variable capacitance diodes in which the energy losses are small, it is usually to measure the energy losses with varying bias voltage or frequency. Bridges or phase-sensitive detectors are commonly used for this purpose. It will be shown below that phase-sensitive detection may lead to significant experimental errors.

2. Analysis

The principle scheme of the measurement is given in Fig.1, where the capacitor with losses, replaced by the ideal lossless capacitance C and the conductance G,

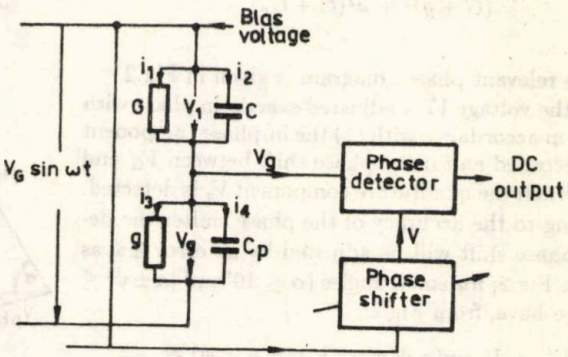

Fig. 1

which represents the losses, is connected in series with the conductance g. The input capacitance of the detector and the capacitances of leads and connectors form the parasitic capacitance C_p. The AC probing voltage of amplitude V_G and angular frequency ω is applied to the system and the voltage V_g is connected to the phase sensitive detector controlled by the reference voltage V_r. The DC voltage on the input of detector is

$$V = \beta V_g \cos\varphi, \tag{1}$$

where φ is the phase shift between V_g and V_r, which can be adjusted by the phase shifter, and β is a constant. For the system as in Fig.1, we can write in harmonic steady-state:

$$\underline{I}_1 + \underline{I}_2 = \underline{I}_3 + \underline{I}_4, \tag{2}$$

$$\underline{V}_G = \underline{V}_1 + \underline{V}_g. \tag{3}$$

Having in view that $\underline{I}_1 = \underline{V}_1 G$, $\underline{I}_2 = \mathrm{j}\omega \underline{V}_1 C$, $\underline{I}_3 = \underline{V}_g g$ and $\underline{I}_4 = \mathrm{j}\omega \underline{V}_g C_p$, one obtains from (2) and (3):

$$\underline{V}_g = V_{ph} + \mathrm{j}V_q \tag{4}$$

with

$$V_{ph} = V_G \frac{G(G+g) + \omega^2 C(C_p + C)}{(G+g)^2 + \omega^2 (C + C_p)}, \tag{5}$$

$$\tan\alpha = \frac{G(G+g) + \omega^2 C(C + C_p)}{\omega(Cg - C_p G)}. \tag{6}$$

The relevant phasor diagram is given in Fig.2.

As the voltage V_r is adjusted exactly in phase with V_G then in accordance with (1) the in-phase component V_{ph} is recorded and if the phase shift between V_G and V_r is 90°then the quadrature component V_g is detected. But owing to the accuracy of the phase shifter the desirable phase shift will be adjusted by an error $\pm\psi$ as shown in Fig.2; for small angles ($\alpha \leq 10°$and $|\alpha \pm \psi| \leq \leq 10°$) we have, from Fig.2:

$$\begin{aligned} V'_{ph} &= V_g \sin(\alpha \pm \psi) \approx V_g \tan(\alpha \pm \psi) \approx \\ &\approx V_g \tan\alpha \pm V_g \tan\psi \approx V_{ph} \pm V_g \psi \end{aligned}, \tag{7}$$

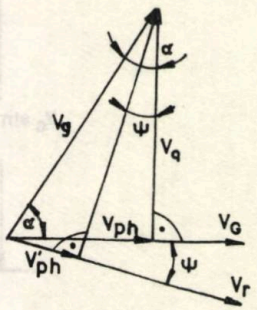

Fig. 2

where V'_{ph} is the voltage recorded by the detector. In practice, one usually has $g \gg G$, $C/C_p \gg G/g$ and $g/\omega \gg C + C_p$; then

$$V_g = V_G \frac{\omega C}{g}, \tag{8}$$

$$V_{ph} = V_G \left[\frac{G}{g} + \left(\frac{\omega}{g} \right)^2 C(C + C_p) \right], \tag{9}$$

$$\tan\alpha = \tan\delta + \frac{\omega}{g}(C + C_p), \tag{10}$$

where the loss tangent of the capacitor is defined as

$$\tan\delta = \frac{G}{\omega C}. \tag{11}$$

Equations (7),...,(9) yield

$$V'_{ph} = V_G \left[\frac{G}{g} + \left(\frac{\omega}{g} \right)^2 C(C + C_p) \pm \frac{\omega}{g} C\psi \right] = V_G \left(\frac{G}{g} + m \right), \tag{12}$$

where

$$m = \left(\frac{\omega}{g} \right)^2 C(C + C_p) \pm \frac{\omega}{g} C\psi.$$

The voltage V'_{ph} (after amplification) is driven to the Y input of the recorder. On the X input the bias voltage V (which induces the changes of G) is supplied. In this way the $G - V$ plot is obtained. It is desirable that

$$|m| \ll \frac{G}{g}, \tag{13}$$

then $V'_{ph} = V_G G/g$, hence V_{ph} is proportional to G. But if $|m| \geq G/g$ the undesirable component m is involved. The first term of m, i.e. $(\omega/g)^2 C(C + C_p)$, is uncertain because of C_p (it is rather difficult to determine the parasitic capacitance of the system exactly); the next term, $\pm(\omega/g)C\psi$, is uncertain because of ψ. Notice that for variable capacitance diodes, the capacitance C is a function of the bias voltage. This also makes the difficulty to correct the results which take into account the component m. For these reasons one assumes tacitly that the

condition (13) is fulfilled experimentally but such a procedure leads to an error ε defined as

$$\varepsilon = \frac{m}{G/g} = \frac{\omega C}{G}\left[\frac{\omega}{g}(C + C_p) \pm \psi\right]. \tag{14}$$

In Fig.3 the error ε is represented as a function of the capacitance C with the conductance G as a parameter. The calculations were performed for a variable capacitance diode βB413 produced by IPRS, Băneasa, with: $g = 0.01$ S, $C_p = 50$ pF, $f = \omega/2\pi = 10^5$ Hz and $\psi = -1°$. It is seen that for some C the error $\varepsilon < -1$, meaning that V'_{ph} is negative and "negative" conductances will be recorded. Since the bias voltage applied to the capacitor varies both C and G, we can consider that $G = f(C)$. Now, owing to bias the capacitance changes from C_1 to C_2 (Fig.3) and for any $C \in [C_1, C_2]$ the conductance G is recorded with positive or negative error. The resulting $G - V$ plot can be strongly deformed and "negative" conductances may occur. Identical calculation performed for $\psi = -0.1°$and $g = 0.1$ S give a maximum negative error $\varepsilon = 5 \times 10^{-3}$ for $G = 10^{-5}$ S and $\varepsilon = 0.5$ for $G = 10^{-7}$ S.

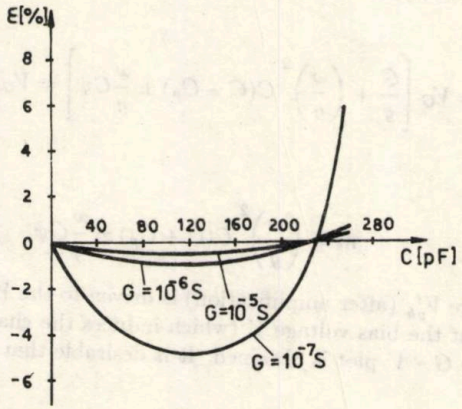

Fig. 3

3. Case of a Real Detector

The relationship (1) is valid only for an ideal detector. In practice a spurious DC output component appears owing to inaccuracy of the detector. Formally this component can be treated as arising from the ideal detection of some fictitious AC voltage which possesses the same frequency as V_g and has amplitude V_f and phase angle φ_f. This voltage generates the spurious in-phase component V_{phf} which adds to V'_{ph}. Usually, V_f and φ_f are not specified but certainly we can write that

$V_{phf} \leq V_g k$, where k is the accuracy of the detector, and with the help of (10) it becomes possible to write (7) as

$$V''_{ph} = V_g \left[\tan\delta + \frac{\omega}{g}(C + C_p) \pm \psi \pm k \right] = V_g(\tan\delta + n), \tag{15}$$

where

$$n = \frac{\omega}{g}(C + C_p) \pm \psi \pm k.$$

From (15) it follows that n is the sum of errors introduced by the electrical system, the phase shifter and the detector since $V_g \tan\delta = V_G G/g$. One would require

$$|n| \ll \tan\delta \tag{16}$$

to measure G exactly, hence the loss tangent of the capacitor determines the accuracy of the phase shifter and the detector (for example, $\tan\delta = 10^{-3}$ and $k < 10^{-3}$ (0.1%)). The last condition seems difficult to accomplish in the case under consideration, while with the help of bridge techniques the measurement of such low losses is possible. Next, for $\tan\delta = 10^{-3}$, $f = \omega/2\pi = 10^5$ Hz, $C = 100$ pF, $C_p = 0$ and $g = 0.1$ S the system error $(\omega/g)(C + C_p)/\tan\delta$ amounts to 63% but for $g = 0.01$ S this error is 630%. Such errors will be made in an ideal case $\psi = 0$, $k = 0$ and $C_p = 0$ and they are induced by the conductance g. Notice that the smaller is ω/g the smaller are the system errors but the reduction of ω/g worsens the signal-to-noise ratio. This case may by alleviated only for a configuration of G, ω and C in which the loss tangent rises appreciably or by the use (if available) of low-noise current preamplifiers with an input $g_{\text{in}} \gg 0.1$ S that can operate at frequencies 100...200 KHz, but the problem of k still remains open. Of course, the system errors disappear when the measurements are performed with the help of the bridge. The capacitance C can be measured exactly (V_g component) if $\tan\delta \ll 1$, $(G \ll \omega C)$, but analogous difficulties appear when $\tan\delta \gg 1$, $(G \gg \omega C)$, and the measurement of G is then correct.

4. Conclusion

Self-balancing bridges seem more appropriate for conductance measurements if the loss tangent of capacitors is low whereas phase-sensitive detection makes it possible to perform conductance measurements over a wide band of frequency.

Received, June 29, 1993

Technical University "Gh. Asachi", Jassy,
Department of Electric Measurements

REFERENCES

1. M i l l e a A., *Măsurări electrice. Principii şi metode.* Ed. Tehn., Bucureşti, 1980.
2. * * * *Catalog diode şi tiristoare.* IPRS Băneasa, Bucureşti, 1982.

MĂSURĂRI DE CAPACITĂŢI ŞI CONDUCTANŢE FOLOSIND DETECTOARE SENSIBILE LA FAZĂ

(Rezumat)

Se analizează performanţele obţinute la măsurarea conductanţelor şi capacităţilor prin metoda detecţiei sensibile la fază.

Erori apreciabile se obţin datorită sistemului electric de măsură, defazorului şi detectorului sincron, în special în cazul condensatoarelor de bună calitate, la care tangenta unghiului de pierderi este mică. Pentru aceste tipuri de condensatoare este justificată măsurarea capacităţii cu ajutorul punţilor de curent alternativ. Metoda detecţiei sincrone prezintă avantaje în cazul condensatoarelor cu pierderi mari.

BULETINUL INSTITUTULUI POLITEHNIC DIN IAŞI
Tomul XL (XLIV), Fasc. 1–4, 1994
Secţia III
ELECTROTEHNICĂ. ENERGETICĂ. ELECTRONICĂ

D.C. 538.551.21; 621.3.066.6; 531.79

ON PARAMETRIC LIMITING RABBETS WITHOUT CONTACTS

BY

I. SUCHAR and RADU URSULEAN

1. Generalities about Electrical Limiting Rabbets without Contacts

The block diagram of the electrical limiting rabbets without contacts is shown in Fig.1.

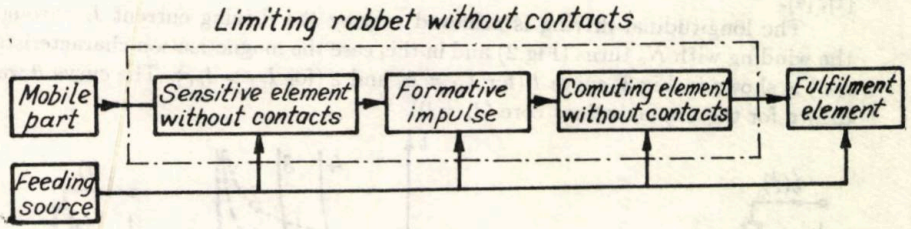

Fig. 1

The diversity of physical principles on which these limiters are based has generated a big number of circuits and constructive solutions for the sensitive elements and for the contacts.

The sensitive element may be parametric or with switched-off radiation. The parametric one may be inductive (e.g. a coil with saturated core, a magnetic amplifier with positive feedback, etc.) or capacitive (e.g. a variable capacitor whose capacitive reactance varies with the moving part).

The inductive limiting rabbets without contacts are more used because the capacitive ones have some disadvantages, namely: a) they need a bridge circuit supplied from a high frequency power supply; b) periodical adjustments of some circuit parameters are needed; c) their accuracy depends on the magnitude and the stability of the frequency of the power supply, the humidity and the shielding of the circuits against unwanted electrical fields.

The principle on which the parametric limiting rabbets without contacts are based is the changing of the magnitude of the magnetic field (the inductive types) or of the electric field (the capacitive types) made by the moving part of the sensitive element. This means a steep changing of the inductivity (or the capacitance) of the sensitive element followed by the steep changing of the state of the circuits of the commuting element, and this drives the fulfilment element (e.g. an electric motor).

The sensitive element with switched-off radiation may be of photoelectric type, with ultrasonic waves or based on radioactivity. The switching-off of the radiation is made by the mobile part when it reaches its extreme position; after this the active element is driven.

When dealing with unsealed limiting rabbets, the sensitive element may be at an important distance (hundreds of meters) from the commuting element (which includes circuits with transistors and thyristors).

2. The Permanent Magnet Drives the Ferroresonant Leap

In what follows a parametric limiting rabbet without contacts which is made by exploiting the relay-like characteristic of the ferroresonant circuits is studied.

It is well known that in the *RLC* series ferroresonant circuit with nonlinear coil the current $i(t)$ and the voltage across the linear capacitor $u_c(t)$ are permitted two steady states: one with small amplitude and another with high one. Changing the states is possible only by means of a leap and can be achieved varying the voltage of the power supply, $u = \sqrt{2}U \sin \omega t$, the frequency f, or any of the parameters R, L or C of the circuit [7].

Modifying the inductivity L of the nonlinear coil can be done by means of longitudinal or orthogonal driving of the magnetization of the ferromagnetic core [1], [4].

The longitudinal driving is achieved varying the driving current I_c through the winding with N_c turns (Fig.2) and in this case the magnetization characteristic $i(\psi)$ is shown in Fig.3, curve *1* (for $I_{c1} \neq 0$) and *2* (for $I_{c2} > I_{c1}$). The curve *0* was drawn for the unmagnetized core ($I_c = 0$).

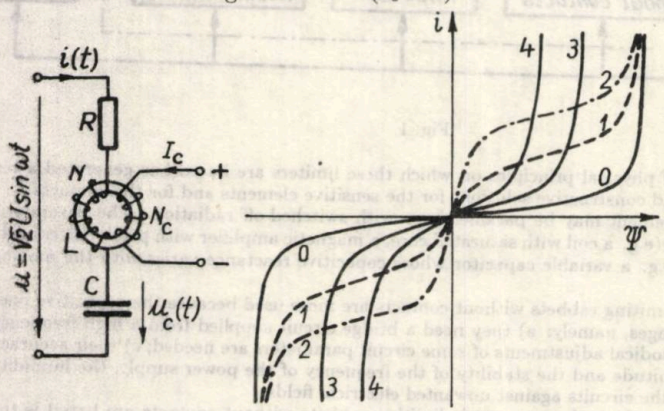

Fig. 2 Fig. 3 Fig. 4

The magnetization characteristic for $I_c \neq 0$ can be approximated by means of a fifth degree polynomial as follows:

$$i = a_1\psi + a_3\psi^3 + a_5\psi^5, \tag{1}$$

where ψ represents the total magnetic flux of the nonlinear coil; a_1, $a_5 > 0$ and $a_3 < 0$ are dimensional coefficients with numerical values depending on the magnetic properties of the core of the coil and of the current I_c.

Rising the longitudinal driving current I_c the $i(\psi)$ characteristic modifies its shape in the weak magnetic fields zone and goes toward greater values of the current $i(t)$; the value of the saturation magnetic induction is maintained unchanged. It is easily understood that the influence of the fifth term of the polynomial (1) becames more important when I_c is rising.

If the nonlinear coil isn't longitudinally driven ($I_c = 0$), ferroresonance occurs in the circuit represented in Fig.2, that is, the circuit has a relay-like characteristic with two stable functioning points. If the double ferroresonance occurs ($I_c \neq 0$), the caracteristic has three points of stable functioning.

The orthogonal drive of a nonlinear coil can be achieved in two ways: a) by means of a drive winding made on the core and a direct current, whose magnetic field is perpendicular on the magnetic field generated by the main winding; b) by means of a permanent magnet.

A study concerning the ferroresonant circuit with nonlinear coil orthogonally driven by the field of a permanent magnet characterized by the induction B_c and moved towards the core of the coil (Fig.4) can be found in [3].

In Fig.3, the magnetization characteristic *3* presents the case of the orthogonal driving of the nonlinear coil, as in Fig.4, with a magnetic field of induction B_{c1}, and the characteristic *4*, with a field $B_{c2} > B_{c1}$.

It can be seen that when B_c grows, the core of the coil can be saturated at smaller values of the induction B of the main field, but the shape of the characteristic around zero doesn't change and remains the same as in characteristic *0* in Fig.3 ($B_c = 0$). That is why when the orthogonal drive B_c grows, the relative magnetic permeability μ_r of the core of the nonlinear coil becames smaller and a linearization of the characteristic $\mu_r(H)_{B_c=\text{const.}}$ occurs. When a certain value of the magnetic induction of the driving field, named critical driving induction B_{ccr}, is reached, the permeability μ_r is practically independent of H (the intensity of the main magnetic field (Fig.5)), so that the nonlinear coil becomes linear.

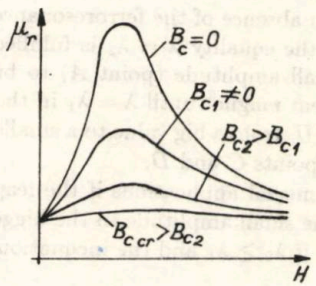

Fig. 5

It can be easy understood that the inductivity L_0 of the undriven nonlinear coil ($B_c = 0$) is greater than the inductivity L of the same coil when its core is orthogonally premagnetized by an external continuous field.

The magnetization characteristic of the core of the orthogonally driven nonlinear coil, represented in Fig.4, can be approximated in a satisfactory manner by means of a third degree polynomial, as follows:

$$i = b_1\psi + b_1 b_3 \psi^3, \tag{2}$$

where the numerical values of the coefficients $b_1 > 0$ (with the dimension 1/H) and

$b_3 > 0$ (with the dimension $1/\mathrm{Wb}^2$) are dependent of the magnetic properties of the core of the coil.

The processes that take place when the conditions for ferroresonant leap of the current are fulfilled were studied in [3]. They are described by a second order nonlinear differential equation of the D u f f i n g type . If we neglect all terms except the harmonic one with the same frequency f as the power supply, the differential equation can be written as follows:

$$\frac{\mathrm{d}^2 v}{\mathrm{d}\tau^2} + k\frac{\mathrm{d}v}{\mathrm{d}\tau} + \frac{1}{\lambda}v + \frac{b_3\psi_n^2}{\lambda}v^3 = \sin\tau, \tag{3}$$

where:

$$\tau = \omega t + \operatorname{arctg} RC\omega, \quad v = \frac{\psi}{\psi_n}, \quad \psi_n = \frac{\sqrt{2}U\sqrt{1+R^2C^2\omega^2}}{\omega}, \quad k = \frac{1}{RC\omega}. \tag{4}$$

The quantity:

$$\lambda = LC\omega^2 \tag{5}$$

represents the normed inductivity of the nonlinear coil. It has the maximum value $\lambda_0 = L_0 C\omega^2$ when the core of the coil isn't orthogonally magnetized ($B_c = 0$).

We shall use the voltage drop U_c across the linear capacitor of the ferroresonant circuit (Fig.4) for driving the transistors of the circuit described in § 4 in the saturation or cut-off regions.

According to the studies begun in [3] and followed by the ones in [7], the function $U_c(\lambda)$ presents a relay-type characteristic (Fig.6). Resuming, we can say that if the magnet M (Fig.4) is sufficiently far away form the nonlinear coil, the normed inductivity is maximum ($\lambda = \lambda_0$) and $U_c(\lambda)$ has a small amplitude (U_1), determined by the small intensity of the current, in absence of the ferroresonance. When the magnet is so closed to the coil so that the equality $\lambda = \lambda_2$ is fulfilled, the ferroresonant leap of the voltage U_c from small amplitude (point A) to big one (point B) occurs. If we withdraw the permanent magnet until $\lambda = \lambda_1$ in that moment there is a reverse jump of the amplitude of U_c from a big value to a smaller one and the operating point oscillate between the points C and D.

The ferroresonant circuit in Fig.4 can have unusual applications if the leaps of the voltage U_c do happen in both ways (from the small amplitude to the bigger one and viceversa). These jumps are possible only if $\lambda_0 \geq \lambda_1$ and the inequations

$$\omega < \sqrt{\frac{1}{C(L_f - R^2C)}}, \tag{6}$$

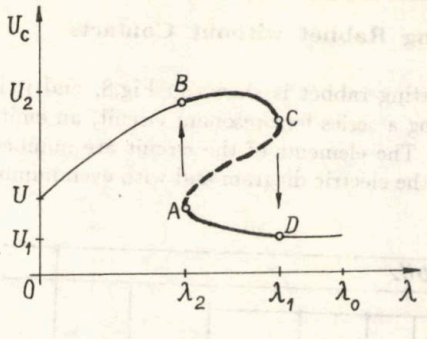

Fig. 6

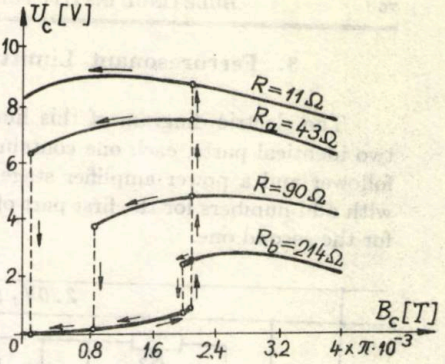

Fig. 7

$$\frac{1+R^2C^2\omega^2}{RC^2\omega^2} \geq \left|\frac{\sqrt{3}}{1/\omega L_f - \omega C/(1+R^2C^2\omega^2)}\right|, \tag{7}$$

are valid, where L_f is the value of the inductivity which determines the ferroresonant jump.

For a given level of the voltage of the power supply the $[\lambda_1\ \lambda_2]$ domain of the relay-like characteristic in Fig.6 can be modified varying the resistance between two limits: R_a and R_b. Although the stability of the functioning of the ferroresonant circuit depends on the value of $R \in [R_a,\ R_b]$ the limits of the useful domain for the resistance can be calculated as follows:

$$R_a = \frac{1}{C\omega}\sqrt{\lambda_f - 1}, \tag{8}$$

$$R_b = \frac{1}{2C\omega}\sqrt{6\lambda_f^2 + 4(\lambda_f - 1)}, \tag{9}$$

where

$$\lambda_f = L_f C\omega^2 > 1 \tag{10}$$

represents the normed inductivity of the nonlinear coil when the ferroresonant leap is achieved, with the magnet near the coil. The characteristic in Fig.7 were drawn utilising the experimental results and give the dependence between the voltage drop U_c and the magnetic induction B_c of the orthogonal drive for the nonlinear coil with resistance R as a parameter. The circuit was supplied with $U = 3.2$ V and $f = 50$ Hz. It can be seen from the experimental results that if $R < R_a$ there is only one leap of the voltage U_c and this leap can be achieved rising the value of B_c. When the value of R aproaches R_b the limits of the domain of the relay-like characteristic are smaller and this is valid for the voltage U_c, too.

3. Ferroresonant Limitting Rabbet without Contacts

The electric diagram of this limitting rabbet is shown in Fig.8, and it has two identical parts, each one containing a series ferroresonant circuit, an emitter follower and a power amplifier stage. The elements of the circuit are numbered with odd numbers for the first part of the electric diagram and with even numbers for the second one.

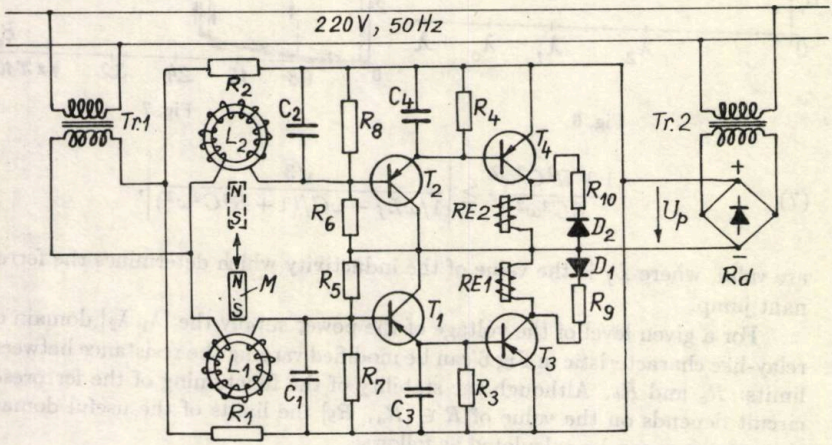

Fig. 8

The ferroresonant circuits have the resistances $R_1 = R_2 = 50\ \Omega$, the linear capacities $C_1 = C_2 = 20\ \mu$F and the coils with nonlinear inductivities $L_1 = L_2$. Each coil, with $N_1 = N_2 = 155$ turns, is made from a torroidal core of ULTRAPERM Z with the surface of the radial cross-section of 75×10^{-6} m^2, the medium diameter of 57.5×10^{-3} m and the maximum magnetic permeability of 0.314 H/m.

The emitter followers are used for impedance matching of the ferroresonant circuits that have a big output impedance with the power amplifier stages with low input impedance.

The resistors $R_3 - R_4$, $R_5 - R_7$ and $R_6 - R_8$ are used for biasing the transistors T_1 and T_2. The capacitors C_3 and C_4 are used for decoupling. The values used are: $R_3 = R_4 = 150\ \Omega$, $C_3 = C_4 = 12\ \mu$F, $R_5 = R_6 = 3.3$ KΩ and $R_7 = R_8 = 4.3$ KΩ. The transistors T_1 and T_2 are of AC 180 K type.

The power amplifier is made with transistors T_3 and T_4 and their loads are the coils of the RE1 and RE2 relays. T_3 and T_4 are of BD 138 type.

The $D_1 - R_9$ and $D_2 - R_{10}$ groups are chosen so that the overvoltage in the collectors of the transistors be in the worst case twice the voltage of the power supply U_p.

The ferroresonant circuits are supplied by means of transformer Tr1 with 220 V/8 V, 4 VA and 50 Hz. For an adequate functioning of the circuit repre-

sented in Fig.8 the amplitude of the sinusoidal voltage of the power supply for the ferroresonant circuits must be smaller than the one necessary for the ferroresonance to occur when the nonlinear coil isn't premagnetized with an orthogonal magnetic field.

If the coils L_1 and L_2 are fixed on the extreme points delimiting the run of a mechanism with linear moving, they can be used as sensitive elements at the position of a permanent magnet placed on the moving part of the mechanism, which is moved in both ways durring the run.

So, when the magnet M in Fig.8 is approaching the nonlinear coil L_1, in the circuit $R_1 - C_1 - L_1$ a leap of the amplitude of the current $i_1(t)$ from a small value to a bigger one is produced; this fact determines a variation of the voltage $u_{c1}(t)$ on the capacitor C_1 which is sufficiently high to turn T_1 on. This signal turns on the transistor T_3 and so the relay RE1 is activated, stops the moving of the magnet and commands the begining of the reverse run.

When the magnet is removed from the coil L_1, there is a reverse leap of the amplitude of the current $i_1(t)$, the voltage $u_{c1}(t)$ becomes suddenly smaller than its former value, the transistors T_1 and T_2 are switched-off and the coil of the relay RE1 isn't supplied any more.

The same happens on the other half of the circuit in Fig.8 when the magnet is close enough to the coil L_2 and then is removed.

Using the theoretical background presented above a limitting rabbet was build according to the circuit in Fig.8, where $L_0 = 0.918$ H, $\lambda_0 = 1.81$, $L_f = 0.544$ H, $\lambda_f = 1.0727$, $R_a = 43\ \Omega$, $R_b = 214\ \Omega$.

4. Conclusions

1. A limiting rabbet without contacts is proposed; it works using the relay-like characteristic of a series ferroresonant circuit with the nonlinear coil orthogonally driven.

2. The orthogonal drive is achieved with the external field of a permanent magnet which is moved towards the nonlinear coil.

3. The limiting rabbet is feeded from the mains power supply and being without contacts it can be used in harsh environments.

4. The precision and the reliability of the circuit are not dependent of the enviromental conditions (temperature and humidity); they are dependent of the frequency and the amplitude of the power supply of the ferroresonant circuits and of the aging of the permanent magnet.

Received, December 16, 1991

Technical University "Gh. Asachi", Jassy,
Department of Electrotechnics
and Electrical Machines

REFERENCES

1. Angel Y., *Commande magnétique orthogonale des systèmes paramétriques.* Acta electronica, **4**, *3*, 359-380 (1960).
2. Hayashi Ch., *Nonlinear Oscillations in Physical Systems.* McGraw-Hill Book Company, New-York, 1964.
3. Lüder E., *Ein kontaktloser Schalter mit Hilfe des Ferroresonanzkreises.* ETZ-A, **90**, *7*, 158-161 (1969).
4. Savin Gh., Rosman H., *Circuite electrice neliniare şi parametrice.* Ed. Tehnică, Bucureşti, 1973.
5. Simion E., Popescu I., *Sprunghafte betriebsweisen der Signale in Ferroresonanzkreisen.* Bul. Inst. polit., Iaşi, **XVII(XXI)**, *1-2*, s.III, 19-30 (1971).
6. Suchar I., *Releu electronic de semnalizare a deplasării.* Romanian Patent, *91319* (1986).
7. Suchar I., Ursulean R., *On Proximity Relays without Contacts.* Bul. Inst. polit., Iaşi, **XXXVII(XLI)**, *1-4*, s.III (1991).

ASUPRA UNUI LIMITATOR PARAMETRIC DE CURSĂ FĂRĂ CONTACTE

(Rezumat)

Se studiază un nou limitator de cursă fără contacte, a cărui funcţionare se bazează pe particularitatea circuitului ferorezonant cu bobină neliniară comandată ortogonal de a prezenta o caracteristică de tip releu. Sunt evidenţiate avantajele şi dezavantajele aparatului propus.

BULETINUL INSTITUTULUI POLITEHNIC DIN IAŞI
Tomul XL (XLIV), Fasc. 1–4, 1994
Secţia III
ELECTROTEHNICĂ. ENERGETICĂ. ELECTRONICĂ

D.C. 518.8; 621.396.6

ABOUT THE USE OF MULTIPLEXERS IN THE SYNTHESIS OF LOGICAL FUNCTIONS

BY

C. POŞA and DORU-FLORIN CHIPER

1. Introduction

The multiplexers can be used in the selection of a signal from several signal sources. They can be used in the synthesis of logical functions, too.

We shall present a method for logical function synthesis based on the use of these circuits. The proposed method is regular and simple and can be easily implemented on digital computers. Thus it is possible to generate implementations which are more simple.

From the truth table and the functional equation of the multiplexer we can observe that for every combination of the selection inputs it is selected one of the multiplexer inputs. We can select a number of the function variables corresponding to the k selection inputs of the multiplexer and we shell connect them at the multiplexer selection inputs. At the other multiplexer inputs, 2^{n-k} other logical functions with $n-k$ variables are connected. Thus at the output of the multiplexer the desired logical function is obtained. If a multiplexer with 8 selection inputs is used we can eliminate three of the function arguments remaining to synthesize eight functions with $n-3$ variables.

In this paper a method to generate these residual functions which have $n-k$ variables, for arbitrary n and k, is presented. The proposed algorithm can be used to choose the proper variables which corresponds to the selection inputs of the multiplexer so that the resulting functions to be as simple as possible or to appear identical several times.

2. Theoretical Considerations

Let consider the decomposition of a logical with respect to one variable:

$$f(x_n, x_{n-1}, ..., x_j, ..., x_1, x_0) = \overline{x}_j f(x_n, x_{n-1}, ..., 0, ..., x_1, x_0) +$$

$$+ x_j f(x_n, x_{n-1}, ..., 1, ..., x_1, x_0)$$

or

$$f(x_n, x_{n-1}, ..., x_j, ..., x_1, x_0) = \overline{x}_j f_0(x_n, x_{n-1}, ..., x_{j+1}, x_{j-1}, ..., x_1, x_0) +$$

$$+ x_j f_1(x_n, x_{n-1}, ..., x_{j+1}, x_{j-1}, ..., x_1, x_0).$$

To obtain the decimal canonical forms (in octal) of the two functions, f_0 and f_1, it is necessary to separate the numbers which have the correspondent of rank 2^j with the value 0 and 1. In this groups of numbers this bit disappears and the bits of superior rank are shifted with one step to the left. We can in this manner to synthesize a function with n variables using one multiplexer with two paths. In this case we have to synthesize two functions of $n-1$ variables. This process can be continued, the number of variables becoming less. Spectacular results can be obtained if we use as addresses of multiplexer the variables of the function which have the biggest ranks. In this case we can directly obtain the decimal canonical forms (in octal) of the 2^k functions (where k is the number of variables which have been eliminated). Indeed:

$$n_f(0, 0, ..., 0, x_{n-k}, ..., x_1, x_0) = (0, 0, ..., 0, 0)2^{n-k} + n_{f_0},$$
$$n_f(0, 0, ..., 1, x_{n-k}, ..., x_1, x_0) = (0, 0, ..., 0, 1)2^{n-k} + n_{f_1},$$
$$\cdots\cdots\cdots\cdots\cdots\cdots\cdots\cdots\cdots\cdots\cdots\cdots\cdots\cdots\cdots\cdots$$
$$n_f(1, 1, ..., 1, x_{n-k}, ..., x_1, x_0) = (1, 1, ..., 1, 1)2^{n-k} + n_{f_{2k-1}},$$

where: n_f is the number of decimal form of the function f and (1,...,1) is a binar number.

The numbers of decimal canonical form of the function $f_j, (j = 0, 1, ..., 2^{k-1})$, can be obtained from the previous function by division with 2^{n-k}. The quotient j identify the function f_j and the remainder represents the decimal canonical form of the function f_j. When we change the quotient we pass to another function. The condition to choose for the selection inputs only the variables to whom was allocated the greatest ranks is not restrictive because this assignation can be permutated remaking the decimal canonical form of the function and applying the algorithm again. We shall obtain other results, of course. We can compare these solutions to choose the optimal solution for that application.

It is also fast the synthesis of the function based on the selection of the least significant k variables for the selection inputs of the multiplexer. In this case the remainders i identify the residual functions f_i and the quotients of the division by 2^{n-k} which have the same remainder, i, will represent the canonical decimal form of the function f_i.

3. Numerical Example

For a better understanding of the presented method let consider the majority function MAJ(a, b, c, d, e) with 5 variables (which yields a logical 1 at the output when at least 3 of the 5 variables are logical 1). We shall synthesize this function with a multiplexer with 8 paths. The decimal canonical form of this function is:

$$\text{MAJ}(a, b, c, d, e) = \bigcup^{abcde} 7, 11, 13, 15, 19, 21, 22, 23, 25, 26, 27, 28, 29, 30, 31.$$

The variable a has the greatest rank 4 and the variable e the smallest one 0. The multiplexer has three selection inputs. So, we divide the numbers of the decimal canonical form by $2^{5-3} = 4$. The 8 residual functions of 5–3=2 variables (d and e) from the multiplexer inputs which we have to synthesize are:

a) $f_0 = 0$ (there is no number which divided by 2^{5-3} gives the quotient 0);

b) $f_1 = \bigcup^{de} 3$; $f_2 = \bigcup^{de} 3$; $f_3 = \bigcup^{de} 1, 2, 3$; $f_4 = \bigcup^{de} 3$;

c) $f_5 = \bigcup^{de} 1, 2, 3$; $f_6 = \bigcup^{de} 1, 2, 3$; $f_7 = \bigcup^{de} 0, 1, 2, 3$.

We can observe that the functions f_1, f_2 and f_4 are identical and they have the logical value 1 when d and e are 1:

$$f_1 = f_2 = f_4 = de; \quad f_3 = f_5 = f_6 = \bar{d}e + d\bar{e} + de = d + e$$

and the function f_7 has the logical value 1 for all of the four possible combinations. So, it will be connected at logical 1 (+5 V). We have to synthesize only two logical function of two variables. It results the implementation from Fig.1.

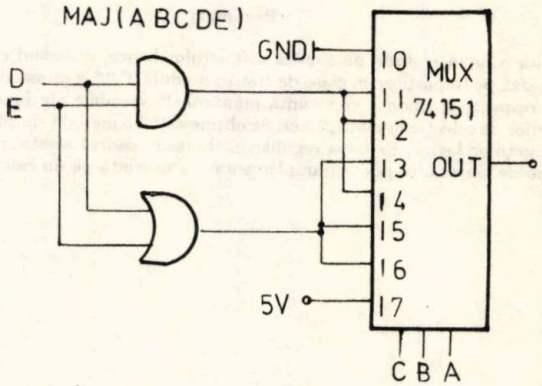

Fig. 1

4. Conclusions

A new method to synthesize logical function using multiplexers is presented. We established some rules which make the synthesis regular and simpler. Based on this rules we have obtained an algorithm which can be implemented on a digital computer. Changing the order of variables we obtain several results which can be compared to obtain the simplest form of the remainder functions or to obtain as many identical functions as possible.

The proposed method can be applied for arbitrary n and k. If we synthesize the function by hand we can manage functions with 10...12 variables.

This method being a numerical one can be solved by digital computers, the number of variables being limited by the memory capacity.

Changing the order of variables we can choose the optimal solution for a certain function. We can, thus, to extend the use of multiplexers in the synthesis of boolean functions.

Received, September 23, 1992

Technical University "Gh. Asachi", Jassy, Department of Applied Electronics

REFERENCES

1. Reus N., *Tratarea simbolică a schemelor de comutaţie.* Ed. Acad., Bucureşti, 1971.
2. Poşa C., Chiper D., *Reducerea numărului de variabile în procesul de sinteză al circuitelor numerice.* Symp. "Achievements in Professional Electronic Field", Snagov, 1987, VI-17.

ASUPRA UTILIZĂRII MULTIPLEXOARELOR ÎN SINTEZA FUNCŢIILOR LOGICE

(Rezumat)

Se prezintă o nouă metodă de sinteză a funcţiilor logice, utilizând circuite multiplexoare. Metoda se bazează pe împărţirea în clase de resturi modulo 2^{n-k} a numerelor de stare ce definesc funcţia logică respectivă, unde n reprezintă numărul de variabile ale funcţiei sintetizate, iar k numărul intrărilor de selecţie în multiplexer. Se obţine astfel o metodă simplă, regulată şi eficientă de sinteză a funcţiilor logice. Pe baza regulilor stabilite în cadrul acestei metode s-a obţinut un algoritm simplu de sinteză, ce poate fi implementat cu uşurinţă pe un calculator numeric.

BULETINUL INSTITUTULUI POLITEHNIC DIN IAŞI
Tomul XL (XLIV), Fasc. 1-4, 1994
Secţia III
ELECTROTEHNICĂ. ENERGETICĂ. ELECTRONICĂ

D.C. 621.394.9

A MODIFIED $M2$ DECODER

BY
N.D. ALEXANDRU and I.F. MASHEH

1. Introduction

In a previous work [6], a method of synthesizing the modified M i l l e r code $M2$ was presented. This code is derived from delay-modulation (DM) code otherwise known as M i l l e r. In order to decrease the d.c. component of the signal, a restriction was introduced for the last mark in a string of at least two successive marks, which is coded like a single space, by a lack of transition.

This code we obtained was called modified $M2$ and exhibits the transition diagram illustrated in Fig.1, where the transition diagram for the DM code is also represented.

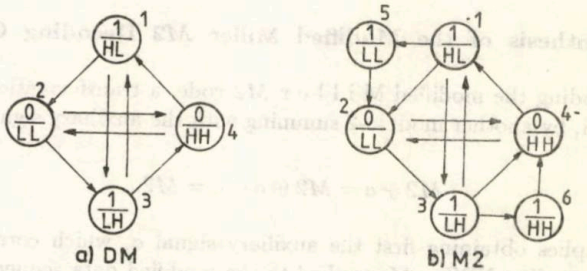

Fig. 1

This code will present besides the time intervals with a length of T, $1.5T$ and $2T$, specific to the DM code, other intervals with a length of $2.5T$ and $3T$, which can be used for eliminating the phase ambiguity as well.

The synthesis method for the modified M i l l e r $M2$ coding circuit, which was outlined in [6], is based on the observation that starting from the DM code, the new code can be obtained as a generalized digital modulation of the PSK or SIK-type, using as a carrier the M i l l e r coded signal M and an auxiliary signal

a as the data input. This signal a is obtained from the NRZ – L coded data signal by replacing every mark by a space, excepting the last mark in a string composed of at least two successive marks, as shown in Fig.2.

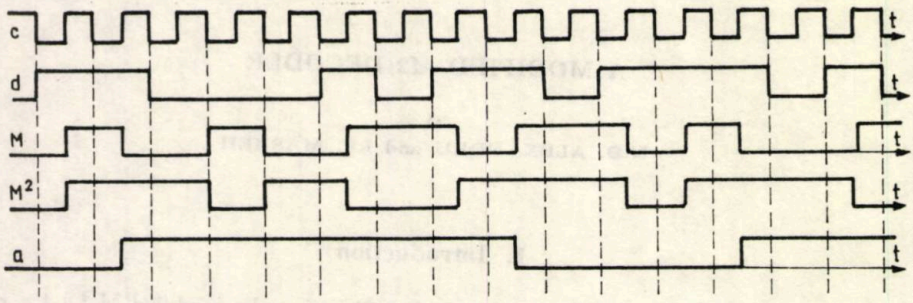

Fig. 2

We can write then

$$M2 = M \oplus a, \tag{1}$$

where $\oplus$ denotes modulo-2 summing (EXCLUSIVE–OR operation).

2. Synthesis of the Modified Miller $M2$ Decoding Circuit

For decoding the modified M i l l e r $M2$ code, a transformation in $M2$ will be performed, by another modulo-2 summing with the auxiliary signal a. Then

$$M2 \oplus a = M2 \oplus a \oplus a = M2. \tag{2}$$

This implies obtaining first the auxiliary signal a, which corresponds to a differential encoding NRZ – M, applied to the modified data sequence, where all marks were replaced by spaces, excepting the last mark in a string composed of at least two successive marks.

From Fig.2 we see that the last mark in a string composed of at least two successive marks determines the appearance in M of intervals with a length of $2.5T$ if the last mark is followed by at least two successive spaces or $3T$ if followed by a single space. This implies the use of differential decoding techniques of comparing the level on a given bit interval with the level on the previous one, as shown in Fig.3.

A first delay by T is followed by the modulo-2 summing of $M2$ and $M2'$ ($M2$ delayed by T). This transforms the intervals with a length of $2.5T$ or $3T$ with the level L or H in intervals with a length of $1.5T$ or $2T$ and level L. This also eliminates time intervals with length T. A new delay by T followed by the

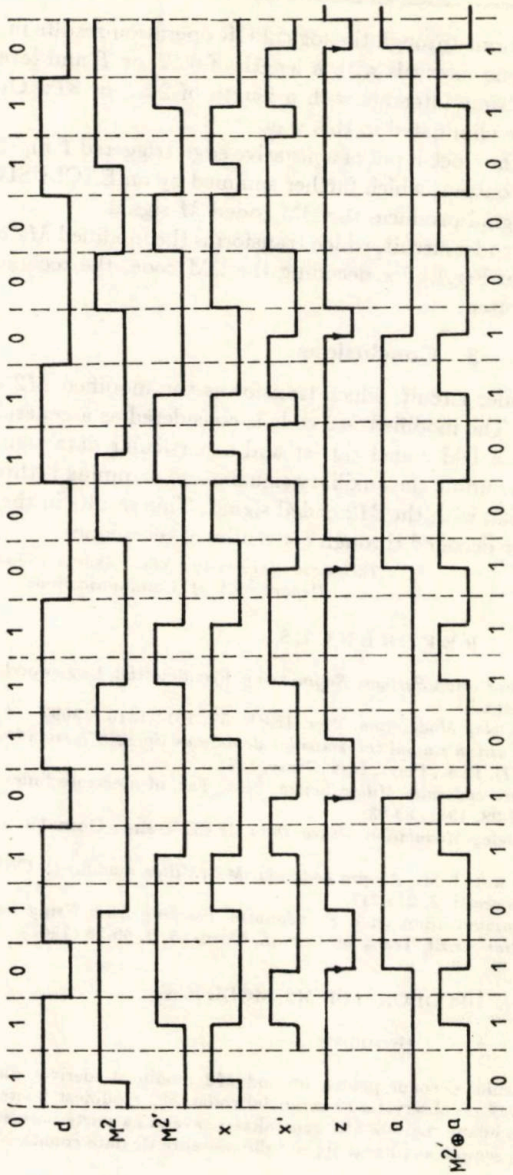

Fig. 3

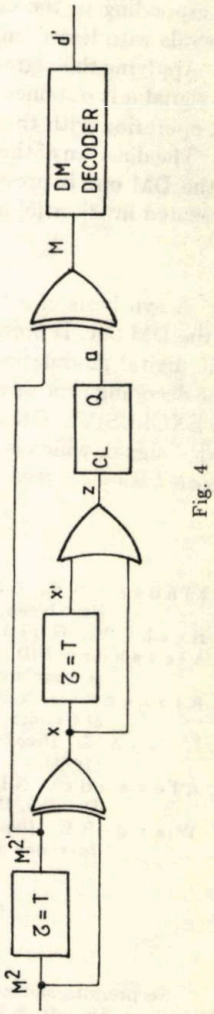

Fig. 4

summing of the implied waveforms through the logical OR operation results in the waveform z, which exhibits time intervals with a length of $0.5T$ or T and level L corresponding to the original time intervals with a length of $2.5T$ or $3T$. Other intervals with lesser length are eliminated in this way.

Applying this signal z at the clock input of a negative edge-triggered T flip-flop, the signal a is obtained at its output, which further summed by an EXCLUSIVE–OR operation with the $M2$ signal produces the DM coded M signal.

The diagram of this transcoder circuit, which transforms the modified $M2$ code in the DM one is presented in Fig.4. For decoding the DM code, the techniques presented in [3] or [5] can be used.

3. Conclusions

A synthesis of a transcoder circuit, which transforms the modified $M2$ code in the DM one, is presented. The modified $M2$ code is considered as a generalized SIK digital modulation with a DM coded carrier and a particular data signal a. The decoding process implies finding the auxiliary signal a and summing it through an EXCLUSIVE–OR operation with the $M2$ coded signal. This results in the DM coded signal, which is further decoded through conventional techniques.

Received, April 13, 1992

Technical University "Gh. Asachi", Jassy,
Department of Communications

REFERENCES

1. L i n d s e y W.C., *Telecommunication Systems Engineering.* Prentice Hall, Englewood Cliffs, New Jersey, 1973, ch.1.
2. H e c h t M., G u i d a A., *Delay Modulation.* Proc. IEEE, **57**, 1314-1316 (1969).
3. A l e x a n d r u N.D., *Contribuţii la studiul transmisiilor de date de tip FSK (privind codarea şi modularea).* Ph. D. Diss., Polyt. Inst., Jassy, 1981.
4. A l e x a n d r u N.D., *Sinteza coderului Miller.* Scient. Sess., Fac. of Electrotechnics, Univ. of Craiova, Nov. 27-28, 1981, 89-93.
5. L e w i n J., *Decoder for Delay-Modulation Coded Data.* IEEE Trans., **Com-19**, 719-723 (1971).
6. A l e x a n d r u N.D., I m a d F.M., *Asupra coderului M2 (Miller modificat).* CNETAC, Dec. 7-9, 1988, Bucureşti, **2**, 215-217.
7. W a r d R.B., *Digital Communication on a Pseudonoise Tracking Link Using Sequence Inversion Modulation.* IEEE Trans. on Comm., **Com-15**, *1*, 69-78 (1967).

ASUPRA DECODORULUI $M2$ MODIFICAT

(Rezumat)

Se prezintă sinteza circuitului decodor pentru un cod $M2$ modificat, derivat din codul M i l l e r. Decodarea se bazează pe observaţia că semnalul codat $M2$ modificat poate fi considerat un caz particular de modulaţie digitală SIK generalizată, având ca purtătoare semnalul codat M i l l e r, iar ca date un semnal auxiliar a obţinut din secvenţa de date codată NRZ – L printr-o codare particulară.

BULETINUL INSTITUTULUI POLITEHNIC DIN IAŞI
Tomul XL (XLIV), Fasc. 1–4, 1994
Secţia III
ELECTROTEHNICĂ. ENERGETICĂ. ELECTRONICĂ

D.C. 621.394.9

A SIMPLIFIED DECODER FOR MILLER CODED DATA

BY

N.D. ALEXANDRU and PAUL COTAE

1. Introduction

In previous works [1], [2], a logic synthesis of the decoder circuit for M i l l e r or delay-modulation (DM) coded data was performed using the symbolic method [3].

This paper presents another technique, which results in a more simple implementation of the decoder.

2. A Simplified Decoding Technique

In Fig.1 we represented the waveforms associated with the operation of the decoder. We denote by c – the clock signal, d – the input data signal, x – the DM coded signal, x' – the signal x delayed by T (a bit interval) and p – the waveform resulted from the modulo-2 summing of x and x'.

We also perform a logical AND operation between $\overline{p}$ and $\overline{c}$ and, respectively, $\overline{p}$ and c, which we denote by A and, respectively, B:

$$A = \overline{p} \cdot \overline{c}, \tag{1}$$

$$B = \overline{p} \cdot c. \tag{2}$$

We can see that using the trailing edge of A and respectively the leading edge of B for setting or respectively resetting a SR flip-flop results in the decoded data sequence at the output of the SR flip-flop.

The resulted circuit diagram is represented in Fig.2.

In Fig.3 a complete diagram of the decoding circuit is represented. A phase-change decision logic [2], [4] is required, because the decoder needs for proper operation the clock signal c with proper phase. As the transitions appear in the DM coded signal both at the center of the bit interval for a mark and at the end of the bit interval for a space, the PLL in the synchronization circuit can only lock

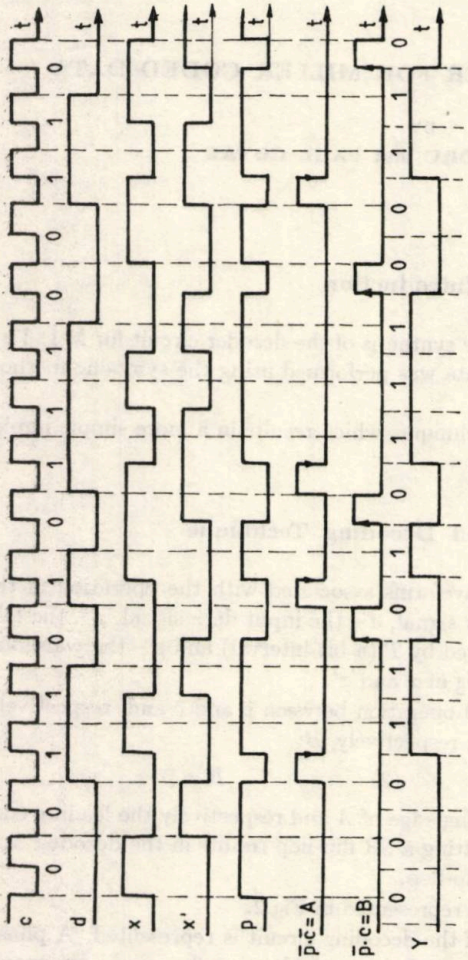
c
d
x
x'
p
p̄·c̄=A
p̄·c=B
Y
t

Fig. 1

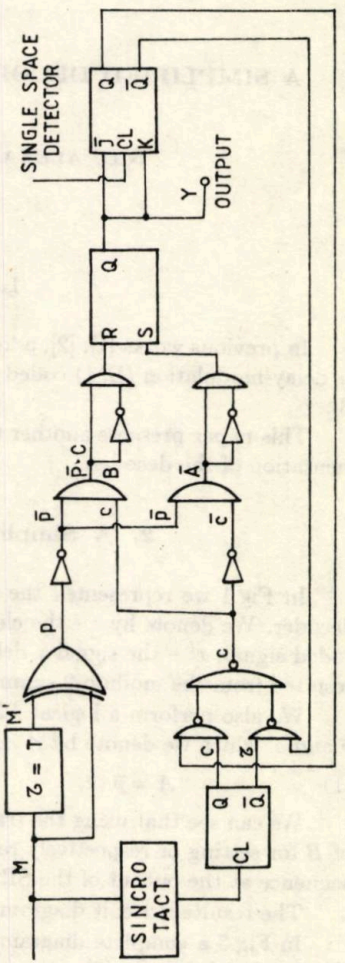
SINGLE SPACE DETECTOR
OUTPUT
SINCRO TACT
Z = T
M
M'
p
p̄
c
c̄
B
Ā
R
S
Q
Q̄
J̄
CL
K
Y

Fig. 3

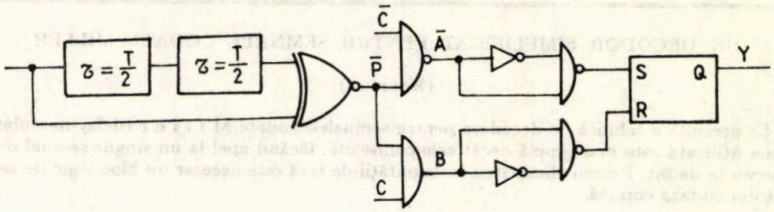

Fig. 2

on the double bit frequency $2f_{bit}$. The clock signal c is extracted by a frequency division by 2 using a T - type flip-flop that introduces a phase ambiguity of 180°.

3. Conclusions

A simple decoding technique for DM coded data signals was presented. The decoding circuit can be implemented very easily. An error appearing in the decoded data due to a lack of transition at its input is propagated until the next edge at its input.

For proper operation, a phase-change decision logic is required.

Received, April 30, 1992

Technical University "Gh. Asachi", Jassy, Department of Communications

REFERENCES

1. Alexandru N.D., *Contribuţii la studiul transmisiilor de date de tip FSK (privind codarea şi modularea).* Ph.D. Diss., Polyt. Inst., Jassy, 1981.
2. Alexandru N.D., Cotae P., *Decoder for Delay-Modulation Coded Data.* Scient. Sess. Development & Application Systems, Suceava, Romania, May 28-30, 1992 (to be published).
3. Reus N., *Tratarea simbolică a schemelor de comutaţie.* Ed. Acad., Bucureşti, 1978.
4. Lewin J., *Decoder for Delay-Modulation Coded Data.* IEEE Trans. on Comm., **Com-19**, 719-723 (1971).
5. Hecht M., Guida A., *Delay Modulation.* Proc. IEEE, **57**, 1314-1316 (1969).
6. Lindsey W.C., *Telecommunication Systems Engineering.* Prentice Hall, Englewood Cliffs, New Jersey, 1973, ch.1.
7. Alexandru N.D., *Sinteza coderului Miller.* Scient. Sess., Fac. of Electrotechnics, Univ. of Craiova, Nov. 27-28, 1981, 89-93.
8. Alexandru N.D., Imad F.M., *Asupra coderului M2 (Miller modificat).* CNETAC, Dec. 7-9, 1988, Bucureşti, **2**, 215-217.
9. Mallinson J.C., Miller J.W., *Optimal Codes for Digital Magnetic Recording.* The Radio and Electronic Engineer, **47**, 172 (1977).
10. Lindholm D.A., *Power Spectra of Channel Codes for Digital Magnetic Recording.* IEEE Trans. on Magnetics, **MAG-14**, *5*, 321-323 (1978).
11. Poo G.S., *Computer Aids for Code Spectra Calculations.* IEE Proc., **128**, Pt. F, *5*, 323-330 (1981).
12. Alexandru N.D., Boariu A., *Power Spectral Density of a Delay-Modulation Coded Random Data Sequence.* COMCONEL 90, Dec. 16-20, 1990, Cairo, Egipt, 83.
13. Cariolaro G.L., Tronca G.P., *Spectra of Block Coded Digital Signals.* IEEE Trans. on Comm., **Com-22**, 1555-1564 (1974).

UN DECODOR SIMPLIFICAT PENTRU SEMNALE CODATE MILLER

(Rezumat)

Se prezintă o tehnică de decodare pentru semnalele codate M i l l e r (delay-modulation). Schema utilizată este mai simplă decât cele cunoscute, făcând apel la un singur semnal de tact pe frecvenţa de bit. Pentru eliminarea ambiguităţii de fază este necesar un bloc logic de selecţie a tactului cu faza corectă.

BULETINUL INSTITUTULUI POLITEHNIC DIN IAŞI
Tomul XL (XLIV), Fasc. 1-4, 1994
Secţia III
ELECTROTEHNICĂ. ENERGETICĂ. ELECTRONICĂ

C.D. 621.365

INTENSIFICATION DU REFROIDISSEMENT DES CONDUCTEURS À L'AIDE DES CALODUCS

PAR

ADRIAN BARABOI, EUGEN HNATIUC et MARICEL ADAM

1. Introduction

Les caloducs sont des dispositifs utilisés pour le transfert de la chaleur. En principe ils sont réalisés (Fig.1) par un tube *1*, métallique, étanché et vidé, dans lequel il y a une certaine quantité de liquide volatil, *2*.

Le fonctionnement en régime permanent des caloducs consiste dans le transport de l'énergie thermique de la source chaude (vaporisateur), *3*, à la source froide (condensateur), *4*. La vaporisation du liquide dans la zone de la source chaude se produit avec absorbtion d'énergie thermique, sous forme de chaleur latente.

La vapeur ainsi obtenue se déplace vers le condensateur où la chaleur transportée est cédée à la source froide. Seulement sous l'action de la gravitation, s'il n'y a pas un réseau capillaire dans les parois intérieures du tube, la phase liquide, résultée par condensation, revient dans la zone de vaporisation et ainsi les cycles peuvent continuer.

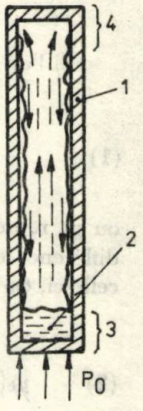

Fig. 1

Selon sa construction, la conductivité thermique équivalente de ce dispositif-ci peut prendre des valeurs très hautes [1], de toute façon agrandies par rapport aux celles qui caractérisent les métaux. Par conséquence, le flux thermique transféré par un tel dispositif peut augmenter d'une telle façon que l'effet de refroidissement exercé sur une pièce chaude, en contact avec le vaporisateur, soit intensifié.

Compte tenu des particularités fonctionnelles ci-dessus, les caloducs peuvent être avantageusement utilisés comme des radiateurs thermiques [1]. À ce point de vue ils se caractérisent par de meilleures propriétés concernant le fonctionnement

en régime permanent et, aussi, par des valeurs agrandies de la vitesse de réponse thermique transitoire.

2. Echauffement en régime permanent des conducteurs

On étudie l'échauffement d'une barre métallique homogène, traversée, en régime permanent, par un courant ayant l'intensité I (Fig.2); ce conducteur est muni par un nombre de $n + 1$ radiateurs de type caloducs, emplacés à des distances égales, chacun transférant le flux thermique P_0.

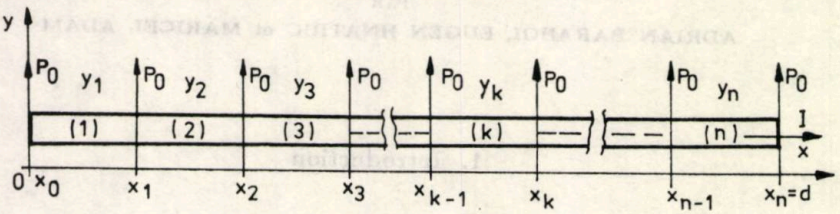

Fig. 2

Si l'on adopte la notation:

$$y_k = \frac{\theta_k}{\theta_0}, \tag{1}$$

où y_k représente la température normée de la zone k, $(k = 1, 2, ..., n)$, θ_k – la différence de température produite par l'échauffement en régime permanent de celle-ci, θ_0 – une valeur de référence pour la température, on peut écrire [2]:

$$y_k(x) = A_k e^{ax} + B_k e^{-ax} + \frac{b^2}{a^2}, \quad x \in [x_{k-1},\ x_k], \quad (k = 1, 2, ..., n), \tag{2}$$

où:

$$a^2 = \frac{p\alpha_t - \rho_0 J^2 s \alpha_R}{\lambda s}, \quad b^2 = \frac{\rho_0 J^2 s + p\alpha_t \theta_a}{\lambda s \theta_0}. \tag{3}$$

Les notations utilisées dans les relations (3) ont les significations suivantes: α_t – le coefficient global de transfert de la chaleur, caractérisant la barre, s, p – la surface, respectivement la longueur du périmètre de la section transversale, ρ_0 – la résistivité du matériel à 0°C, J – la densité du courant, α_R – le coefficient thermique de la résistance, λ – la conductivité thermique, θ_a – la température ambiante.

On peut déterminer les coefficients A_k, B_k à l'aide des conditions à la limite, ayant la forme:

$$\left.\frac{dy_1}{dx}\right|_{x=0} = -\left.\frac{dy_n}{dx}\right|_{x=n} = \frac{P_0 + \alpha_t s(\theta_0 y_c - \theta_a)}{\lambda s \theta_0}, \qquad \left.\frac{d}{dx}(y_k - y_{k-1})\right|_{x=x_{k-1}} = \frac{P_0}{\lambda s \theta_0}, \tag{4}$$

$$y_1(0) = y_n(d) = y_c, \quad y_{k-1}(x_{x-1}) = y_k(x_{k-1}), \quad (k = 2, 3, \ldots, n).$$

3. Application numérique

On a calculé la possibilité d'intensifier le refroidissement d'une barre en aluminium 60×10 mm, traversée par un courant de charge ayant l'intensité $I = 1000$ A.

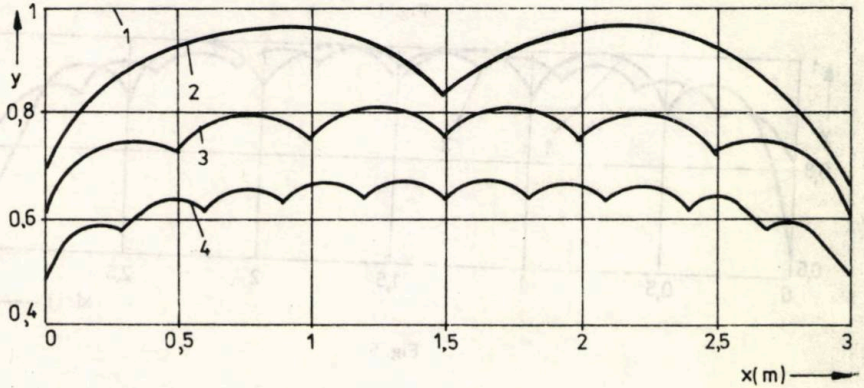

Fig. 3

Dans la Fig. 3 on a représenté graphiquement, à titre de comparaison, les courbes de l'échauffement $y(x)$, obtenues par voie de calcul, dans des conditions différentes: *1* – barre initiale, *2, 3, 4* – barre munie par un certain nombre de radiateurs, emplacés à distances égales, chacun transférant le flux thermique P_0=10 W.

On met en évidence la diminution de la valeur maximum, y_m, de la température, due à l'accroissement du nombre de radiateurs utilisés.

Si l'on note avec P le flux thermique total, cédé par les radiateurs:

$$P = (n+1)P_0, \tag{5}$$

on peut étudier l'influence de ce flux-ci sur la valeur maximum, y_m, de la température; les résultats des calculs sont représentés dans la Fig.4. On constate que, pour des valeurs raisonnables du flux thermique P, la valeur maximum de la température, enregistrée sur la barre fonctionnant avec des radiateurs, peut accuser une diminution d'environ 40% par rapport à celle de la barre initiale.

On met en évidence, aussi, que pour une valeur donnée du flux thermique, P, la diminution de la valeur maximum de la température s'avère plus forte si l'on utilise un nombre agrandi de radiateurs, caractérisés par des valeurs plus faibles du flux thermique, P_0.

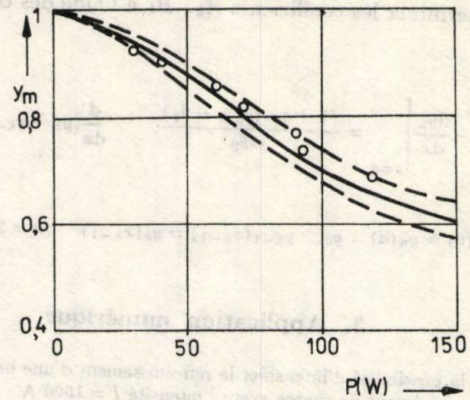

Fig. 4

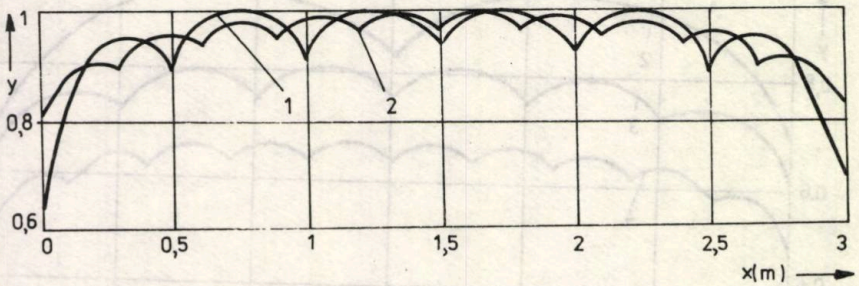

Fig. 5

L'intensification du refroidissement permet l'augmentation de l'intensité du courant de charge. Dans la Fig.5 sont représentées les courbes d'échauffement calculées pour la même barre, munie par 6 radiateurs avec $P_0 = 18,5$ W (courbe *1*), respectivement 11 radiateurs avec $P_0 = 10$ W (courbe *2*), mais, cette fois, obtenues pour une surcharge de 25% en courant ($I = 1\,250$ A).

4. Conclusions

On présente une possibilité d'intensifier le refroidissement des conducteurs, traversées par des courants de charge, à l'aide des radiateurs de type caloduc.

On met en évidence que, par cette voie et dans des conditions acceptables concernant la construction des radiateurs, la diminution de la température peut atteindre des valeurs jusqu'à 40%; par conséquence on peut compter sur l'accroissement, d'environ 25%, du courant de charge.

La solution proposée s'avère utile dans le cas des conducteurs fonctionnant temporairement surchargées. La même solution peut être appliquée dans le but d'uniformiser l'échauffement au long des conducteurs hétérogènes sous rapport thermique; en ce qui concerne ce dernier cas, les radiateurs peuvent être emplacés,

par exemple, dans les zones des contacts électriques [3].

Reçue le 11 juin 1993

Université Technique „Gh. Asachi", Jassy, Chaire d'Énergétique

BIBLIOGRAPHIE

1. B i l e g a n I.C., *Tubul termic.* Ed. Tehn., Bucureşti, 1983.
2. S u c i u I., *Bazele calculului solicitărilor termice ale aparatelor electrice.* Ed. Tehn., Bucureşti, 1981.
3. B a r a b o i A., A d a m M., H n a t i u c E., L e o n t e P., *Utilizarea tuburilor termice în construcţia contactelor electrice.* III-ème Symp. „Optimisation de l'exploitation et du développement des installations énergétiques", Jassy, 1991, **III**, 209.

INTENSIFICAREA RĂCIRII CĂILOR DE CURENT CU AJUTORUL TUBURILOR TERMICE

(Rezumat)

Se studiază regimul permanent de încălzire prin efect J o u l e – L e n z a unui conductor omogen, în ipoteza amplasării, din loc în loc, pe lungimea acestuia, a unor radiatoare de tip tub termic.

Se evidenţiază, prin exemple de calcul, efectul de aplatizare a curbelor de repartiţie a temperaturii în lungul conductorului, de unde rezultă posibilitatea supraîncărcării acestuia în curent.

BULETINUL INSTITUTULUI POLITEHNIC DIN IAŞI
Tomul XL (XLIV), Fasc. 1–4, 1994
Secţia III
ELECTROTEHNICĂ. ENERGETICĂ. ELECTRONICĂ

C.D. 537.523.5

SUR LE BILAN DES PUISSANCES POUR LES INSTALLATIONS D'ALIMENTATION DES GÉNÉRATEURS DE PLASMA FROID DE TYPE „GLIDARC"

PAR
EUGEN HNATIUC, ALBIN CZERNICHOWSKI,
JEAN-MARIE CORMIER et FRÉDÉRIC RICHARD

1. Introduction

Le fonctionnement des générateurs de plasma froid de type GLIDARC, réalisés par une équipe de chercheurs de l'Université d'Orléans, assure une décharge de haute tension (1...4 KV) et de faible courant (1...10 A), entre les électrodes de l'installation, situées dans une tuyère dans laquelle circule un gaz, qui permet d'y obtenir de nombreuses espèces excitées très réactives et intéressantes pour diverses applications de chimie et de dépollution.

Afin de mettre en valeur les qualités des réacteurs électrochimiques et pour imposer leur utilisation dans l'industrie il faut tout d'abord améliorer les performances énergétiques de ces installations, vu que la tension électrique d'amorçage, par exemple, est beaucoup plus grande que celle de la décharge.

Dans ce qui suit on présente des informations concernant la mesure des puissances électriques dans une installation GLIDARC, pour mieux évaluer le rendement de celle-ci.

2. Alimentation électrique des réacteurs GLIDARC

Le schéma électrique pour l'alimentation des réacteurs GLIDARC en courant alternatif monophasé (Fig.1) comporte tant le transformateur T (220 V/5000 V) que l'autotransformateur AT qui assure le réglage de la tension sur les électrodes.

La puissance active absorbée du réseau est mesurée à l'aide du wattmètre W_1 et la puissance qu'on retrouve dans la décharge est indiquée par le wattmètre W_2. La même puissance électrique dans la décharge peut être évaluée à l'aide d'un

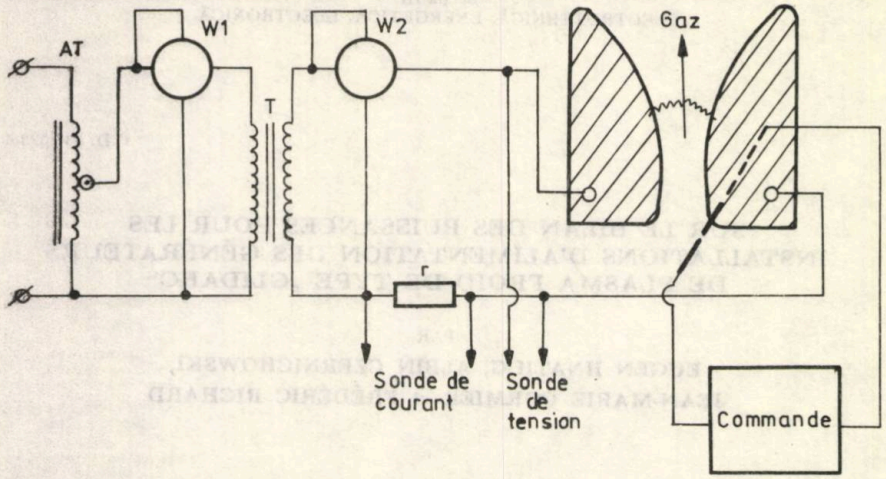

Fig. 1

oscilloscope numérique à quatre voies type GOULD 1604; l'aquisition des tensions se réalise par l'intermédiaire des sondes ayant le rapport de division 1:1 000 tandis que celle des courants est obtenue à l'aide des sondes à effet Hall (LEM–Suisse), les enregistrements comportant 10 240 points pour une voie. La courbe de la puissance instantanée en fonction du temps est calculée point par point après le transfert des informations vers un ordinateur; la puissance moyenne est déduite en calculant la valeur moyenne de la courbe de la puissance instantanée sur les 10 240 points (Fig.2).

Si on change soit le débit du gaz soit le réglage électrique (tension où courant), on modifie la puissance P_1 indiquée par W_1 et bien sûr aussi la puissance de la décharge, P_2, indiquée par W_2.

À souligner qu'il y a de grosses différences entre les valeurs P_2 indiquées par W_2 et celles obtenues à l'aide de l'ordinateur, qu'on peut les justifier par les composants harmoniques de la tension de la décharge (Fig.2). Les taux des composants harmoniques pour une tension ayant la forme indiquée dans la Fig.2 sont évaluées à partir de la Fig.3, obtenue à l'aide du même ordinateur et sont présentés dans le Tableau 1.

Tableau 1

Taux des composants harmoniques

Ordre de l'harmonique	I	II	III	IV	V	VI	VII	VIII	IX
U, [%]	80,50	9,000	53,100	–	7,50	–	21,00	–	11,000
B, [%]	97,43	5,446	21,420	–	1,81	–	3,63	–	1,479
I, [%]	84,24	7,560	51,468	6,3	9,45	–	7,35	–	3,781

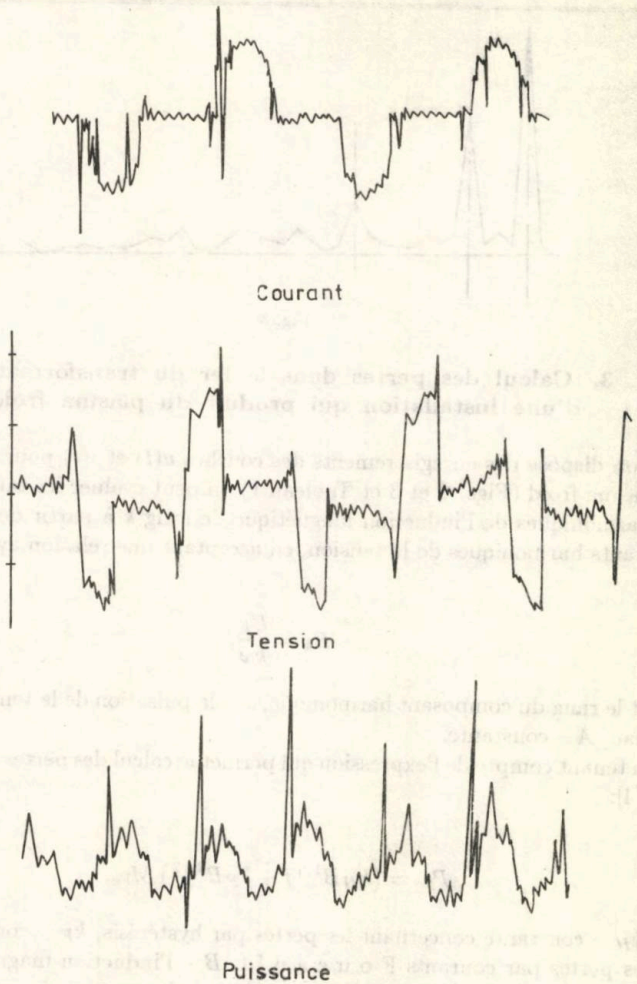

Fig. 2

Évidemment il faut tenir compte de ces composants harmoniques de la tension de décharge pour calculer d'une façon plus précise les pertes dans le noyau de fer du transformateur si on désire de mieux évaluer les performances énergétiques d'une installation GLIDARC.

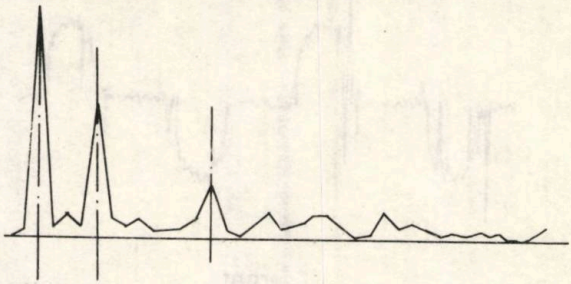

Fig. 3

3. Calcul des pertes dans le fer du transformateur d'une installation qui produit du plasma froid

Si on dispose des enregistrements des courbes $u(t)$ et $i(t)$ pour des décharges type plasma froid (Figs. 2 et 3 et Tableau 1) on peut évaluer les taux des composants harmoniques de l'induction magnétique de rang k à partir des taux U_k des composants harmoniques de la tension, en acceptant une relation ayant la forme:

$$B_k = \frac{U_k}{k\omega}, \tag{1}$$

ou k est le rang du composant harmonique, ω – la pulsation de la tension électrique du réseau, A – constante.

En tenant compte de l'expression qui permet le calcul des pertes dans un noyau de fer [4]:

$$P_{\mathrm{Fe}} = \left(k_H B^{1,6} f + k_F B^2 f^2\right) M_{\mathrm{Fe}}, \tag{2}$$

avec: k_H – constante concernant les pertes par hystérésis, k_F – constante concernant les pertes par courants F o u c a u l t, B – l'induction magnétique dans le noyau de fer, f – la fréquence de la tension, M_{Fe} – la masse de fer, on peut évaluer les pertes pour chaque composant harmonique de rang k:

$$P_{\mathrm{Fe}k} = \left(k_H B_k^{1,6} k f + k_F B_k^2 k^2 f^2\right) M_{\mathrm{Fe}}, \tag{3}$$

et par conséquent les pertes totales sont:

$$P_{\mathrm{Fe}}^{\Sigma} = \sum_{i=1}^{n} P_{\mathrm{Fe}k} \tag{4}$$

Les valeurs P_{Fe}^{*} ainsi obtenues dépassent sensiblement celles qui correspondent à des signaux supposés sinusoïdaux, pour le même transformateur (vers 20 W); cet aspect est confirmé par le bilan des puissances pour une telle installation (Tableau 2).

Tableau 2
Bilan des puissances

P_1 W	ΔP_1 W	P_2 W	ΔP_2 W	P_{Fe} W	$(P_2 + \Delta P_1 + \Delta P_2 + P_{Fe})/P_1$
1125	564,48	354,47	145,46	60	0,99947
1867,5	933,12	450,98	372,38	65	0,9753589
2025	1076,48	423,82	391,24	70	0,9686597

On propose de substituer la relation (2) pour le calcul des pertes dans le fer du noyau par une expression plus simple ayant la forme:

$$P'_{Fe} = Q f^{\alpha} B^{\beta} M_{Fe}, \tag{5}$$

où on conserve les notations de la relation (2) et on ajoute les coefficients Q, α, β, qu'on peut les déterminer.

Si on analyse les valeurs de α et β indiquées dans les Tableaux 3 et 4 on peut affirmer que ces coefficients sont peu sensibles aux changements usuels de la fréquence f où de l'induction magnétique B.

Tableau 3
Valeurs des coefficient α

B, [T] / f, [Hz]	0,1	0,2	0,3	0,4	0,6	0,8	1,0	1,2	1,4
25...75	1,903	1,916	1,927	1,935	1,944	1,950	1,954	1,957	1,959
50...150	1,942	1,956	1,962	1,966	1,971	1,974	1,976	1,978	1,980
100...300	1,970	1,977	1,980	1,983	1,985	1,987	1,988	1,989	1,990
250...500	1,984	1,988	1,989	1,990	1,992	1,993	1,993	1,994	1,994

Tableau 4
Valeurs des coefficients β

f, [Hz] / B, [T]	25	50	75	100	150	200	250	300	500
0,1...0,2	1,940	1,968	1,978	1,983	1,988	1,991	1,993	1,994	1,996
0,2...0,3	1,951	1,974	1,982	1,986	1,991	1,993	1,994	1,995	1,997
0,3...0,4	1,956	1,977	1,984	1,988	1,992	1,994	1,995	1,996	1,997
0,4...0,6	1,961	1,980	1,986	1,989	1,993	1,995	1,996	1,996	1,998
0,6...0,8	1,966	1,982	1,988	1,991	1,994	1,995	1,996	1,997	1,998
0,8...1,0	1,969	1,984	1,989	1,992	1,994	1,996	1,997	1,997	1,998
1,0...1,2	1,971	1,985	1,990	1,992	1,995	1,996	1,997	1,997	1,998
1,2...1,4	1,973	1,986	1,991	1,993	1,995	1,996	1,997	1,998	1,998

4. Conclusions

On propose une méthode pour évaluer d'une façon plus précise les pertes dans le noyau de fer des installations à plasma froid (GLIDARC) à partir des composants harmoniques de la tension, ayant le but de mieux estimer les performances énergétiques de l'ensemble. Les résultats du calcul sont bien confirmés par des mesures dans une installation type GLIDARC.

On propose également une relation plus simple qui permet de déterminer les pertes dans le noyau de fer, bien soutenue par les faibles influences des valeurs de la fréquence et de l'induction magnétique sur les exposants α et β de la relation (5).

Reçue le 21 décembre 1993

Université Technique „Gh. Asachi", Jassy,
Chaire d'Energétique
et
Université d'Orléans, France

BIBLIOGRAPHIE

1. Savin Gh., Rosman H., *Circuite electrice neliniare şi parametrice.* Ed. Tehnică, Bucureşti, 1973.
2. Chapelle J., Czernichowski A., *Traitement des gaz par décharges froides à haute pression.* R.G.E., *2* (1993).
3. Puşcaşu S., Marcovici J., *Mărimi şi regimuri electrice nesinusoidale.* Ed. Scrisul Românesc, Craiova, 1974.
4. Taev I.S., *Osnovy teorii električeskih apparatov.* Izd. Vysšaia Škola, Moskva, 1987.

CU PRIVIRE LA BILANŢUL DE PUTERI ÎN INSTALAŢIILE DE ALIMENTARE A GENERATOARELOR DE PLASMĂ RECE DE TIP „GLIDARC"

(Rezumat)

Se urmăreşte evaluarea randamentului instalaţiilor de alimentare a reactoarelor electrochimice cu plasmă rece, ca indicator al performanţelor acestora. Pentru evaluarea mai precisă a pierderilor în fier se propune considerarea spectrului de armonici din componenţa inducţiei magnetice din miez, ce poate fi estimat dacă se dispune de înregistrarea dependenţei de timp a tensiunii electrice din secundarul transformatorului de alimentare.

BULETINUL INSTITUTULUI POLITEHNIC DIN IAŞI
Tomul XL (XLIV), Fasc. 1–4, 1994
Secţia III
ELECTROTEHNICĂ. ENERGETICĂ. ELECTRONICĂ

D.C. 621.313.2-9

SHUNTING OF THE ARMATURE OF THE SEPARATELY EXCITED D.C. MOTOR*)

BY

MIRCEA-SORIN OPRIŞOR and ANA-SIMONA CABA

1. Introduction

The shunting of the d.c. motor armature, for all excitation types, is known as a method for obtaining reduced speeds. The rigidity of the mechanical characteristics obtained by this way is comparable with that obtained during the adjustment of the rotor voltage, but the installation is cheaper.

The shunting regime of the rotor is summarily and incorrectly dealt with in the specialized literature [1],...,[4] and the predetermination posibilities of the electric parameters or speed are not known.

The aim of this paper is to correct the analytical representation of this speed control type. On this basis, could be established the designing conditions for obtaining a certain regime speed and a certain mechanical characteristic slope. The losses caused by this method does not influence essentialy the total losses and the system. Consequently, these are not taken into account, especially when the regime duration is small.

2. Classic Representation

The equations of the voltages

$$(1)\quad U = E + R_a I_a + R_s(I_a + I_p), \qquad (2)\quad U = R_p I_p + R_s(I_a + I_p),$$

are valid for the separately excited d.c. motor, supplied according to the diagram presented in Fig.1. The speed of the armature, obtained from here, is

$$(3)\quad \Omega = r\Omega_0 - \Delta'\Omega,$$

where

*) Presented at the Eighth National Conference of Electrical Drives, Jassy, Romania, October 22-24, 1992.

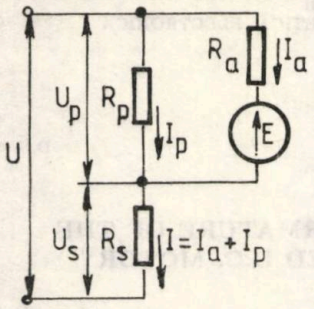

Fig. 1.– The diagram for classic representation of the shunting of the armature of the separately excited d.c. motor.

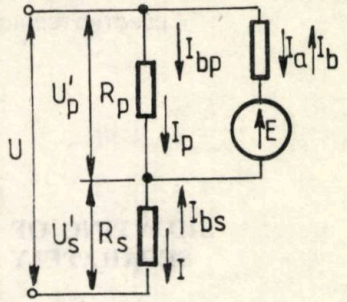

Fig. 2.– The diagram for the corrected representation of the in Fig.1 indicate case.

$$r = \frac{R_p}{R_s + R_p} = \frac{1}{1 + R_s/R_p} < 1. \tag{4}$$

The Eq.(3) represents a motor-regime machine supplied with a reduced voltage $rU < U$. By shunting the armature, the ideal idle running speed decrease:

$$r\Omega_0 = r\frac{U}{K} \tag{5}$$

and the speed drop increase:

$$\Delta'\Omega = \frac{R_a I_a}{K} f \tag{5'}$$

by multiplying with the factor

$$f = 1 + r\frac{R_s}{R_a} = 1 + \frac{1}{1/R_s + 1/R_p} \cdot \frac{1}{R_a} = 1 + \frac{R_{ext}}{R_a} > 1. \tag{6}$$

R_{ext} represents the resistance of the machine external circuit, where R_s and R_p are seen in derivation. This would presume that I_a passes partially through R_s (in the direction mentioned in Fig.1) and partially through R_p (in the reverse direction as I_p), a fact difficult to be admitted and not taken into account in Eqs.(1), (2). The diminishing of the speed, given by Eq.(3), assumes the decrease of the ratio r and the increase of the factor f. With this end in view, R_s must increase, because the variations of R_p determine opposite effects by means of the r and f values. Taking in consideration the potential difference at the terminals of the resistance R_p, we obtain, by using Eq.(1):

$$U_p = R_p I_p = R_a I_a + E = U - R_s(I_a + I_p). \tag{7}$$

From here it results:

$$I_a = \frac{U - (E + R_s I_p)}{R_a + R_s}, \tag{8}$$

$$I_p = \frac{U - R_s I_a}{R_s + R_p}. \tag{9}$$

One can notice that an increased value of R_s diminishes both currents I_a and I_p, a fact explainable by their compounding on R_s, but an increased value of R_p determines only the decrease of I_p. Considering the other two solutions given by Eq.(7):

$$I_a = \frac{U}{R_s} - \left(1 + \frac{R_p}{R_s}\right) I_p, \tag{10}$$

$$I_p = \frac{U - [E + (R_a + R_p) I_a]}{R_s}, \tag{11}$$

the variation of R_p is apparently once again contradictory.

From the above discussed problems, it does not result the superimposing of a dynamic braking regime on the motor regime. If we admit that the introduction of the resistances R_s and R_p in the diagram decreases the rotor current as compared to that of the motor supplied directly from the source, this fact could be explained only by considering the superimposing of the two working regimes.

3. Corrected Representation

We assume that the rotation direction and the E sign are kept in the shunting regime of the armature (Fig.2). Consequently, the dynamic braking current I_b has an opposite direction as compared with the rotor current for the motor regime I_a. That is why, in the shunting regime of the armature, the current for the motor regime will be:

$$I'_a = I_a - I_b. \tag{12}$$

On the external circuit, I_b is branched, being summed up partially with I_p:

$$U'_p = R_p(I_p + I_{bp}) \tag{13}$$

and decreased partially from the current supplied by the power unit:

$$U'_s = R_s(I_a + I_p) - R_s I_{bs}, \tag{14}$$

where:

$$I_b = I_{bp} + I_{bs}. \tag{15}$$

The Eqs.(13) and (14) are justified by two arguments, namely: a) the resistance R_{ext} has been seen, from the motor side, as being composed of R_p and R_s in parallel; b) the voltage at the R_p terminals is increased by the new distribution of the voltages on the resistive divider $U = U'_s + U'_p$, but the decrease of the speed imposes the increase of R_s and the decrease of R_p, i.e. a complete concordance with the adjustment necessary for the diminishing of the ideal idle running speed $r\Omega_0$.

Under this condition, the balances of the voltages on the circuits shown in Fig.2 will be:

$$U = R_p(I_p + I_{bp}) + R_s(I_a + I_p - I_{bs}), \tag{16}$$

$$U = E + R_a(I_a - I_b) + R_s(I_a + I_p - I_{bs}). \tag{17}$$

Replacing I_p from Eq.(16) into Eq.(17), we obtain:

$$\Omega = r\Omega_0 - \frac{R_a(I_a - I_b)}{K} f. \tag{18}$$

This means that Eq.(3) is valid only if associated with Eq.(12), by which the overlap of the dynamic braking regime is taken into account.

Decomposing the Eq.(18) and using Eq.(6), one can notice that

$$\Omega = \left[r\Omega_0 - (R_a + R_{ext})\frac{I_a}{K}\right] + (R_a + R_{ext})\frac{I_b}{K}; \tag{19}$$

the total resistance of the machine circuit $(R_a + R_{ext})$ influences, as expected, in the same degree the speed drop both in the motor regime and in the dynamic braking regime. On the other hand, it is obvious that the speed given by Eq.(19) represents the results of the direct summing of the mechanical characteristics for the motor regime and the dynamic braking one. Consequently, the resultant mechanical characteristics has a smaller slope as compared to that of the supplementary resistance motor R_{ext}, especially because of the dynamic braking. The magnitude of the resultant characteristic slope

$$\Omega = r\Omega_0 - f\left(1 - \frac{I_b}{I_a}\right)\Delta\Omega \tag{20}$$

decreases in proportion as the ratio I_b/I_a and the factor f are increased.

4. Predetermination Possibilities

Let us consider the particular case of the equality of the slopes of the natural and shunting characteristics:

$$f\left(1-\frac{I_b}{I_a}\right)=1. \tag{21}$$

It results the condition:

$$I_b=\left(1-\frac{1}{f}\right)I_a=\frac{1}{1+R_a/R_{\text{ext}}}I_a<I_a. \tag{22}$$

A higher slope of the shunting characteristic imposes an I_b lower than that given by Eq.(22). This is obtained by limiting any of its components, by increasing R_s or R_p, but with a corresponding effect on the factor f.

Subtrating Eq.(16) from (17), we find:

$$E=R_a(I_b-I_a)+R_p(I_{bp}+I_p). \tag{23}$$

The initial assumption determines the condition $E>0$ and hence:

$$I_p+I_{bp}>(I_a-I_b)\frac{R_a}{R_p}. \tag{24}$$

Based on economic reasons we can consider $I_p+I_{bp}\cong I_a$; it results:

$$I_b<\left(1-\frac{R_p}{R_a}\right)I_a \tag{25}$$

and having in view the condition (22), at limit, we obtain

$$R_p>2R_a. \tag{26}$$

From Eq.(4) it results:

$$R_s=R_p\left(\frac{1}{r}-1\right) \tag{27}$$

and for $r<0.5$ the condition

$$R_s>R_p \tag{28}$$

is deduced, for which $f<5$. The condition that the slopes of the natural and shunting characteristics should remain equal becomes:

(29) $$I_b < \frac{4}{5} I_a.$$

If, for the same reasons, we choose $I_b = I_a/2$, from Eq.(22) we obtain $f = 2$ and, from Eq.(6) it results:

(30) $$R_{\text{ext}} = rR_s = R_a.$$

Then, on the basis of conditions (26) and (27), $r < 0.5$ is imposed, a value usually searched for.

5. Experimental Tests

We have used the raising system of a table driven by a separately excited d.c. motor, with $U_n = 24$ V, $P_n = 100$ W and $R_a = 4.5\ \Omega$. The static resistant torque has been modified by varying the weight put on the table, in the domain $F = 0...10$ Kg. The linear speed, v, of the table, has been measured. The shunting of the armature has been done only when raising the table. The natural mechanic characteristics $v = f(F)$, experimentally obtained (Fig.3), for both directions (raising and descending), indicate:

(31) $$v_0 \cong 13.4 \ \text{[mm/min]}, \qquad \Delta V_{F=10} \cong 0.4 \ \text{[mm/min]},$$

i.e.:

(32) $$v = v_0(1 - 3 \times 10^{-3} F).$$

The obtaining of a mechanical characteristic with the same slope with that of the natural characteristic has been imposed, under the conditions in which:

$$r = 0.333, \quad I_b = 0.5 I_a \quad \text{and} \quad f = 2.$$

From Eqs.(30) and (27) it results:

(33) $$R_s = \frac{R_a}{r} = 13.5\ \Omega, \qquad R_p = \frac{R_s}{2} = 6.75\ \Omega.$$

From constructive reasons we adopted $R_s = 15\ \Omega$ and $R_p = 7.5\ \Omega$. In this way the condition $R_s = 3.333 R_a$ has been assured. Consequently, a reduced speed mechanical characteristic with the rigidity given by the condition (21) is obtained:

(34) $$v = 0.333 v_0 - 1.05 \times 0.04 F = v_0(1/3 - 3 \cdot 10^{-3} F), \quad \text{[mm/min]}.$$

The experimental curve shown in Fig.3 confirms this result.

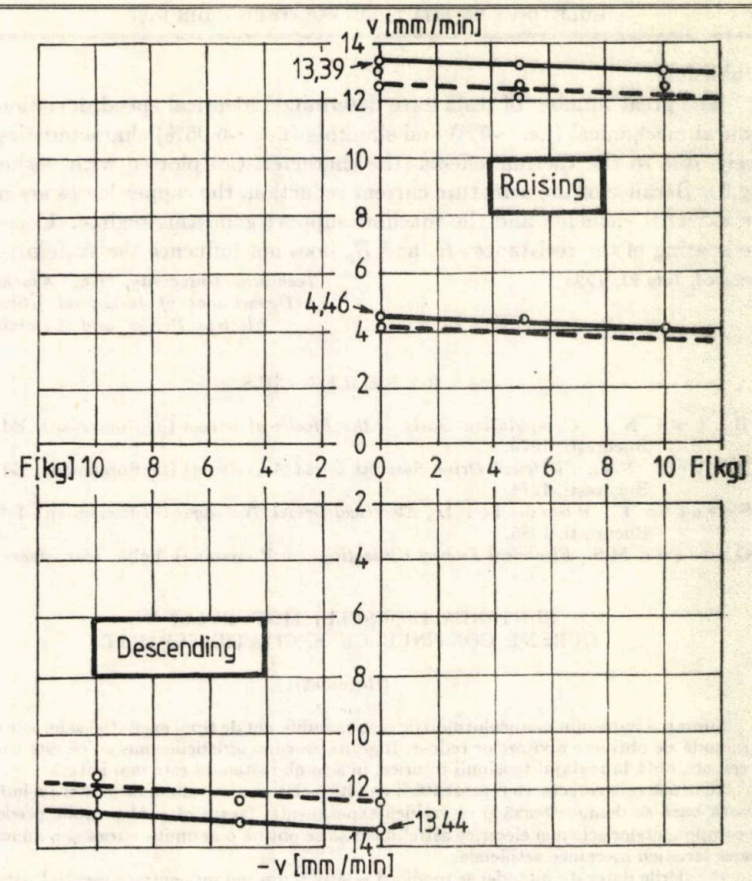

Fig. 3.– Experimentally obtained curves speed vs. resistant force in both motor and shunting regimes.

6. Conclusions

The suggested solution for the representation of the mechanical characteristics, obtained by shunting the armature of the d.c. motor, is confirmed by the accomplished experimental tests. Its was confirmed too the overlap of both motor and dynamic braking regimes.

Knowing the natural mechanic characteristic of the motor, marked by Ω_0 and $\Delta\Omega$, the armature resistance, R_a, and the current imposed by the given load, I_a, the estimations of the resistances R_s and R_p are possible; thus a certain ideal idle running speed and a certain regime speed, Ω, should be obtained. According to the examples given by Eqs.(21)...(29), some other designing conditions could be

established.

The great number of tests have determined identical speed deviations on the natural mechanical (i.e. ~6%) and shunting (i.e. ~6.05%) characteristics, respectively, due to the thermal effects (the characteristics plotted with dashed line in Fig.3). Because of the armature current reduction, the copper losses are moved on the external elements and the machine support good this regime. Consequently, the heating of the resistances R_s and R_p does not influence the system.

Received, July 21, 1993

Technical University "Gh. Asachi", Jassy,
Department of Industrial Utilizations,
Electric Drives and Automation

REFERENCES

1. Boţan N.V., *Computation Basis of the Electrical Drives* (in Romanian). Ed. Tehnică, Bucureşti, 1970.
2. Boţan N.V., *Electrical Drive Systems Speed Adjustment* (in Romanian). Ed. Tehnică, Bucureşti, 1974.
3. Seracin E., Popovici D., *Electrical Drives Technique* (in Romanian). Ed. Tehnică, Bucureşti, 1985.
4. Oprişor M.S., *Electrical Energy Utilizations* (in Romanian). Polyt. Inst., Jassy, 1992.

ŞUNTAREA INDUSULUI MOTORULUI DE CURENT CONTINUU CU EXCITAŢIE SEPARATĂ

(Rezumat)

Şuntarea indusului motorului electric de c.c., indiferent de tipul excitaţiei sale, este cunoscută ca metodă de obţinere a vitezelor reduse. Rigiditatea caracteristicilor mecanice este comparabilă cu cea obţinută la reglajul tensiunii rotorice, în schimb instalaţia este mai ieftină.

Se urmăreşte corectarea reprezentării analitice clasice a regimului de şuntare a indusului. Pe această bază se demonstrează şi se verifică experimental faptul că sunt posibile predeterminări ale componentelor schemei electrice astfel încât să se obţină o anumită viteză şi o anumită pantă a caracteristicii mecanice artificiale.

Pierderile datorate metodei se modifică relativ puţin, nu influenţiază esenţial sistemul şi nu trebuie luate în considerare atunci când durata regimului este redusă. Deoarece curentul rotoric scade, pierderile în cupru sunt deplasate pe elementele exterioare şi maşina suportă bine acest regim.

BULETINUL INSTITUTULUI POLITEHNIC DIN IAŞI
Tomul XL (XLIV), Fasc. 1–4, 1994
Secţia III
ELECTROTEHNICĂ. ENERGETICĂ. ELECTRONICĂ

C.D. 537.314; 621.317.736

QUELQUES ASPECTS THÉORIQUES CONCERNANT LA PROPAGATION DES SIGNAUX ÉMIS PAR LES INDICATEURS DE DÉFAUT SUR LES LIGNES DE MOYENNE TENSION

PAR

C. ASAFTEI, N. GAVRILAŞ, MIRCEA GUŞĂ et MARCEL ISTRATE

1. Introduction

La localisation à distance des défauts d'isolement dans une ligne électrique de moyenne tension suppose l'émission et la réception des signaux électriques qui se transmettent sur les conducteurs de phase [1].

L'évaluation du niveau du signal à la réception, en partant du niveau du signal dans le point d'émission, représente un problème important de ce système de signalisation. Il faut préciser que cette évaluation peut être réalisée facilement par des essais, mais l'étude théorique préliminaire s'impose. À l'aide d'une telle étude on peut tirer au clair le phénomène de la propagation des signaux sur les lignes de moyenne tension, les facteurs dont l'influence est importante et finalement on peut obtenir une limitation des essais nécessaires.

L'étude théorique complète doit considérer tous les éléments qui exercent une influence sur la propagation des signaux sur la ligne: la présence des dérivations sur l'axe principal et des dérivations aux dérivations, les transformateurs aux extrémités des dérivations, les caractéristiques du défaut (lieu, type, résistance de terre), les paramètres électriques et géometriques de la ligne, l'influence de la terre, etc.

On envisage l'utilisation d'une méthode de calcul grapho-analytique en réunissant la méthode des ondes directes et reflétées et celle des composantes modales.

2. Analyse modale dans l'étude de la propagation des signaux électriques le long des lignes

La méthode des ondes directes et reflétées est basée sur la solution des équations des télegraphistes.

Pour une ligne de longueur infinie, la solution du système d'équations, concernant la tension entre les conducteurs (dans le point x) est donnée par la relation connue [2]:

$$\|\underline{U}\| = \|\underline{U}_1\| e^{-\|\underline{\gamma}_u\| x}, \tag{1}$$

ou $\|\underline{\gamma}_u\|$ est la matrice des coefficients de propagation exprimés commes grandeurs de phase et $\|\underline{U}_1\|$ – la tension à l'entrée de la ligne.

Pour le cas d'un système de signalisation sur une ligne de longueur finie, l, en considérant le signal émis à l'entrée de la ligne, $x = 0$, $U(0)$, le signal à la sortie (tout près du récepteur, $x = l$) sera

$$\|\underline{U}(l)\| = \|\underline{U}(0)\| e^{-\|\underline{\gamma}_u\| l}. \tag{2}$$

Dans cette rélation $\|\underline{U}(l)\|$, $\|\underline{U}(0)\|$ sont les vecteurs tension dans les points considérés $x = l$ et $x = 0$.

Il est difficile d'obtenir les expressions des ondes directes de tension de phase pour les conditions réelles de propagation. Une simplification considérable du calcul offre l'analyse utilisant les composantes modales. L'expression de l'onde directe de tension, écrite en composantes modales, est similaire à la relation (2):

$$[\underline{U}_m(l)] = [e^{-\underline{\gamma}_m l}][\underline{U}_m(0)], \tag{3}$$

où $[\underline{U}_m(l)]$, $[\underline{U}_m(0)]$ représentent les vecteurs de tension, en composantes modales, dans les points $x = l$, respectivement $x = 0$; $[\underline{\gamma}_m]$ est la matrice de propagation modale [3].

En partant des relations qui expriment la liaison entre les composantes de phase et modales pour les tensions et tenant compte des relations (2) et (3), on peut obtenir la liaison entre les ondes directes de tension écrites en composantes de phase:

$$\|\underline{U}_d(l)\| = [T_u][\underline{U}_m(l)] = [T_u][e^{-\gamma_m l}][\underline{U}_m(0)] =$$
$$= [T_u][e^{-\gamma_m l}][T_u]^{-1}\|\underline{U}(0)\| = [F]\|\underline{U}(0)\|,$$

où $[T_u]$ est la matrice de conversion en composantes modales; $[F] = [T_u][e^{-\gamma_m l}][T_u]^{-1}$ – la matrice de transfert.

Maintenant on peut poser le problème de trouver les éléments de la matrice $[F]$. Tout d'abord il faut déterminer les éléments des matrices $[\gamma_m]$ et $[T_u]$. Dans ce but on commence avec la definition de la matrice modale des coefficients de propagation

$$[\gamma_m]^2 = [T_u]^{-1}\|\underline{\gamma}_u\|^2[T_u],$$

tenant compte du fait que cette matrice doit être diagonale. À cause de cette condition, les éléments de la matrice $[\gamma_{-m}]$ seront les valeurs propres de la matrice $\|\underline{\gamma}_u\|^2$ tandis que les éléments de la matrice $[T_u]$ seront les vecteurs propres correspondants. Ainsi on peut déterminer directement le vecteur des ondes directes de tension dans un point de la ligne en connaissant le vecteur des tensions dans

le point d'émission en composantes de phase et les coefficients de propagation en composantes modales.

La méthode des ondes directes et reflétées dans sa forme particulière – la méthode du diagramme-latice – permet d'établir le niveau du signal dans un point quelconque de la ligne comme résultat des reflexions multiples.

On peut calculer, pour un réseau complexe, les valeurs de la tension dans un noeud, pour un certain moment, avec la relation

$$\|\underline{U}_i\| = \sum_j \|\underline{\alpha}_{ij}\| \|\underline{U}_{ji}\|,$$

où: α_{ij} sont les coefficients de reflexion dans le noeud i pour la branche de liaison avec le noeud j; U_{ji} – les ondes directes de tension qui arrivent dans le noeud i, provenant du noeud j.

Les ondes reflétées provenues du noeud i vers le noeud j ont l'expression

$$\|\underline{U}_{ij}\| = \|\underline{U}_i\| - \|\underline{U}_{ji}\|.$$

3. Considérations sur le schéma équivalent du réseau

Pour effectuer les calculs ci-dessus il faut établir le schéma équivalent du réseau de moyenne tension contenant l'axe principal, les dérivations, les transformateurs, etc. Un transformateur MT/BT sera modélé comme une capacité de 500...3000 pF [4]. L'impédance phase – terre équivalente de cette capacité, pour les fréquences basses (jusqu'à l'ordre des KHz), est assez grande (de l'ordre des KΩ) de sorte qu'on peut négliger l'influence du transformateur.

En ce qui concerne une dérivation, son impédance d'entrée dépend de la valeur du rapport entre sa longueur et la longueur d'onde du signal qui la parcourt.

On peut calculer l'impédance d'entrée d'une ligne sans pertes avec la relation connue

$$\underline{Z}_i = -\mathrm{j}Z\mathrm{ctg}\beta l = -\mathrm{j}Z\mathrm{ctg}2\pi\frac{l}{\lambda},$$

où: β est le coefficient de phase, λ – la longueur d'onde du signal utile, l – la longueur de la ligne, Z – l'impédance d'onde de la ligne. La valeur de l'impédance d'entrée devient nulle si la longueur de la ligne est un multiple impair de $\lambda/4$, c'est à dire $l = (2k+1)\lambda/4$. Dans cette situation l'entrée d'une dérivation sera un point directement relié à terre, ce qui diminue fortement le niveau du signal utile. Par exemple, on connaît la correspondance suivante entre différentes fréquences et les longueurs minima de ligne ($k = 0$) pour lesquelles $\underline{Z}_i \to 0$:

f, [KHz]	4	8	12	16
$l_{\min}$, [Km]	18,75	9,38	6,25	4,69

Ayant en vue que les dérivations des réseaux de moyenne tension sont assez courtes, afin d'éviter un phénomène de forte diminution du signal utile, on préfère les basses fréquences pour le signal de l'émetteur. Ce résultat est valable aussi pour l'axe principal.

Les considérations ci-dessus tirent au clair les difficultés de l'étude théorique de la propagation des signaux électriques sur une ligne de moyenne tension. Il est très utile d'adopter certaines hypothèses pour simplifier le schéma équivalent en vue de diminuer les calculs sans affecter le sens des résultats.

4. Conclusions

L'analyse théorique de la propagation des signaux émis par des dispositifs émetteurs installés sur les lignes de moyenne tension, faisant partie des systèmes de localisation des défauts, est importante pour déceler les facteurs qui exercent une influence sur ce processus.

L'étude rigoureuse est particulièrement difficile dans le cas des lignes de moyenne tension à cause de la complexité du schéma équivalent. Pourtant, cette étude théorique est possible, en utilisant l'analyse modale, avec la considération des phénomènes de reflexion dans les noeuds de la ligne, pour un schéma simplifié. On présente la succession des étapes du calcul et quelques indications sur le choix de la fréquence du signal utile.

Reçue le 18 mai 1993

Université Technique „Gh. Asachi", Jassy, Chaire d'Energétique

BIBLIOGRAPHIE

1. Asaftei C., Guşă M., Gavrilaş N., *Contributions to Centralized Short-Circuits Signalling in Medium Voltage Overhead Electric Lines.* Conférence Nationale de l'Énergie, juin 1992, Neptun, Roumanie.
2. Péricart J., *L'étude des lignes polyphasées nonsymmétriques à l'aide du calcul matriciel.* R.G.E., *1* (1959).
3. Cristescu D., Oláh R., *Supratensiuni şi izolaţia reţelelor electrice.* EDP, Bucureşti, 1983.
4. * * * *Directives pour la représentation des éléments d'un réseau lors du calcul des phénomènes transitoires.* Electra, *128* (1980).

ASPECTE TEORETICE CU PRIVIRE LA PROPAGAREA SEMNALELOR EMISE DE INDICATOARELE DE DEFECT PE LINIILE DE MEDIE TENSIUNE AERIENE

(Rezumat)

Sistemele de semnalizare centralizată a producerii defectelor de tip scurtcircuit în reţelele aeriene de medie tensiune reprezintă o etapă avansată de supraveghere a exploatării acestora, în vederea reducerii duratelor întreruperilor în furnizarea energiei. Buna lor funcţionare este condiţionată de recepţionarea unui semnal de calitate, în condiţiile dificile ale acestor reţele.

Studiul teoretic al propagării este deosebit de dificil datorită schemei echivalente complicate. Folosind însă o schemă simplificată şi aplicând metoda componentelor modale cu considerarea reflexiilor în punctele nodale, se pot obţine rezultate utile, care pot fi folosite la proiectarea echipamentelor sistemului de semnalizare.

BULETINUL INSTITUTULUI POLITEHNIC DIN IAŞI
Tomul XL (XLIV), Fasc. 1–4, 1994
Secţia III
ELECTROTEHNICĂ. ENERGETICĂ. ELECTRONICĂ

D.C. 538.551.3; 517.512; 621.316.1

SOME ASPECTS ABOUT THE SPECTRAL ANALYSIS OF LOAD CURVES OF ELECTRIC DISTRIBUTION NETWORKS

BY

GH. GEORGESCU and M. GAVRILAŞ

1. Introduction

Compared to classical methods which consider as reference the maximum load, modelling demands from the nodes by means of typical load curves [1], [2] has permitted to tackle more accurate a great number of problems concerning the optimum design and use of distribution networks.

The main advantage of this method is the improvement of accuracy when calculating the energy losses and a more accurate estimation of the efficiency of those means used to reduce the losses. On the other hand the disadvantage of this approach is the increase of the number of input data, of memory used and of the computational time.

A number of recent studies has suggested new possibilities for the application of load curves in optimization problems which mainly intend to minimize energy losses in distribution networks. In this context a significant simplification of calculation may be achieved by using statistical methods based on the estimation of correlation coefficients or on the Fourier's series decomposition [3], [4].

The paper presents some results regarding the harmonic spectrum of typical load curves from distribution networks, emphasizing the utility of spectral analysis of load in optimization studies.

2. Mathematical Model

Typical load curves, representing the most probable variation of active and reactive powers consumed in a given time interval T (usually 24 hours), have been built-up for different consumers and characteristic days by statistically processing a great number of recorded diagrams [2]. Thus, the typical load curves for the urban and rural domestic consumption as well as for a series of social-cultural users (schools, hospitals, policlinics, department stores, etc.), have been obtained. For each type of consumer corresponds four typical load curves, reflecting the demand variation for four characteristic days of the year: summer (winter) – work day

(leissure day). Usually a typical load curve is represented by 24 hours levels diagram and is expressed in relative units, obtained by division to the average load.

Let be $P(t)$ and $Q(t)$ two periodical functions, representing typical load curves for active and reactive powers, with a period T; these could be decomposed in Fourier's series as follows:

$$(1)\quad \begin{cases} P(t) = \overline{P} + \sum\limits_{K=1}^{N} A_K^P \sin\left(\frac{2K\pi}{T}t\right) + \sum\limits_{K=1}^{N} B_K^P \cos\left(\frac{2K\pi}{T}t\right), \\ Q(t) = \overline{Q} + \sum\limits_{K=1}^{N} A_K^Q \sin\left(\frac{2K\pi}{T}t\right) + \sum\limits_{K=1}^{N} B_K^Q \cos\left(\frac{2K\pi}{T}t\right). \end{cases}$$

Here: N – number of harmonics taken into consideration; t – time variable ($t = 1, \ldots, T$); $\overline{P}$, $\overline{Q}$ – average values for active and reactive powers over period, T; A_K^P, B_K^P, A_K^Q, B_K^Q – Fourier's coefficients, corresponding to harmonic K, for active and reactive powers respectively.

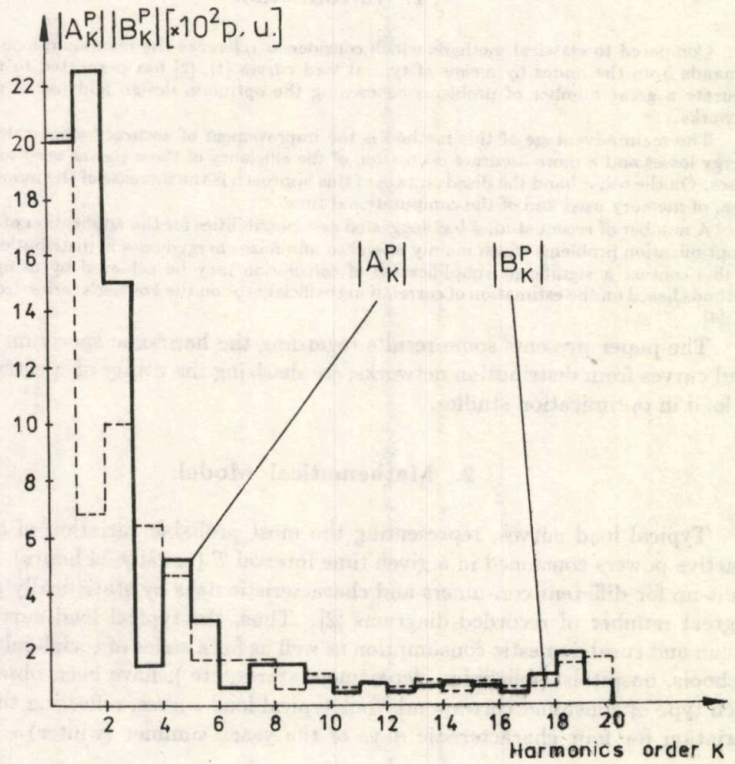

Fig. 1

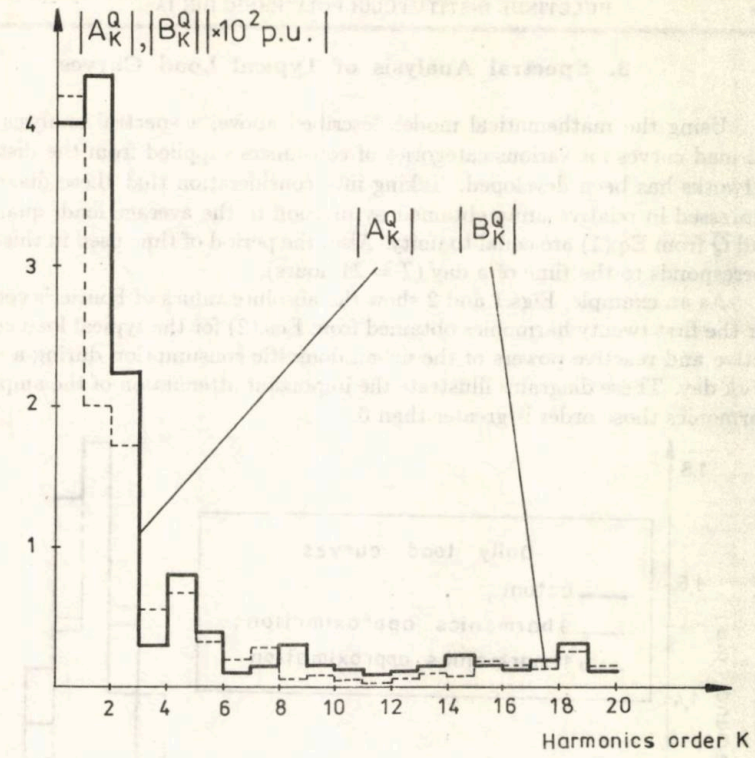

Fig. 2

The Fourier's coefficients could be determined using the well known equations:

$$(2)\quad \begin{cases} A_K^P = \frac{1}{K\pi} \sum_{t=1}^{T} P_t \left[\cos \frac{2K\pi}{T}(t-1) - \cos \frac{2K\pi}{T} t\right], \\ B_K^P = \frac{1}{K\pi} \sum_{t=1}^{T} P_t \left[\sin \frac{2K\pi}{T} t - \sin \frac{2K\pi}{T}(t-1)\right], \\ A_K^Q = \frac{1}{K\pi} \sum_{t=1}^{T} Q_t \left[\cos \frac{2K\pi}{T}(t-1) - \cos \frac{2K\pi}{T} t\right], \\ B_K^Q = \frac{1}{K\pi} \sum_{t=1}^{T} Q_t \left[\sin \frac{2K\pi}{T} t - \sin \frac{2K\pi}{T}(t-1)\right], \end{cases}$$

where P_t and Q_t are the active and reactive powers from level t of the typical load curves.

3. Spectral Analysis of Typical Load Curves

Using the mathematical model described above, a spectral analysis of typical load curves for various categories of consumers supplied from the distribution networks has been developed. Taking into consideration that these diagrams are expressed in relative units obtained by division to the average load, quantities $\overline{P}$ and $\overline{Q}$ from Eq.(1) are equal to unity. Also, the period of time used in this analysis corresponds to the time of a day ($T = 24$ hours).

As an example, Figs.1 and 2 show the absolute values of Fourier's coefficients for the first twenty harmonics obtained from Eqs.(2) for the typical load curves for active and reactive powers of the urban domestic consumption during a summer-work day. These diagrams illustrate the important attenuation of the amplitude of harmonics those order is greater than 6.

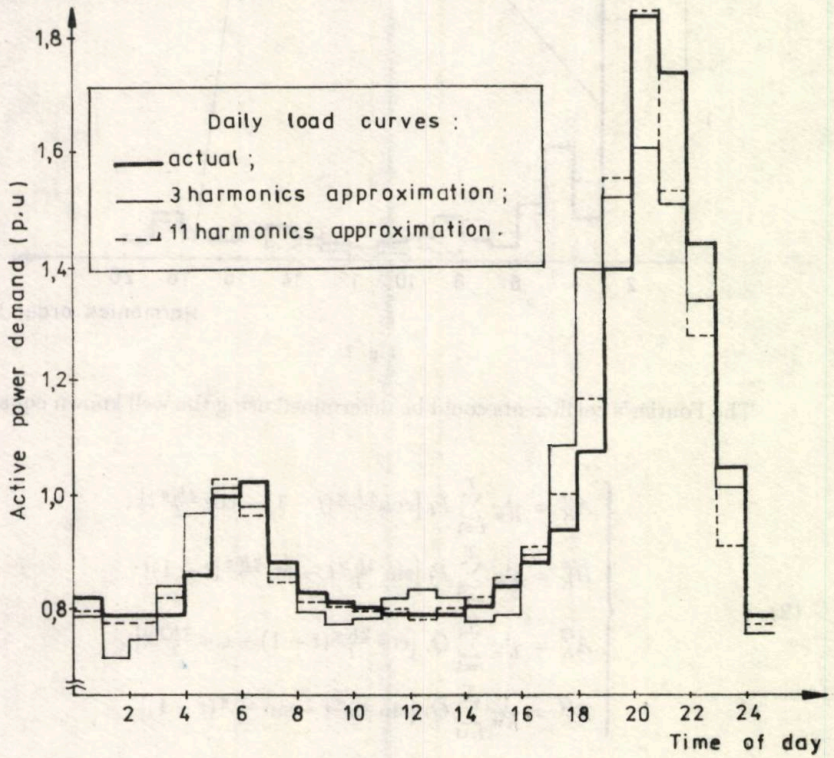

Fig. 3

Using the value of Fourier's coefficients thus determined, the approximated load curves for the same type of consumer and the same regime has been obtained

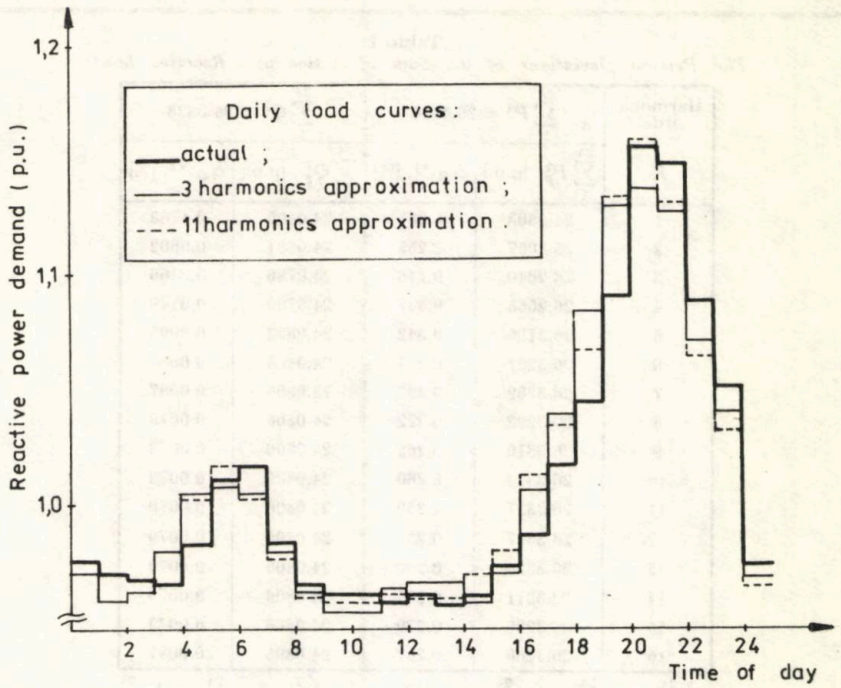

Fig. 4

considering 3 and 11 harmonics respectively. The obtained results are shown in Figs. 3 and 4, together with the typical diagram used as reference. The analysis of these diagrams shows little deviations of the approximated curves from the actual one. At the same time there is no significant improvement when using 11 instead of 3 harmonics.

By the way, taking also into consideration the final aim of this analysis, namely the calculation of energy losses, Table 1 shows the percent deviations of the sum of square values of active and reactive loads from the approximated diagrams with 1...16 harmonics, compared to the typical load curve. The values in this table demonstrate that is sufficient to consider only 3 harmonics, the error occurring when estimating the energy losses being less than 1%.

Similar results were obtained for other types of consumers and regimes. Consequently it can be said that for any category of consumer is sufficient an approximation of load curves using the first 3 harmonics of Fourier's series decomposition. Thus, Tables 2 and 3 ilustrate the values of Fourier's coefficients for the first 3 harmonics determined for representative consumers from the distribution networks.

Table 1

The Percent Deviations of the Sum of Active and Reactive Loads

Harmonic order	$\sum_1^{24} P^2 = 26.4010$		$\sum_1^{24} Q^2 = 24.0826$	
K	$\sum_1^{24} P_F^2$, [p.u.]	Δ_P *), [%]	$\sum_1^{24} Q_F^2$, [p.u.]	Δ_Q *), [%]
1	24.9803	5.381	24.0400	0.1765
2	25.8057	2.255	24.0681	0.0602
3	26.2040	0.746	24.0786	0.0166
4	26.2565	0.547	24.0790	0.0149
5	26.3106	0.342	24.0803	0.0095
6	26.3227	0.297	24.0805	0.0087
7	26.3252	0.287	24.0805	0.0087
8	26.3292	0.272	24.0806	0.0079
9	26.3310	0.265	24.0806	0.0079
10	26.3324	0.260	24.0806	0.0079
11	26.3327	0.259	24.0806	0.0079
12	26.3327	0.259	24.0806	0.0079
13	26.3324	0.260	24.0806	0.0079
14	26.3311	0.264	24.0806	0.0079
15	26.3296	0.270	24.0806	0.0079
16	26.3266	0.282	24.0805	0.0087

*) $\Delta_P = \left(\sum_1^{24} P^2 - \sum_1^{24} P_F^2\right) / \sum_1^{24} P^2 \times 100$; $\Delta_Q = \left(\sum_1^{24} Q^2 - \sum_1^{24} Q_F^2\right) / \sum_1^{24} Q^2 \times 100$.

Table 2

Fourier's Coefficients for an Urban Domestic Consumption

	$A_1^{P(Q)}$	$A_2^{P(Q)}$	$A_3^{P(Q)}$	$B_1^{P(Q)}$	$B_2^{P(Q)}$	$B_3^{P(Q)}$
Active power	Summer-working day					
	−0.1980	−0.2528	−0.1501	0.2064	−0.0698	−0.1032
	Summer-leissure day					
	−0.1981	−0.3008	−0.1728	0.2693	0.0357	−0.0910
	Winter-working day					
	−0.2466	−0.2047	−0.0412	0.0920	−0.1462	−0.0861
	Winter-leissure day					
	−0.2983	−0.2313	0.0001	0.0863	−0.1212	−0.0852
Reactive power	Summer-working day					
	−0.0406	−0.0439	−0.0241	0.0425	−0.0201	−0.0172
	Summer-leissure day					
	−0.0412	−0.0408	−0.0268	0.0527	0.0061	−0.0220
	Winter-working day					
	−0.0569	−0.0426	−0.0121	0.0255	−0.0257	−0.0075
	Winter-leissure day					
	−0.0586	−0.0445	−0.0010	0.0247	−0.0214	−0.0184

Table 3

Fourier's Coefficients for a Rural Domestic Consumption

	$A_1^{P(Q)}$	$A_2^{P(Q)}$	$A_3^{P(Q)}$	$B_1^{P(Q)}$	$B_2^{P(Q)}$	$B_3^{P(Q)}$
Active power	Summer-working day					
	−0.1827	−0.2481	−0.1297	0.1404	0.0022	−0.0387
	Summer-leissure day					
	−0.2727	−0.2298	−0.1341	0.0900	0.0614	−0.0202
	Winter-working day					
	−0.2889	−0.2617	−0.0221	−0.0017	−0.2735	−0.0299
	Winter-leissure day					
	−0.3046	−0.2161	−0.0432	−0.0150	−0.2112	−0.0319
Reactive power	Summer-working day					
	−0.1571	−0.1716	−0.0597	0.0906	−0.0357	−0.0235
	Summer-leissure day					
	−0.1870	−0.1431	−0.0618	0.0779	0.0271	−0.0167
	Winter-working day					
	−0.1728	−0.1609	−0.0316	0.0016	−0.1390	−0.0151
	Winter-leissure day					
	−0.2109	−0.1465	−0.0370	−0.0305	−0.1342	−0.0103

4. Conclusions

The use of load curves from the nodes of distribution networks for the optimization of their working conditions leads to the increasing of the accuracy of results. The approximation of load curves using Fourier's series decomposition method has the main advantage of making up the inputs as data bases of a reduced size.

Received, September 15, 1992

Technical University "Gh.Asachi", Jassy, Department of Energetics

REFERENCES

1. Codiasse A.M., Guillevic M., Giraud D., *Connaissance des charges moyenne tension en vue de leur prise en compte dans les études de planification.* Rev. gén. de l'électr., *7-8* (1982).
2. Georgescu Gh., Poeată Al., Poeată N., *Contribuţii la modelarea sarcinilor din nodurile reţelelor de distribuţie urbană.* Bul. Inst. polit., Iaşi, **XXIX(XXXIII)**, *1-2*, s.III (1983).
3. Cârţină Gh., Alexandrescu V., *Utilizarea modelelor statistice în optimizarea regimurilor de funcţionare ale sistemelor electroenergetice.* Energetica, *8* (1988).
4. Potrebič A.A., *Rasčet poteri energyi v električeskih setiah s učetom grafikov nagruzok.* Električestvo, *6* (1990).

CONTRIBUŢII PRIVIND ANALIZA SPECTRALĂ A GRAFICELOR DE SARCINĂ ALE REŢELELOR ELECTRICE DE DISTRIBUŢIE

(Rezumat)

În comparaţie cu metodele clasice, care folosesc ca referinţă sarcina maximă, se prezintă avantajele pe care le oferă descompunerea în serii Fourier a graficelor de sarcină din punctul de vedere al optimizării exploatării şi proiectării reţelelor electrice de distribuţie.

BULETINUL INSTITUTULUI POLITEHNIC DIN IAŞI
Tomul XL (XLIV), Fasc. 1–4, 1994
Secţia III
ELECTROTEHNICĂ. ENERGETICĂ. ELECTRONICĂ

D.C. 621.317.333.4

GENERAL CONSIDERATIONS ON THE DETECTING AND THE LOCATION OF THE SHORT-CIRCUITS ON OVERHEAD DISTRIBUTION LINES

BY

N. GAVRILAŞ, C. ASAFTEI, MIRCEA GUŞĂ et MARCEL ISTRATE

1. Introduction

The up-to-day concerns with the improvement of the electric power supplied to the consummers, especially from the point of view of the supply continuity, are well known. The evaluation refers to the number of the utility breakings and to the mean duration of the latters. Some researches [1] have proved that as far as the transport and distribution power systems are concerned the longest breakings are determined by the incidents that occur in the medium voltage systems; as nearly 34% from the total amount of the unsupplied power is caused by these ones.

These are the reasons that have lately determined to take some major measures related to the modernizing of the medium voltage systems, such as the change of the latters architecture, the increase of the reliability of their component parts, the introduction of the automatization and remote controls, the equipping with the computer technology, the improvement of the maintenance quality, and so on.

As far as our country is concerned, we have to specify that, according to the present standards, there is accepted a relatively larger duration of the utility breakings within the limits of 8...72 hours, depending of the consummers category.

Unfortunately, we lack a strict national evidence concerning the incidents that occured on the medium voltage systems.

The data registered to the F.R.E. (Electric Network Branch), Iaşi, in 1991, render evident the existence of nearly 150 utility breakings whose duration are comprised between a few and 200 minutes. The total time is of 470 hours which is too much in relation to the requirements practiced in the world.

The reduction of the breakings duration is related to the possibility of detecting the fault in the line section as fast as possible and to isolate it. The effective intervention in order to eliminate the fault occurs immediately after that. The detection of the faulty section depends upon the degree of providing the power system with switching devices. In our country, in the case of the medium voltage systems, the circuit breakers are fitted only with the outgoings of the lines in the transformer stations while in the case of the branches, there are connected just with separating switches that can be operated manually and locally. The detection of the faulty section is achieved through the method of "testing and error" that lies the successive opening of the separating switches followed by a reconnection of the automatic circuit-breaker in the station. These operations are performed until the reconnection is successfull, that is until the faulty section is separated.

This is a real tough method because it takes much time, necessary for the trouble-gang to move in the field, it disturb the consummers by repeated connections and disconnections, it leads to the early wear of the breakings due to the repeated running on the fault of these ones and so on.

As far as the power systems in our country are concerned, as for the moment being there is no anticipation to the replacement of the disconnectors on derivation with automatic switching devices, the limitation of the negative effects related to the method of "testing and error" can be performed only if it is possible to get operatively information accurate enough and related to the location of the fault and if this is achieved right immediately after the automatic disconnection of the line from the station.

To this purpose, some researches have been done in a previous paper [2] in order to implement a local signalling system for the faults on the line; the researches aim to achieve a centralized signalling of the faulty section in the station where the line is connected to the bars [3].

This system requires the disposition of some specialized devices in some points of the power system [3] that should provide and/or remote local signalling of the appearance of the insulation failure down the assembling point which allows an operative intervention in order to eliminate the fault; no further operations are performed in the system.

In what follows some achievements concerning the signalling devices are presented.

2. Functional Requirements and Principles of Performing some Local Indicators for the Section with an Insulation Failure

In order to make them useful to the operating staff, the signalling devices must meet a sequence of functional requirements, namely: a) the signalling of appearance of a short-circuit down the assembling point; b) the cancelling of this signalling, without any intervention from the part of the operating staff, the moment when the electric line is reactuated; c) reliability in time under different environmental conditions; d) an extremely simple maintenance, having in view the wide range and the great number of locations; e) extremely reduced dimensions and weight so that its connection should not influence over the present size of the lines and over their level of insulation, respectively.

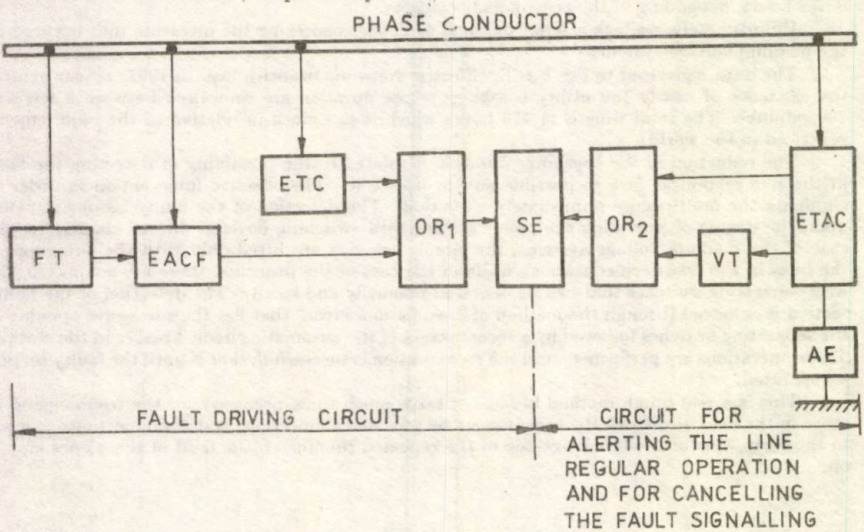

Fig. 1.– Block diagram of a signalling device.

Starting from these considerations, by means of a block diagram (Fig.1), the concern with the performing of the signalling devices are presented. In this figure were utilised the following notations: ETC – energy transfer circuit; EACF – energy accumulating circuit for fault driving; FT – fault transducer; OR_1, OR_2 – output regulators; SE – signalling element; VT – voltage transducer; ETAC – energy transfer and accumulating circuit; AE – additional element.

We have to specify that the concerned device are fitted with the control of the medium voltage lines where the neutral earthing is achieved through a resistance and where the supply is made radially. Then there are given some considerations related to the two components of the signalling device, as they where elaborated.

2.1. Fault Driving Circuit

The driving with the view of the fault signalling can be performed either by using the line potential energy previously to the fault generation or by directly using the electromagnetic energy of the short-circuit current.

In the first case, the potential energy in the condensers of the EACF block is used for driving of the OR_1. This is determined by a FT that is induced by the electromagnetic energy of the short-circuit current. As a result of this, the output regulator will determine a position reversal of the SE and thus it will physically indicate the generation of the fault, down the assembling point of the device.

In the second case, the driving of the OR_2 will be performed right by means of the electromagnetic energy of the short-circuit current that is transferred by the ETC block (for instance a current transformer).

2.2. The Circuit for Alerting the Line Regular Operation and for Cancelling the Fault Signalling (Reversal Circuit)

In order to cancel the fault state, the reversal circuit, like in the previous case, uses the energy transfered from the line after the return of the operating voltage. The signal cancelling can be performed instantaneously or with a certain delay after the return of the operating voltage.

In the first case, the AE and ETAC blocks generally constitute a voltage divider to which the OR_2 is connected. In such a case it is possible that, the moment when the operating voltage returns, the position reversal of the SE, so the cancelling of the fault signalling should be produced instantaneously.

In the second case, after the return of the operating voltage the electrostatic energy is firstly stored in the condensers of the ETAC block (the latter for instance, can be a rectifying circuit with voltage multiplication). This transfer of energy can be performed by electromagnetic induction from the load current of the phase wire or by a capacitive coupling due to the capacity currents that circulate between the phase wire and earth (in this last case, the AE is supplied by the stray capacitance between the device case and the earth).

When the direct voltage to the ETAC output block reaches the value of the starting voltage of the VT, the latter induces and determines the transfer of the

potential energy to the OR_2 that will operate the SE.

Among the variants elaborated, the "Tehnoton" Entreprise in Iaşi has made its option in order to introduce it in serial production and has chosen the variant that uses the electromagnetic energy of the short circuit current for operating in view of fault signalling. In order to cancel the signalling it uses the electrostatic energy transferred from the line by a capacitive coupling. Some of its technical characteristics are to be mentioned: the minimum fault working current $I_{min} = 40$ A and the signalling cancel time $t = 10...20$ sec.

3. Conclusions

The elaboration of the local fault indicators on the medium voltage power systems constitutes a world-wide matter of great interest having in view its obvious advantages: simple and fast detection of the faulty sections, diminution of the strain degree of the automatic circuit-breakers in the stations which means a time reduction of the utility breakings to consummers but it also means the elimination of the unpleasant faults caused by repeated reswitchings of the circuit-breakers, efficiency in use of the operating staff and so on.

In accordance with these trends, some general considerations on the necessity of elaborating such indicators as well as some original achievements are presented.

Received, May 18, 1993

Technical University "Gh. Asachi", Jassy, Department of Energetics

REFERENCES

1. L a t u r n u s G., *Politique d'EDF GDF Services en matière de qualité de la fourniture dans le domaine rural.* R.G.É., *1* (1991).
2. G u ş ă M., A s a f t e i C., G a v r i l a ş N., I s t r a t e M., *Contribuţii privind semnalizarea locală a scurtcircuitelor în reţele electrice aeriene de medie tensiune.* Energetica, *10-12* (1990).
3. A s a f t e i C., G u ş ă M., *Sur la signalisation à distance des défauts d'isolement dans les réseaux de moyenne tension.* Conférence Nationale d'Énergie, Neptun, Roumanie, 15-18 juin 1992.

CONSIDERAŢII PRIVIND DETECTAREA ŞI LOCALIZAREA SCURTCIRCUITELOR ÎN REŢELELE ELECTRICE AERIENE DE DISTRIBUŢIE

(Rezumat)

Alimentarea cu energie electrică a consumatorilor din zonele rurale nu s-a bucurat de aceeaşi preocupare în privinţa calităţii ca în mediul urban şi industrial. În ultimul timp se fac eforturi pentru corectarea acestei situaţii, unul din mijloace fiind şi reducerea la minimum a duratei întreruperilor. Folosirea în acest scop a dispozitivelor de indicare locală a zonelor cu defect constituie o preocupare amplă pe plan mondial având în vedere avantajele evidente pe care le oferă.

Se concepe o serie de asemenea dispozitive de semnalizare, ale căror principii de realizare şi de funcţionare sunt descrise pe baza unei scheme bloc. Aceste dispozitive au fost testate în laborator şi în reţele reale, în urma cărora varianta considerată cea mai convenabilă de către beneficiar (F.R.E., Iaşi) a fost încredinţată pentru producţie de serie unei întreprinderi electrotehnice (Tehnoton, Iaşi).

BULETINUL INSTITUTULUI POLITEHNIC DIN IAŞI
Tomul XL (XLIV), Fasc. 1–4, 1994
Secţia III
ELECTROTEHNICĂ. ENERGETICĂ. ELECTRONICĂ

D.C. 621.316.1

CONSUMER CATEGORY IDENTIFICATION OF THE LOADS FROM ELECTRIC DISTRIBUTION SYSTEMS USING ARTIFICIAL NEURAL NETWORKS

BY

M. GAVRILAŞ and GH. GEORGESCU

1. Introduction

Urban and rural power distribution networks supply a great number of loads, which in their turn are characterized by different operating conditions. In order to perform the optimal control and planning of these systems a series of power flows analysis for each individual operating conditions is required. Up to the present the following specific loads are considered to be sufficient in power flow analysis of distribution networks: warm / cold season load and work / leisure day load.

An essential stage that has to be surpassed when solving this problem and that also influence to a great extent the accuracy of results is the manner in which load from the buses are taken into consideration. An answer frequently meat in the literature [1],...,[3] suggests to model the loads from the buses using typical load curves associated to different categories of consumers and a number of measurements in the network.

For a distribution network, a typical load curve refers to a category of consumers having the same operating conditions; it is usually drawn out by statistically processing a great number of actual load curves recorded at LV or MV buses of the transformers and represents the probable variation of the load during 24 hours.

For an easier application of this method the make up of a Data Base consisting of a great number of typical load curves for different categories of consumers and operating conditions could show useful. Such a Data Base would permit to recompose the structure of a complex load using an actually recorded load curve. Also, if one wishes to enter in the Data Base a new type of consumer (i.e., a new typical load curve), this would be carried out if and only if the load curve of the consumer considerably differs from those already memorized.

Recently, a lot of interest has been focused on the applications of *Neural Networks* (NN) in the optimal control and planning of power systems [4],...,[6]. In these studies the NN technique has been applied for load forecasting, harmonic sources identification, optimal line routing, etc., and the results seem to be very promising.

The advantage of NN consists in their ability to model a multivariable problem not requiring any rigorous analytical representation of their complex dependency. At the same time NN eliminate nonlinearities that appear between input variables, nonlinearities that are specific in power systems analysis. Furthermore, they are characterized by a great processing speed, a great tolerance to the possible errors in input data and by their adaptability (the improvement of their performances as they gain more experience).

2. Neural Networks. A General View

A Neural Network (NN) is a system that fulfils a parallel and distributed processing of information made up of a set of known input variables and supplies the unknown variable(s) at the output.

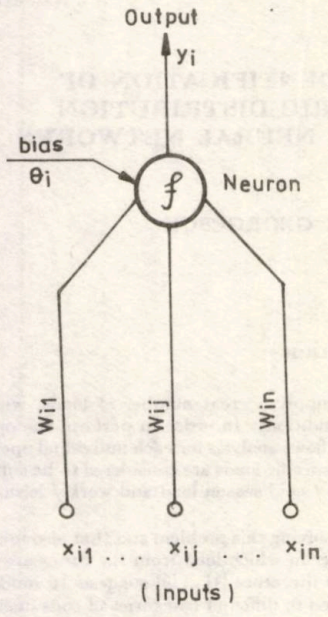

Fig. 1

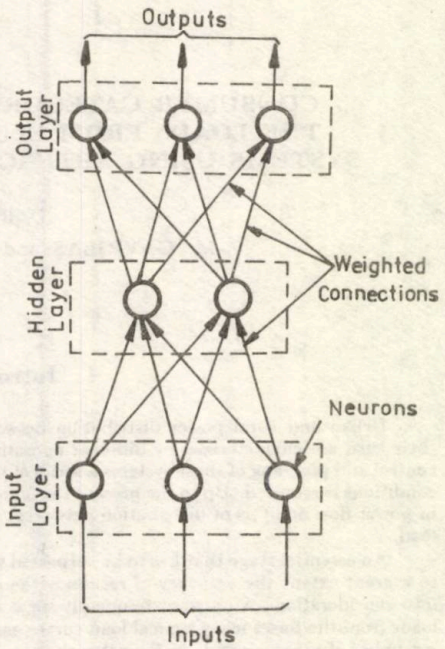

Fig. 2

The essential part of an NN is the neuron (Fig.1) which receives one or more input information x_{ij} from the other processing elements (neurons) or external sources; this input information is modified afterwards by certain weighted coefficients, or simply weights, w_{ij}. When the information comes from an external source the associated weight equals 1. The output y_i results as the weighted sum of the inputs and bias (threshold) θ_i, passed through the nonlinear transfer (activation) function proper to the neuron, $y_i = f(\sum_j x_{ij} w_{ij} - \theta_i)$. Some of the most common transfer functions used with NN are represented in Fig.3.

One of the most known NN configuration is the feedforward backpropagation network from Fig.2. This network consists of three layers of neurons: the *input layer* which gets information from the external sources and provides the inputs for the next, *hidden layer*; the outputs of the hidden layer are distributed afterwards to the neurons in the last, *output layer*.

The operation of an NN comprises two major stages: the "learning" stage and the "recall" one. During the learning stage several sets of input and corresponding output data are supplied to the NN, which iterates using specialized learning algorithms in order to determine the weights w_{ij} and biases θ_i that most accurately correlates the input to the output data. In the recall stage the NN receives a set of input data from an external source and has to point out to an unknown output. This output will be determined using the weights and biases computed during the previous stage. Again, applying another set of input data, the network will process it following the rule established by the learning stage and will output the appropriate answer.

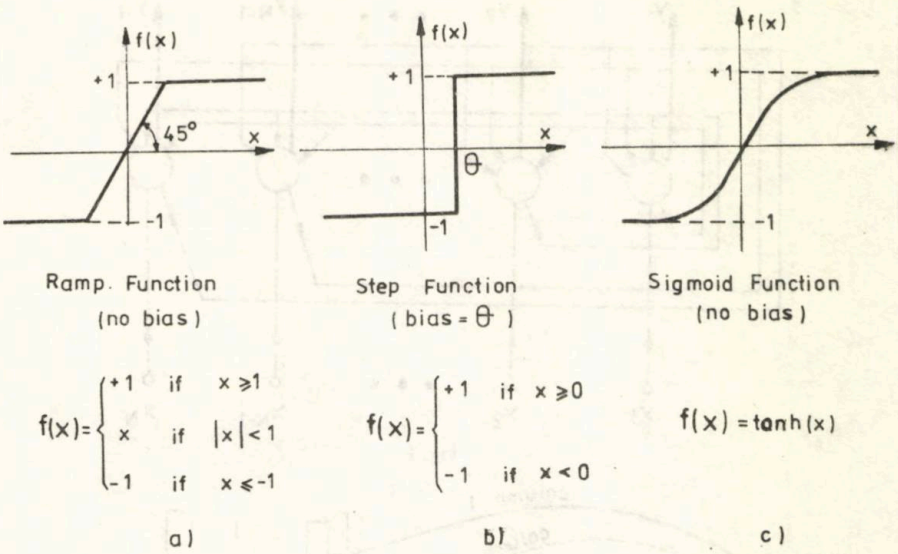

Fig. 3

Among the most frequently mentioned learning algorithms are [7]: Hebbian Correlation, Principal Component Learning, Competitive Learning, Min-Max Learning, Error Correction Learning, Stochastic Learning.

3. Consumer Category Identification Using Neural Networks

In order to design a Data Base that could be used to model the loads from the buses of a distribution network and afterwards to retrieve the structure of the loads, it is convenient to apply a NN specially meant for image recognition. Such a NN could be the H o p f i e l d Net; even if the performances of this type of network are not quite good, we have considered it satisfactory to the goal of this paper.

By comparison to the general configuration of an NN from Fig.2, the H o p f i e l d Net consists of a single neurons layer that acts simultaneously as the input and the output layers (Fig.4) [7]. As a result of this particular configuration each neuron is connected to the others from the same layer.

A typical load curve will be quantified by matrix $[T]$ whose elements are $+1$ or -1 following the rule illustrated in Fig.5. The input variables of the H o p f i e l d Net are the elements of another matrix $[X] = [x_i^K]$; each column K of this matrix, obtained by chaining down the columns of matrix $[T]$, is associated to one of the typical load curves that the Net has to learn (s. Fig.5).

The operation of the H o p f i e l d Net is described by the following algorithm.

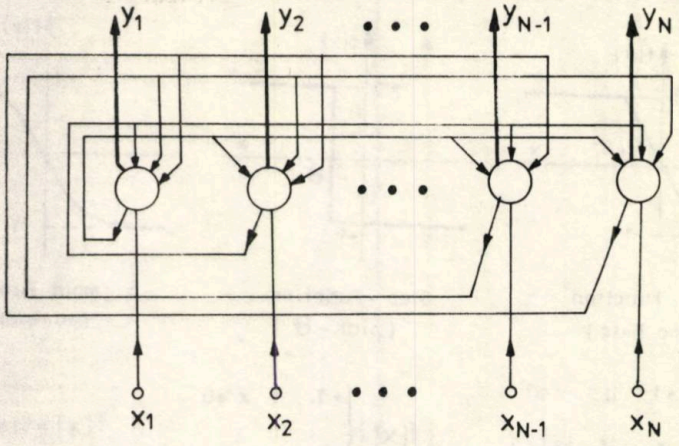

Fig. 4

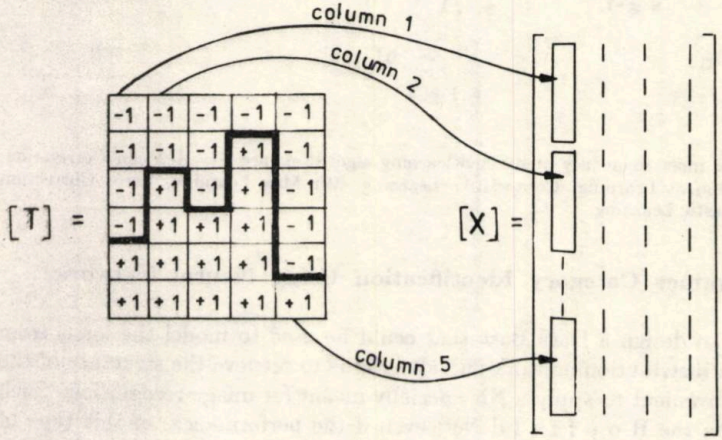

Fig. 5

3.1. Learning Stage

One of the most simple learning algorithm used with H o p f i e l d Net [7] computes the weights of the connection between neurons i and j as:

$$w_{ij} = \begin{cases} \sum_{K=1}^{G} x_i^K x_j^K & \text{if} \quad i \neq j, \\ 0 & \text{if} \quad i = j, \end{cases} \qquad (i, j = \overline{1, N}),$$

where: x_i^K – the i-th element of the K-th typical load curve; G – number of typical load curves considered; N – number of neurons in the Net, that equals the number

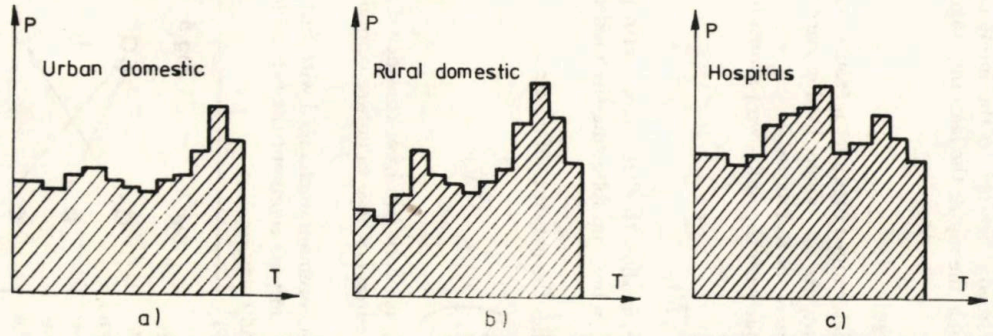
P
Urban domestic
T
a)
P
Rural domestic
T
b)
P
Hospitals
T
c)

Fig. 6

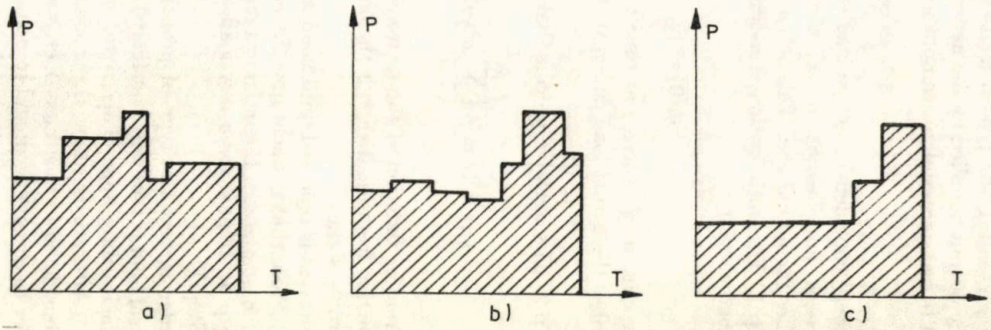
P
T
a)
P
T
b)
P
T
c)

Fig. 7

of rows in matrix $[X]$.

A more complete learning algorithm that computes not only the weights but also the biases is described in [8].

After the learning stage is completed a network test follows; this is accomplished by presenting the typical load curves already "learnt" to the input network. If the output supplied by the network equals the input, the learning stage is considered to be successfully accomplished.

3.2. Recall Stage

This stage considers an actual load curve, determined by direct measurements in the network, and classifies it, i.e. the NN outputs the typical load curve that best matches the actual one. This action is carried out as follows:

S t e p 1. The initialization of network input with the unknown pattern (the recorded load curve):

$$y_i(0) = x_i, \quad (i = \overline{1,N});$$

$y_i(t)$ is the output of neuron i at time t, and x_i is the i-th element of vector $[X]$ that describes the actual load curve; vector $[X]$ is built up following the model in Fig.5.

S t e p 2. The iterative process that classifies the actual load curve:

$$y_i(t+1) = f\left(\sum_{j=1}^{N} w_{ij} y_j(t) - \theta_i\right), \quad (i = \overline{1,N});$$

f is the transfer function of the neurons in the network (we have considered the Ramp Function from Fig.3 a); θ_i is the bias of neuron i, whose value was computed in the learning stage.

The process is repeated until neurons outputs remain unchanged with further iterations. From that moment now the network outputs represent the typical load curve that best matches the unknown input load curve.

S t e p 3. Repeat for a new load curve by going to Step 1.

In order to test the type of proposed NN, three typical load curves were considered as input data for the learning stage. This curves are shown in Fig.6. Afterwards other three load curves (Fig.7), considered as measured ones, were studied in order to classify them and to point out the consumer category to which they belong. After processing the information the load curves presented to the network were classified according to Fig.8.

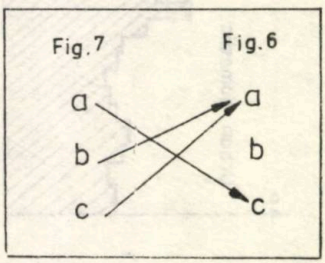

Fig. 8

4. Conclusions

The neural network considered in this paper is useful for classifying the diversity of consumers from the nodes of a power distribution network.

Using this neural network, a more reasonable design of the Data Base containing the typical load curves for different categories of consumers becomes possible. This Data Base could be applied in the optimal control planning of urban and rural power distribution systems.

Received, August 7, 1993

Technical University "Gh. Asachi", Jassy,
Department of Energetics

REFERENCES

1. Codiasse A.M., Guillevic M., Giraud D., *Conaissance des charges moyenne tension en vue de leur prise en compte dans les études de planification.* Rev. Gén. de l'Electr., *7-8* (1982).
2. Markuševič N.S., *Avtomatizirovannoe upravlenie rezhimami elektrosetei 6-20 KV.* Izd. Energyia, Moscou, 1980.
3. Georgescu Gh., Poeată N., *Contribuţii la modelarea sarcinilor din nodurile reţelelor electrice de distribuţie urbane.* Bul. Inst. polit., Iaşi, **XXIX(XXXIII)**, *1-2*, s.III (1983).
4. Chen S.-T., Yu D.C., Moghaddamjo A.R., *Weather Sensitive Short-Term Load Forecas2ting Using Nonfully Connected Artificial Neural Networks.* IEEE Trans. on Power Systems, **7**, *3*, 1098-1105 (1992).
5. Rutisurhata K.H., Richards G.G., *Constrained Neural Network-Based Identification of Harmonic Sources.* IEEE Trans. on Industry Appl., **29**, *1*, 202-208 (1993).
6. Mori H., Itou K., Uematsu H., Tsuzuki S., *An Artificial Neural Net Based Method for Predicting Power System Voltage Harmonics.* IEEE Trans. on Power Delivery, **7**, *1*, 402-409 (1992).
7. Lippmann R.P., *An Introduction to Computing with Neuronal Nets.* IEEE ASSP Magaz., 4-22 (1987).
8. Li J.H., Michel A.N., *Analysis and Synthesis of a Class of Neural Networks: Linear Systems Operating on a Closed Hypercube.* IEEE Trans. on Circuits and Systems, **36**, *11*, 1405-1422 (1989).

IDENTIFICAREA CATEGORIILOR DE CONSUM ALE SARCINILOR REŢELELOR ELECTRICE DE DISTRIBUŢIE CU AJUTORUL REŢELELOR NEURONALE

(Rezumat)

Folosind un tip de reţea neuronală specializată în recunoaşterea formelor, se indică un procedeu de identificare a categoriilor de consum ale sarcinilor din reţelele de distribuţie urbane şi rurale, pe baza graficelor tip de sarcină.

BULETINUL INSTITUTULUI POLITEHNIC DIN IAŞI
Tomul XL (XLIV), Fasc. 1–4, 1994
Secţia III
ELECTROTEHNICĂ. ENERGETICĂ. ELECTRONICĂ

RECENZII BOOK REVIEWS

JOSHI N.V., *Photoconductivity Art, Science, and Technology.* Marcel Dekker, Inc., NY, 1990, 309 pp., ISBN 0-8247-8321-2.

Featuring detector technology capable of sensing even a few photons, this valuable reference guide provides criteria for selecting techniques and equipment appropriate to various types of faint signals. It highlights many important facets of photoconductivity and photodetection, including the measurement of weak photosignals in the presence of noise...statistics relating to the creation, annihilation, and transport of charge carriers...and time-dependent behavior, photoquenching, negative photoconductivity, and photosensitivity.

Complete with more than 125 diagrams and tables, *Photoconductivity Art, Science, and Technology* gives special attention to modern two dimensional photodetectors...describes various configurations for experimental techniques in photoconductivity measurements...survey a band structure properties, with useful reference to such contemporary structures as $n - i - p - i$ and modulation doped materials...illustrates the concept of noise in photoconductors and its role in detector technology...and observes unusual photoconducting properties in diluted magnetic semiconductors.

Photoconductivity Art, Science, and Technology serves as an indispensable resource for optical, electrical, laser, and aerospace engineers, physicists, materials scientists, photonic scientists, and graduate students interested in these disciplines.

KHAKZAR H., *Entwurf und Simulation von Halbleiterschaltungen mit SPICE.* Kontakt & Studium, Bd.**321**, Ehningen bei Böblingen, Expert Verlag, 493 S., ISBN 3-8169-0650-8.

Das Netzwerkanalyseprogramm SPICE basiert auf dem Transistormodell von G u m m e l und P o o n, ergänzt um Modelle für Si- und GaAs-Feldeffekttransistoren. SPICE ist weit verbreitet und rechnet mit ca. 40 Parametern bei Bipolaren Transistoren sowie bei MOS-FET und mit 10 bis 15 Parametern bei Sperrschicht-FET sowie bei GaAs-MESFET. Das Parameter-Extraktionssystem TECAP ersetzt die langwierige Parametermessung bzw. die Verwendung von oft nicht optimalen Ersatzwerten für die Parameter. Dadurch werden Entwurf und Simulation analoger Schaltungen enorm erleichtert. Der Themenband stellt die Handhabung von SPICE dar, erläutert den Umgang mit dem Programm anhand praktischer Übungen und beschreibt Entwurf und Simulation von Breitbandigen, rauscharmen und klirrarmen Verstärkern.

KRAMMLING P.E., *Bündelfunk. Einführung in die Signalisierung nach MPT 1327 und MPT 1343.* Expert Verlag GmbH, Fachverlag für Wirtschaft & Technik, 1993, 145 S., ISBN 3-8169-0947-7.

Das Buch: a) gibt einen Überblick über die Technik des Bündelfunks allgemein; b) erläutert die Funktionsweise und Einsatzmöglichkeiten eines Bündelfunknetzes nach MPT 1327 (Chekker und Lizenz A-Netze); c) gibt praxisbezogene Beispiele zur Signalisierung zwischen Mobil- und Basisstation; d) dient als Nachschlagewerk für alle in der Spezifikation MPT 1327 möglichen Signalisierungstelegramme bezüglich ihrer Verwendung und Zusammenhänge; e) vermittelt die notwendige Kenntnis über die wichtigen Signalisierungsparameter; f) kann als Nachschlagewerk

bezüglich der z.Z. bekannten Netzdaten des Chekkernetzes dienen; g) gibt einen Einblick in die notwendige Messtechnik.

Es wendet sich an: a) Servicetechniker; b) Entwicklungs- und Produktionsingenieure; c) Ingenieure für Typenabnahme; d) Schüler und Studenten von Fernmeldetechnischen Schulen; e) Netzbetreiber.

I n h a l t: Überblick über Bündelfunk allgemein; Erläuterung der Begriffe „MPT 1327", „MPT 1343" und „MPT 1352"; Architektur des Bündelfunknetzes; Signalisierungsstruktur: Das Dynamo Frame Length Slotted Aloha Verfahren; Signalisierungstelegramme und -parameter-Überblick über die Netzdaten der deutschen Chekkernetze; MPT 1327 Netze in Europa; Überblick über die Messtechnik; Ausblicke in die Zukunft: das digitale paneuropäische Bündelfunknetz TETRA.

RUMMICH E., *Elektrische Schrittmotoren und -antriebe.* Kontakt & Studium, Bd. **365**, Ehningen bei Böblingen, Expert Verlag, 1992, 292 S., ISBN 3-8169-0678-8.

Dieses Buch vermittelt: a) Kenntnisse über Aufbau, Wirkungsweise und Betriebsverhalten sämtlicher gängigen Schrittmotorarten; b) Grundlagen und praktische Hinweise über elektronische Ansteuerschaltungen und Signalverarbeitung; c) Kenntnisse über Untersuchungsmöglichkeiten des dynamischen Verhaltens und der Stabilität von Schrittmotorantrieben in der Phassenebene; d) Auslegungskriterien für den optimalen Entwurf von Schrittmotorantrieben und deren Komponenten; e) Kenntnisse über verschiedene Messmethoden und Messeinrichtungen zur Ermittlung statischer und dynamischer Motor- bzw. Antriebsparameter; f) Anwendungsbeispiele und praktische Hinweise für den optimalen Einsatz von Schrittmotoren.

Das Buch wendet sich an Entwickler, Konstrukteure und Anwender von Positionierantrieben sowie an alle auf den Gebieten Antriebstechnik, Mechatronik, Automatisierungstechnik, Robotik, etc., tätigen Ingenieure, ferner an Studenten der einschlägigen Fachrichtungen.

WUNSCH G., *Elektromagnetische Felder.* VEB Verlag Technik, Berlin, 1989, 336 S., ISBN 3-341-00679-6.

Das Buch ist aus Vorlesungen, die an der Technischen Universität Dresden gehalten wurden, hervorgangen.

In einem vorbereitenden Teil werden die erforderlichen mathematischen Hilfsmittel anwendungsbereit und physikalisch anschaulich dargelegt. Nach einer Einführung in die gebräuchlichsten Koordinatensysteme und Angabe der Feldintegrale wird ein Überblick über die Differentialoperatoren gegeben und die wichtigsten Integralsätze erklärt.

Von den Grundeigenschaften des elektromagnetischen Feldes ausgehend werden die L a p l a c esche und P o i s s o nsche Differentialgleichung in verschiedenen Koordinatensystemen gelöst. Die elektromagnetischen Felder werden unterteilt in elektrostatische Felder, stationäre Strömungs- und Magnetfelder, quasistationäre und schnellveränderliche Felder und nach steigendem Schwierigkeitsgrad behandelt.

Die Autoren konnten ihre grossen pädagogischen Erfahrungen einfliessen lassen, um die nicht immer leichten mathematisch-physikalischen Zusammenhänge folgerichtig und verständlich darzulegen.

Übungsaufgaben am Ende jedes grösseren Abschnitts des Buches dienen der Vertiefung und Festigung des Stoffes.

NGUYEN PHUNG QUANG, *Praxis der Feldorientierten Drehstromantriebsregelungen.* Kontakt & Studium, Expert Verlag GmbH, Fachverlag für Wirtschaft & Technik, Ehningen, 1993, 248 S., ISBN 3-8169-1047-5.

Das Buch: a) vermittelt parxisbezogen und verständlich die Entwurfsgänge eines feldorientiert geregelten Drehstromantriebssystems; b) gibt einen Überblick über die modernen Systemstrukturen unter Einsatz von Asynchronmaschine und Kurzschlussläufer oder permanentmagneterregter Synchronvollpolmaschine; c) behandelt ausführlich die Systemkomponenten wie vektorielle Ständerstromregelung, Rotorflusschätzung, Raumzeigermodulation, Koordinatentransformation, Feldorientierung und Istwerterfassung; d) verwendet diskrete Zustandsmodelle der Maschinen als Ausgangspunkt; e) gibt die Systemlösungen auf dem aktuellsten Stand wieder.

Es wendet sich an alle, die mit dem Entwurf eines Drehstromantriebssystems, mit dessen Implementierung oder mit dem Betrieben eines solchen Systems konfrontiert sind, wie: a) Entwickler und Konstrukteure; b) Betriebsingenieure, Betreiber von Drehstromantrieben; c) in der Forschung Tätige; d) Studenten des Fachgebiets Antriebstechnik.

I n h a l t: Systemübersicht; Raumzeigermodulation als Schnittstelle zwischen Regelung und Pulswechselrichter; Anwendungsbeispiele für Raumzeigermodulation unter Einsatz von Hochleistungsmikroprozessoren; Koordinatentransformation; Asynchronmaschine mit Kurzschlussläufer und permanentmagneterregte Synchronvollpolmaschine; Kontinuierliche und diskrete Maschinenmodelle; Probleme der Istwerterfassung, Sollwertvorgabe und Feldorientierung; Übersicht über vorhandene Stomregelverfahren; Vektorielle Ständerstromregelung mit Dead-Beat-Verhalten oder mit Einstellung auf Endliche Enstellzeiten (EEZ-Verhalten); Stromzustandsregelung-Stromvektorregelung; Stellgrössenbegrenzung und deren Berücksichtigung; Überlagerte Regelungen aus der Sicht der quasiverzögerungsfreien Stromregelung.

NEWI G., *Biologische Wirkungen elektrischer, magnetischer und elektromagnetischer Felder.* Kontakt & Studium, B. **106**, Expert Verlag, 1983, 170 S., ISBN 3-88508-830-4.

In steigendem Masse wird uns bewusst, dass Menschen sowie Tiere und Pflanzen neben den naturgegebenen luftelektrischen und magnetischen Erscheinungen in ihrer Umwelt auch zivilisatorisch bedingte künstliche Felder erfahren. Beispiele dafür sind niederfrequente elektrische Felder unter Hochspannunsleitungen und magnetische Felder in der Industrie, hochfrequente elektromagnetische Felder in der Nähe leistungsstarker Sender oder auch elektrostatische Felder infolge von Influenz und durch Ladungstrennung beim Zusammenwirken von Kunststoffen.

Die biologischen Auswirkungen werden seit Jahrzehnten erforscht und in Fachkreisen von Spezialisten wissenschaftlich diskutiert. Durch das z.Z. verschärfte Bewusstsein für die menschliche Umwelt beschäftigen mögliche günstige oder ungünstige Einflüsse aber auch eine weit über die Fachdisziplinen hinausgehende Öffentlichkeit: Unsicherheit entsteht durch widersprüchliche Veröffentlichung über tatsächliche oder vermeintliche Wirkungen und durch Angabe von zulässigen Grenzwerten, die sich um Grössenordnungen unterscheiden. Es wird ferner versucht, mit gezieltem Einsatz verschiedener Feldarten auch im nichtthermischen Bereich günstige Wirkungen als medizinische Anwendung zu erzielen. Die Grenze zwischen geschäftlichem Interesse und wissenschaftlich fundierten Heilaussichten ist schwer erkennbar geworden.

In dieser Situation soll das Buch die heutigen Erkenntnisse darstellen und zu einer versachlichten Meinungsbildung beitragen, dieses vor dem Hintergrund eigener Forschung und langjähriger kritischer Verarbeitung der Literatur. Der Schwerpunkt bezieht sich dabei auf die Verhältnisse beim Menschen. Als Autoren wurden auf ihrem Arbeitsgebiet international anerkannte Fachleute gewonnen, die die Gewähr für eine objektive Information über den derzeitigen Stand geben.

VOIGT E., *Signal- und Systemtheorie in Beispielen.* Expert Verlag GmbH, Fachverlag für Wirtschaft & Technik, Ehningen, 1993, 251 S., ISBN 3-88169-0987-6.

Das Buch gibt einen Überlick über wesentliche Zusammenhänge der modernen Signal- und Systemtheorie; kann als Nachschlagewerk für Spektren praxisrelevanter Signalformen dienen; ermöglicht die selbstständige Erarbeitung anwendungsbereiten Wissens über Methoden und Ergebnisse der Signal- und Systembeschreibung anhand umfangreicher, nach didaktischen Gesichtspunkten ausgewählter Übungsaufgaben mit ausführlichen Lösungen.

Es wendet sich an Studenten und praktisch tätige Ingenieure der Nachrichtentechnik, Mess- und Regelungstechnik, Signalverarbeitung und artverwandter Gebiete.

I n h a l t: Determinierte zeitkontinuierliche Signale und lineare Systeme (F o u r i e r reihe, F o u r i e r- und L a p l a c e transformation, Faltung, Frequenzverhalten linearer Systeme); Zufällige Prozesse (Verteilungsfunktionen, Momente, Korrelationsfunktionen, Spektren stochastischer Prozesse, Transformation an Kennlinien, Reaktion linearer dynamischer Systeme auf zufällige Prozesse); Zeitdiskrete Signale und Systeme (Folgen, Z-Transformation, diskrete F o u r i e r transformation, Differenzegleichung und Strukturen zeitdiskreter Systeme, zeitdiskrete stochastische Prozesse, Systemreaktionnen).

v. PATTAY W., (Federführend), *Informationstechnische Verkabelung von Gebäudekomplexen. Ein Netz für alle Anwendungen.* Expert Verlag GmbH, Fachverlag für Wirtschaft & Technik, Renningen, 1993, 280 S., ISBN 3-8169-0994-9.

Mit der zunehmenden Dichte der Daten- und Textstationen ist es unwirtschaftlich, die zu ihrem Anschluss an Rechner und Fernmeldedienste benötigten Kabel bedarfsorientiert zu verlagen. Mit dem Übergang vom analogen Telefon zu ISDN steigen die physikalischen Anforderungen an die meist vorsorglich verlegten Telefonkabel. Mit der zunehmenden Verbreitung und Vielfalt der LANs ist es wirtschaftlich untragbar, für jedes LAN ein eigenes Kabel zu verlegen.

Die Informationstechnische Verkabelung muß als Bestandteil der gebäudetechnischen Infrastruktur geplant werden und sich den verschiedensten Nutzerprofilen anpassen können.

Dieser Themenband schlägt eine Brücke zwischen der Verkabelung und der Datenverarbeitung/Organisation, indem er dem Organisator Grundkenntnisse über Kabel und Verkabelung vermittelt und dem Fernmeldetechniker die Anforderungen von LANs und ISDN an die Verkabelung nahebringt. Die in internationalen Normgremien diskutierten Strategien und Komponenten für Verkabelungsstrategien werden ebenso dargestellt wie die von einzelnen Firmen angebotenen Konzepte und Produkte. Der Leser lernt die Andorderungen an zukunftssichere Verkabelungen kennen und erfährt, wie sie zu planen und zu verwalten und wie ihre Komponenten auszuwählen sind.

Das Buch ist geschrieben für Führungskräfte und Mitarbeiter der Fachgebiete Nachrichtentechnik, EDV und Organisation in Unternehmen ab ca.50 Büroarbeitsplätzen sowie für Fachkräfte in Planungsstellen und Ingenieurbüros, die nachrichtentechnische Infrastruktur von Büros planen.

PEAKE S., *Transport in Transition. Lessons from the History of Energy.* Brookings Institution, Washington, 1994, 113 pp., ISBN 1-85383-209-X.

"Transport is a central and complex sector that is the focus of growing controversy in many OECD countries. It is frequently identified as posing particular problems for energy and environmental policy, and in many of these countries it is also the largest and fastest-growing energy end-use sector.

It is for these reasons that the Energy and Environmental Programme decided to undertake a research study on transport. Dr.Stephen P e a k e, having recently completed his doctoral thesis on transport trends and policies and the lessons which might be derived from the energy experience, was an ideal candidate to undertake such research... His report *Transport in Transition* draws partly upon the ideas he developed in collaboration with his doctoral supervisor, Dr.Chris H o p e, at the Department of Engineering, Cambridge University.

...The study argues that transport is entering a turbulent phase with potentially radical changes, and explores some of the lessons which may be drawn from the rich and complex history of energy trends, analysis and policy itself. It is challenging approach which should stimulate much fresh thinking about the analysis and implications transport trends and policies".

Dr.Michael Grubb

Head, Energy and Environmental Programme

C o n t e n t s: 1. Introduction: Energy in transition; Transport in transition; Aims and structure of the report; 2. Transport trends, problems and prospects: the case of the U.K.; The growth of transport in the U.K.: structure and influences; The environmental and social impacts of transport; Transport in transition?; 3. Energy in transition: U.K. energy 1950–1992; The impact of the energy crisis; Conceptualizing energy: information and measurement; U.K. energy conservation and energy efficiency policy; Energy futures: forecasts, scenarios, top-down and bottom-up; 4. Using the analogy between energy and transport: Limitations and basis of the analogy; Structural similarities between the energy and transport sectors; 5. The conceptual analogue: measuring transport and economic activity; Transport: what move when things change and what changes when things move; Measuring overall transport activity in the economy: gross and net mass movements; Micro-interpretations and derivates of gross mass movement: carrier mass productivity; Macro-interpretations and derivates of gross mass movements: environmental impact and economic intensity indicators; Aggregate transport trends in the U.K.: 1952–92; Conclusions; 6. The policy analogue: transport efficiency; Introduction; U.K. energy efficiency; Transport efficiency: lessons from the energy sector; 7. The futures analogue: planning under uncertainty; New uncertainties for the analysis of transport futures in the U.K.; Two alternative scenarios for the U.K. up to 2025; Conclusions: transport in macroeconomic transition; Appendix.

1883 ORSZÁGOS KÖZPONTI MŰSZAKI ÉS KÖNYVTÁR INFORMÁCIÓS

ISSN 0258-9109